Evolutionary Constraints on the Second Most Stable
Optical Clock known : ZZ Ceti

by

Anjum S. Mukadam, M.S., B.S.

Thesis

Presented to the Faculty of the Graduate School of

The University of Texas at Austin

in Partial Fulfillment

of the Requirements

for the Degree of

Master of Arts

The University of Texas at Austin

December 2000

Evolutionary Constraints on the Second Most Stable Optical Clock known : ZZ Ceti

Approved by
Supervising Committee:

_____

_____

_____

_____

This thesis is dedicated to ZZ Ceti (R548), without whose altruistic co-operation,

it would certainly not have been possible.

Acknowledgments

Evolutionary Constraints on the Second Most Stable Optical Clock known : ZZ Ceti

Anjum S. Mukadam, M.A.

The University of Texas at Austin, 2000

Supervisor: D. E. Winget

White Dwarfs (WDs) are ideal chronometers as they demonstrate a simple relation between age and effective temperature. A calibration of their cooling curve is essential to reduce one of the theoretical uncertainties in WD cosmochronology. Such a calibration requires actual measurements of the rate of cooling for a few WDs at different temperatures. We expect pulsating WDs, which are otherwise normal WDs, to demonstrate a change in stable periods with time ($\dot{P}$) due to cooling. By measuring such a secular change of their periods, we will effectively be measuring their rate of cooling. DAs constitute about 80% of the WD population and are observed to pulsate in a temperature strip 11000 - 12000 K. We analyzed data on the DAV ZZ Ceti, also called R548, spanning 30 years and we conclude that the rate of period change with time for two of its pulsation periods is less than $(4.6 \pm 2.1) \times 10^{-15}$ s/s. This implies a cooling time-scale greater than or equal to about 1.5 billion years, thus constraining the theoretical evolutionary models. This measurement is consistent with the 215.2s pulsation in G117-B15A, which shows a $\dot{P}$ of $(2.3 \pm 1.4) \times 10^{-15}$ s/s.

Contents

List of Tables

List of Figures

Chapter 1

Introduction

1.1   White Dwarfs as Chronometers

Of all the stars that ever burn hydrogen (to exclude brown dwarfs), 98-99% will eventually become white dwarfs (Wiedemann 1990, Kepler & Bradley 1995). White Dwarf stars (WDs) are high-gravity objects with log g $\approx$ 8 (in C.G.S. units), an average mass of 0.6 $M_\odot$ and a size close to that of planet Earth. They represent a relatively simple stellar state with no central nuclear fusion, though shell burning may be present. Electron pressure provides the main support against gravity. These electrons also make the core isothermal due to their high conductivity. The outer layers, composed of lighter elements because of gravitational settling, are non-degenerate. They control the rate at which the residual thermal energy of the ions in the electron degenerate isothermal core is radiated into space. WD evolution is dominated by cooling, leading to a simple relation between effective temperature and age of the WD, as given by Mestel theory (Mestel 1952, van Horn 1971). These properties combine to make WDs very reliable chronometers.

WDs are very hot initially, just after the ejection and expansion of the planetary nebulae, and expected to cool rapidly. The cooling rate decreases as their

temperature drops, allowing even the oldest WDs to remain visible. Detecting WDs with faint absolute luminosities and average masses, is then synonymous with detecting the oldest WDs. Also, the exponential decrease in the cooling rate causes a pile up of WDs at lower temperatures. The volume density of WDs per unit absolute bolometric magnitude plotted as a function of their luminosity, i.e. the luminosity function (LF), is expected to show more and more WDs in lower temperature bins. However, the best current observational determinations of the WD LF for the disk indicate a turn-down in the space density of low luminosity stars (Liebert, Dahn & Monet 1988; Leggett, Ruiz & Bergeron 1998; Oswalt, Smith, Wood & Hintzen 1996), presumed to be a signature of the finite age of the disk. The luminosity where this turn-down occurs, in conjunction with theoretical cooling calculations, allowed Winget et al. (1987) to estimate the age of the galactic disk. The determination of the halo luminosity function would enable us to make the same sort of estimate for the halo. This process is referred to as WD cosmochronology.

WD cosmochronology involves observational and theoretical uncertainties: the observational uncertainties come from an inability to locate the turn-down in the luminosity function accurately, because these cool WDs are faint and consequently hard to detect. Note the location of the turn-down is not determined solely by the few WDs detected at low temperatures, but because none are detected at temperatures lower than that. Most of the theoretical uncertainty in the age estimation comes from uncertainties in the constitutive physics and the basic parameters that are used in the estimation of the cooling rates. These include calibration of the cooling curve, core composition, crystallization and phase separation. We can calibrate the cooling curve by measuring the cooling rate of WDs at different temperatures. Nature has provided us with a way to measure the cooling rate of a WD by giving us pulsating WDs.

1.2 An Introduction to Asteroseismology with Pulsating White Dwarfs

Pulsations in stars can be used to probe their interiors, just like earthquakes are used to deduce the Earth's interior. This is one of the few existing techniques to peek inside stars and is called asteroseismology. We can use the asteroseismological technique of identifying the normal modes of pulsation to infer the stellar mass, effective temperature, luminosity and consequently the star's distance from the Sun, masses of the surface layers, rotation rate, magnetic field strength, fractional crystallization and neutrino luminosity (especially in pre-white dwarfs).

The observed properties of the currently known classes of pulsating WDs place them in three different temperature ranges: the high temperature instability strip consists of the PNNV and the DOV stars at an effective temperature of 140000 to 70000 K, $\log g = 6$. The DBV instability strip occurs around 25000 K, while the DAV instability strip is found between 11000 K to 12000 K (Winget 1998). The periods are typically 100 s to 1000 s, consistent with nonradial g-mode pulsations. WDs have high gravity ($\log g \approx 8$), so nonradial g-mode pulsations are energetically favored as they are dominated by motion along equi-potential surfaces, rather than radial or nonradial p-mode pulsations, which are dominated by motion along the radial direction. At the blue edge of the instability strip, we observe the pulsation periods to be stable. This confirms our theoretical expectation that WD evolution is simple cooling at almost a constant radius.

1.3 Changes in Pulsation Periods due to Cooling

Pulsating WDs are not defective or special in any way. It has been shown that all known DAs pulsate in the ZZ Ceti instability strip (McGraw & Robinson 1976; Lacombe & Fontaine 1980; Giovannini et al. 1998), i.e., it is an evolutionary effect.

So, when we measure the cooling rate for a pulsating WD, it applies to all WDs at that temperature and mass. As cooling of the WD changes the pulsation period by a very small amount, measuring the change in pulsation period with time, i.e., $\dot{P}$, actually constrains the rate of cooling.

There are two competing processes that govern $\dot{P}$ in the theoretical models of the ZZ Ceti stars: cooling of the star that increases the periods as a result of the increasing degeneracy (Winget, Hansen & van Horn 1983) and residual gravitational contraction that decreases the periods. This can be expressed as follows (Kepler et al. 2000):

$$\frac{d \ln P}{dt} = -a \frac{d \ln T_c}{dt} + b \frac{d \ln R}{dt} \tag{1.1}$$

where a and b are constants associated with the rate of cooling and contraction respectively, and are of order unity. Following Kawaler, Winget & Hansen (1985) and Kepler et al. (2000), we can write

$$\frac{d \ln P}{dt} = (-a + bs) \frac{d \ln T_c}{dt} \tag{1.2}$$

where s is the ratio of the contraction to the cooling rate.

$$s = \frac{d \ln R}{d \ln T_c} \tag{1.3}$$

Spectroscopic $\log g$ values suggest that R548 has a mass of 0.52 $M_\odot$ (Bergeron et al. 1995). Bradley (1998) obtain a preferred seismological mass range of 0.54 - 0.56 $M_\odot$. For a DA WD near 12000 K, models predict a radius around 9.6×10^8 cm and a contraction rate of about 0.1 cm/yr (Bradley; private communication). (Note that the contraction rate quoted by Kepler et al. (2000) has been mistyped and reads as 1 cm/yr). Models also give a core temperature of 1.2×10^7 K and a cooling rate of 0.05 K/yr (Kepler et al. 2000). These numbers imply that s is 0.025

and hence we conclude that $\dot{P}$ is dictated by the rate of cooling of the pulsating star.

The rate of cooling decreases as the temperature drops and the cooling curve is theoretically expected to be exponential. As we are using pulsating WDs to measure the rate of cooling, we can only measure the cooling rate for the hot DOV and PNNV stars at effective temperatures between 140000 to 70000 K, for the DBVs around 25000 K and for the DAVs between 11000 K to 12000 K. Thus, estimating a $\dot{P}$ for hot pre-white dwarfs forms one end-point of the calibration curve, while the cool DAV pulsators form the other end-point. Interpolation between these two end-points would result in a nicely calibrated cooling curve. We could then measure the $\dot{P}$ for the DBVs and see if it is consistent with the cooling curve.

The DOV star PG-1159-035 revealed a rate of period change for the 516 s mode (Costa, Kepler, & Winget 1999) of $(13.0 \pm 2.6) \times 10^{-11}$ s/s. This value of $\dot{P}$ agrees in sign with the theoretical models, but is an order of magnitude larger. At the cool end, G117-B15A has a measured $\dot{P} = (2.3 \pm 1.4) \times 10^{-15}$ s/s (Kepler et al. 2000). None of the DBVs have a measured $\dot{P}$ yet. But a decade of data now exists on GD358 and it should be possible to measure $\dot{P}$.

1.4   Motivation for choosing a DAV

There are three good reasons to choose a DAV and they are outlined below.

1. **Results to be applied to an Ensemble :** By measuring the cooling rate of another DAV, which has a different stellar mass, we are providing a second independent measurement of the cooling rate of a low temperature WD. A second measurement gains importance as we will be applying the results to DA WDs as a class and they constitute 80% of the WD population.

5

2. **Core Composition :** The rate of cooling of a WD depends on core composition and stellar mass. For different core compositions there are families of cooling curves. The heavier the core, the faster the star cools. Comparing the measured $\dot{P}$ with theoretical evolutionary models would give us an idea of the mean core composition. Using a Mestel-like cooling law, Kepler et al. (1991) wrote a relation between the rate of period change and the core mean atomic weight A as:

$$\dot{P}(A) = 4.3 \times 10^{-15} \frac{A}{12} \tag{1.4}$$

   This will also prove to be a testing ground for models with substantially heavier cores, as they would produce a faster rate of period change. $\dot{P}$ measurements for G117-B15A indicate a C/O core.

3. **Motivation for choosing R548 (ZZ Ceti) :** Now that we have established our motivation for choosing a DAV, we have 29 choices. Using standard evolutionary theory, Bradley, Winget & Wood (1992) estimated the cooling time-scale, i.e., $\frac{T}{\dot{T}}$, for a DA at about 12000 K to be a few billion years. We thus expect the $\dot{P}$ to be positive and of the order of 10^{-15} s/s for a DAV. This is consistent with the measurements for G117-B15A. If the size of the $\dot{P}$ that we have set out to measure is 10^{-15} s/s, it would take us a few decades of data to measure a detectable change in the period. With that criterion in mind, and noting that only stars in the blue edge have really linear stable pulsations, our choice of a suitable candidate amongst all the pulsating DAVs, is limited to exactly three. These are G117-B15A, R548 (ZZ Ceti) and L19-2, the only ones to have archival data spanning a few decades. Kepler is working on G117-B15A and L19-2 is not observable from McDonald Observatory, TX. We therefore chose to work on R548 and acquired an opportunity to extend the time-base by seven years. We observed R548 extensively in 1999 and 2000. Along with the previous data, we now have a time-base of 30 years, from 1970

6

to 2000.

We have established our motivation for attempting to measure the $\dot{P}$ for the known pulsations in R548. In the subsequent chapters, we will see how the proposed work was carried out and examine its implications.

Chapter 2

Observations and Data Reduction

Our main goal is to measure the $\dot{P}$ for the four known pulsations in R548. With that in mind, we obtained archival data on R548 (1970 - 1993) from S. O. Kepler, for which we are very grateful to him. By observing the star in 1999 and 2000, we extended the time-base by seven years. We did high speed time series aperture photometry on R548 in September and October 1999 as well as in August, September and October 2000 at McDonald Observatory. We were also fortunate enough to have R548 included as a secondary target star in the Whole Earth Telescope (WET) campaign XCov 18 in November 1999 and in XCov 20 in November 2000. We profusely thank all the WET community for these data sets. A journal of observations is given in table 2.1 for all the data acquired in 1999 and 2000. Of these, the Wise Observatory CCD data could not be used due to severe extinction problems.

Observing Run	Date	Time (TCB)	Duration (hours)	Telescope	Observatory
asm-0003	September 5, 99	7:36:30	3.7	0.9m	McDonald Observatory
asm-0004	September 6, 99	8:24:30	2.1	0.9m	McDonald Observatory
asm-0005	September 7, 99	9:09:00	2.5	0.9m	McDonald Observatory
asm-0007	September 8, 99	9:58:00	1.5	0.9m	McDonald Observatory
asm-0010	September 10, 99	9:08:00	2.5	2.1m	McDonald Observatory
asm-0013	September 15, 99	6:21:30	5.2	0.9m	McDonald Observatory
asm-0016	September 17, 99	7:51:00	2.1	0.9m	McDonald Observatory
asm-0017	September 18, 99	8:38:00	3.1	0.9m	McDonald Observatory
asm-0019	September 19, 99	7:12:30	4.5	0.9m	McDonald Observatory
asm-0021	September 20, 99	5:27:30	6.4	0.9m	McDonald Observatory
asm-0031	October 15, 99	3:29:00	2.8	0.9m	McDonald Observatory
asm-0032	October 15, 99	4:36:01	6.0	0.9m	McDonald Observatory
asm-0039	October 16, 99	2:51:00	8.0	0.9m	McDonald Observatory
asm-0040	October 19, 99	2:56:30	7.7	0.9m	McDonald Observatory
asm-0041	October 20, 99	2:37:30	8.0	0.9m	McDonald Observatory
asm-0042	October 21, 99	2:19:00	8.2	0.9m	McDonald Observatory
mdr066	November 6, 99	2:01:00	1.4	1.5m	CTIO
n49-0425	November 8, 99	18:37:50	3.2	1m	UPSO
n49-0426	November 9, 99	16:51:00	4.5	1m	UPSO
dmk124	November 9, 99	18:36:01	2.1	1m	SAAO
wccd-004	November 9, 99	17:25:08	0.8	1m(CCD)	Wise Observatory
wccd-007	November 10, 99	16:56:20	1.4	1m(CCD)	Wise Observatory
n49-0427	November 10, 99	14:03:10	2.5	1m	UPSO
dmk126	November 10, 99	18:32:00	2.0	1m	SAAO
no1199q1	November 11, 99	6:46:00	0.9	0.6m	Mauna Kea Observatory
no1199q2	November 11, 99	11:26:40	4.1	0.6m	Mauna Kea Observatory
wccd-012	November 11, 99	16:40:00	1.8	1m(CCD)	Wise Observatory
tsm-0065	November 12, 99	2:00:00	1.0	2.1m	McDonald Observatory
mdr083	November 13, 99	00:54:30	1.6	1.5m	CTIO
mdr086	November 14, 99	00:45:50	1.4	1.5m	CTIO
tsm-0068	November 14, 99	1:32:00	1.4	2.1m	McDonald Observatory
no1499q1	November 14, 99	7:32:00	3.5	0.6m	Mauna Kea Observatory
mdr088	November 15, 99	0:13:30	1.9	1.5m	CTIO
no1599q2	November 15, 99	9:36:50	1.8	0.6m	Mauna Kea Observatory
no1699q1	November 16, 99	6:35:20	4.4	0.6m	Mauna Kea Observatory
asm-0057	August 24, 00	7:35:11	4.0	2.1m	McDonald Observatory
asm-0058	August 25, 00	7:37:20	4.0	2.1m	McDonald Observatory
asm-0059	August 28, 00	7:31:21	3.4	2.1m	McDonald Observatory
asm-0060	September 24, 00	8:42:30	3.2	2.1m	McDonald Observatory
asm-0063	September 26, 00	5:14:20	6.7	2.1m	McDonald Observatory
asm-0065	September 27, 00	8:28:50	3.5	2.1m	McDonald Observatory
asm-0070	September 29, 00	8:55:50	3.0	2.1m	McDonald Observatory
asm-0072	September 30, 00	6:16:00	5.7	2.1m	McDonald Observatory
asm-0075	October 1, 00	8:40:20	3.3	2.1m	McDonald Observatory
asm-0077	October 2, 00	7:38:30	4.4	2.1m	McDonald Observatory
gh-0500	October 7, 00	0:39:30	0.9	2.1m	McDonald Observatory
gh-0501	October 7, 00	1:41:40	0.9	2.1m	McDonald Observatory
gh-0502	October 10, 00	2:16:40	1.0	2.1m	McDonald Observatory

Table 2.1: Journal of Observations for the 1999 and 2000 data on R548

2.1 Observations

R548 is a 14th magnitude WD and we observed it with the 36" and 82" telescopes at McDonald Observatory. The data were acquired using a 3-star photometer (Kleinman, Nather & Phillips 96) and a software program called "QUILT 9.14", written by Ed Nather. R548 has two main doublets, the details of which have been given in table 2.2 (Tomaney 1987; private communication).

Period (s)	Amplitude (mma)	Frequency (μHz)
213.132603	6.7	4691.9
212.768428	4.1	4699.9
274.250835	4.1	3646.3
274.774510	2.9	3639.3

Table 2.2: Previous data on the R548 pulsational doublets

Note that an amplitude of 1 mma (milli modulation amplitude) implies an amplitude of one part in a thousand. In order to resolve the two closely spaced frequencies in each of the doublets, a time-base of 35 to 40 hours is required. This necessitates observing R548 for a few days. An integration time of 5 to 10 s provides a suitable time resolution to observe the pulsation periods. This also sets the Nyquist frequency, the largest observable frequency, at 0.05 Hz. R548 shows nonradial g-mode pulsations, which have periods in the range of a 100 s to a 1000 s, i.e., frequencies lower than 0.01 Hz only. We do not use a filter during observation to maximize the signal to noise ratio. This does not constitute a problem as the nonradial g-mode pulsations have the same phase in all colors (Robinson, Kepler & Nather 1982; Nitta et al. 1999). However, if the phototube is red-sensitive or a CCD is being used to acquire the data, then we will get correct phases, but the amplitudes can be under-estimated by as much as 20% for a DAV (Kanaan et al. 2000; in press). In order to get the correct amplitudes, we do have to use a filter to cut the red part of the spectrum. This reduces the signal to noise ratio, but yields

correct amplitudes. We need a good signal to noise ratio and a long time-base for accurate measurement of period and phase for each of the pulsations. Hence we observe the target as long as possible each night.

2.2 Observing with the 3-channel photometer

The photometer, we used on most observations, has 3 channels, allowing us to observe 3 different patches of sky at the same time. Typically, we choose the target star to be in channel 1, as this channel is aligned with the center of the field and light loss due to reflections is minimized. A comparison or guide star becomes the subject of channel 2, while channel 3 is generally used to observe sky. Brightness variations in the sky can be removed from channels 1 and 2 using data from channel 3. The 3 photo-tubes, belonging to the respective channels have different sensitivities. The ratio of their sensitivities must be taken into account for sky subtraction, to be done later, during data reduction. So, in order to determine this ratio, we observe sky at the beginning and end of each observing run in all 3 channels.

We are doing aperture photometry, and ideally need the target star at the center of the aperture throughout the observing run. However, since the telescope does not track perfectly, we need to check whether the target star is centered at least every few minutes and more frequently if necessary. This process of checking would normally require light to the photo-tube to be cut-off and sent to the eye-piece instead. This would prove to be a disastrous effect on the light curve of the target star and the resultant data would be marginal. To avoid this, a second channel is built into the instrument for a guide star. So, we choose a suitable guide star at the beginning of the observing run and center both stars simultaneously in their respective apertures. We can now guide throughout the run using the guide star. The comparison or guide star has to be within a certain distance from the target star, determined by the plate scale and the instrument design. It cannot be too

close or too far away from the target star. We try to choose a non-variable guide star. However, more than once in the history of the WET, a variable comparison star has led to the discovery of a new pulsating star.

We choose an aperture size for channel 1 according to the seeing. A rough rule of thumb is that the aperture size should be ten times the seeing disk. Aperture size of channel 2 is chosen to be smaller than that for channel 1, or at maximum, the same size as channel 1. This would facilitate an early warning of a guide error. A careful observer would check every few hours if channel 1 is still centered. This is to avoid having channel 2 centered and the target star at the edge of the aperture, due to flexure or any motion of the XY stage that is used to find and center the guide star. Also, atmospheric dispersion and differential extinction can cause the same effect as the target star is probably more blue than the comparison star.

Manual guiding, as has been described above, can be very tedious and even if the observer guides every 3-4 minutes, there can be substantial drifts and the stars may not be centered during the time between guiding. This is specially true for extreme positions of the telescope, when the tracking is unreliable or if the seeing is bad or in case of wind bounce. To get better quality of data in these and other conditions, we resorted to a remote guider, the SBig system. The light from the guide star is split into two beams by a dichroic. Red light is sent to the red-sensitive CCD of the SBig and blue light is sent to the blue-sensitive Photo Multiplier Tube of channel 2. The SBig then provides a CCD image to an observer sitting in the control room, who can now guide every 5-10 s, if necessary, and keep the guide star well centered. As the telescope tracks through differing air-masses, the centers of red and blue images may not coincide due to differential refraction. So, the observer must simultaneously center both target and guide stars and the SBig CCD image every 2-3 hours or so, depending on the change in air-mass.

2.3 Data Reduction

Reducing data is an art with many steps being subjective to individual assessment. It involves excluding from the data what is not due to the star, but due to Earth's atmosphere and the instrument.

We reduced and analyzed the data in the manner described by Nather et al. (1990) and Kepler (1993) using the software called QED (Clemens 1993), also written by Ed Nather. The preliminary step is to identify all the data points that contain sky. At this stage, we edit out bad points as may have been caused by guiding errors, dome errors, clouds, flashlight shining down the tube, lightning and bugs crawling in the aperture among the few things that could go wrong, not even beginning to mention the electronics or the RS-232 communication cables from Cassegrain to control room.

The following steps are involved in data reduction using QED :

1. **Dead-time Correction :** The photo-tube has a finite response time, during which it cannot distinguish between the time of arrival of two photons. This non-zero response time is called dead-time. For the R647 Hamamatsu photo-tubes used in the photometer, the dead time is 15 nanoseconds (Nather; private communication). Note that the electronics for the photometer is so designed that it does not care about the energy of the individual photons. Pulses produced by each photon are tailored to be the same height. Hence, two photons coming in within the dead time are not counted as a single photon with twice the energy, but as a single photon. If the source is very bright, then the fraction of photons lost due to dead-time can be large. R548 is a 14th magnitude star and we got about 2000 counts per second after subtracting the sky counts on the 36" telescope at McDonald Observatory in bright time and using an aperture of 2 mm. This implies a counting rate loss of 0.003% due to dead-time, which is pretty small. On the 82" telescope, we got 3000 cps

in dark time and therefore a loss of 0.0045%. We got about 13000 cps on the 82" telescope in bright time and an implied loss of 0.02%. Note that all these count rates have been quoted for an aperture size of 2 mm after subtracting the sky counts. If you compare the count rates from bright time on the 36" telescope *vs.* bright time on the 82" telescope, they do show a ratio similar to a simple scaling of the areas of the primary mirrors. However, if you compare the count rates from bright time on the 36" telescope to the dark time on the 82" telescope, they do not scale as the ratio of the areas of the primary mirrors.

2. **Sky Subtraction :** Variations in the seeing, transparency of the sky, etc. during the course of the night increase the amount of noise in the data, especially at low frequencies. Assuming the sky fluctuations in channel 3 are correlated to the sky fluctuations in channels 1 and 2, we can eliminate such variations by subtracting the sky in channel 3 from channel 1 and 2 light curves, after the sky has been smoothed. This averaging process is done to reduce the amount of noise added to the 2 light curves, as the atmospheric cells responsible for the scintillation are smaller than the distance between the apertures.

   As mentioned earlier, the sensitivities of the tubes are different. Simultaneous observations of the sky in all 3 channels at the beginning and end of the run are used to obtain the sensitivity ratios, which we can then use in sky subtraction.

3. **Extinction Correction :** As we track the target with the telescope, we are observing it through a varying air-mass. The program corrects the light curves of the target and comparison star for extinction, a wavelength dependent effect, using a given extinction co-efficient. The parameters for this exponential correction are determined by the stellar co-ordinates, location of the observatory and time of observation.

4. **Division by Channel 2 :** This is an optional step and is used to eliminate slow variations affecting both channels in the same way, only if the other steps have been unsuccessful in doing so. This step is particularly advantageous while recovering data from cirrus, or even a relatively mild error due to guiding or dome obstruction. But this increases the amount of noise and hence one must always smooth channel 2 before any such division. We also verified whether such an operation affects the phase determination and we conclude that it does not. Here extreme caution is necessary, and experience is the best guide.

5. **Polynomial Correction :** It is not possible most of the times to completely eliminate slow variations (slow compared to the pulsations), as we have not really measured extinction variations throughout the night, These could be remnants of incorrect sky subtraction or extinction correction. Such variations increase the noise at the low frequencies, when you take the Fourier transform of the light curve. To reduce this, we subtract a polynomial of specified order and remove these variations, at least to some extent. This step gains importance in our work as we need very precise phase information. The linear least square fits on the data do not account for such slow variations and therefore the fit is affected by their presence. This too is an optional step and we consider the length of the observing run before deciding on the order of the polynomial to be subtracted. The higher the order of the polynomial, the greater is the interference at the low frequency end of the pulsation spectrum. Suppose the observing run is one hour long and we subtract a polynomial of order 3, then we are interfering up to a frequency region of 278 μHz. The main frequencies in R548 are at 4692 μHz and 3646 μHz. We have never gone beyond subtracting a polynomial of order 3 from the reduced data, which is conservative enough.

6. **Bridging Gaps :** Gaps maybe caused in the data due to clouds, guiding, errors, etc. If the data is single-site, then there is a gap during day time. Such gaps introduce aliases in the Fourier transform (Nather 1995). Since we are looking at variable WDs, we bridge a gap only if it is less than quarter of a pulsation cycle. We use our best judgement whether or not a bridge does justice to the missing data in the gap. If we cannot bridge the data, we write it as separate chunks or files.

After this preliminary reduction, we bring the data to the same fractional amplitude scale. We convert the times of arrival of photons to a Barycentric Coordinated Time TCB (Standish 1998). At this juncture, the light curves look as shown in figures 2.1-2.5.

Next, we compute a Fourier Transform (FT) of all the data sets. Note that if you take a FT of a sinusoidal signal that is finite in length and has gaps, then you would get a "window" pattern, as shown in the lower panel of figure 2.6.

The true frequencies have to be disentangled from the aliases, as seen in the window. Once the genuine frequencies are identified, then we synthesize a light curve with those frequencies and subtract it from the real data sets. This process is called pre-whitening. Pre-whitening with the true frequency results in a disappearance of most of the power in the FT, while pre-whitening with an alias results in a considerable amount of remnant power. This serves as a confirmatory test that we have correctly identified the pulsation frequencies. The FT thus gives us approximate values for period, phase and amplitude for all the four pulsations. The uncertainty in period being related to the peak width in the FT.

We improve our values for period, phase and amplitude for the four main pulsations by taking each data set through the following two step procedure. The approximate values for periods known from the FT are fed into a linear least squares program. Since we are dealing with two closely spaced doublets, we initially fit the

16
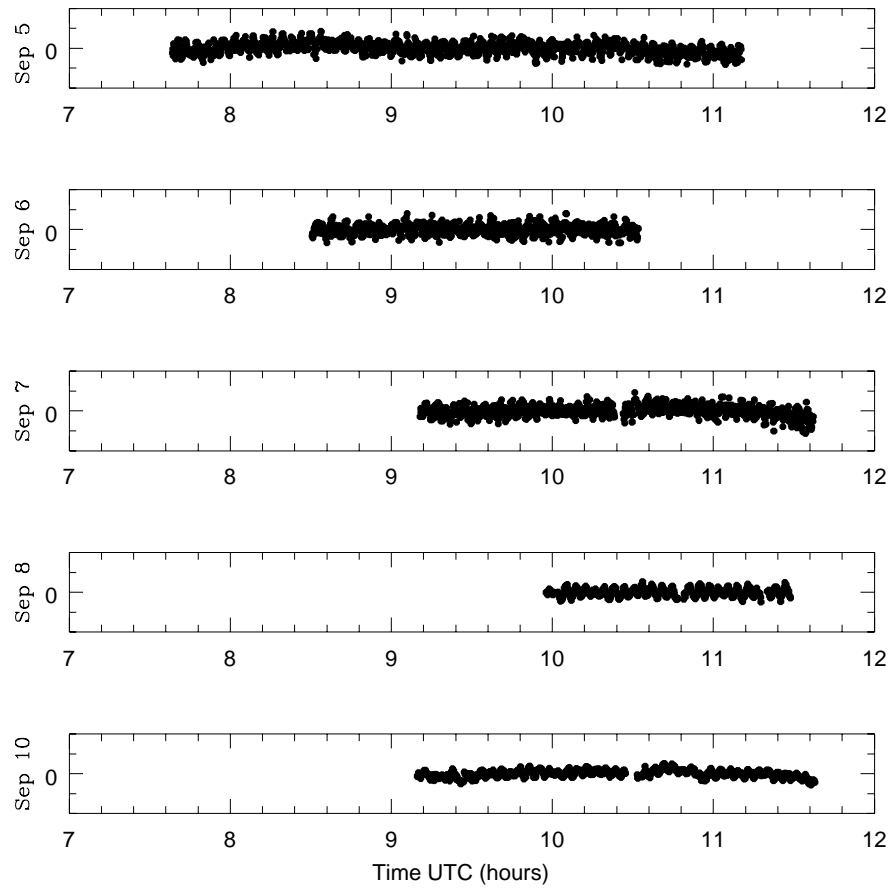
Figure 2.1.—: Light Curve of the reduced data on R548 from September 5 - 10, 1999

17
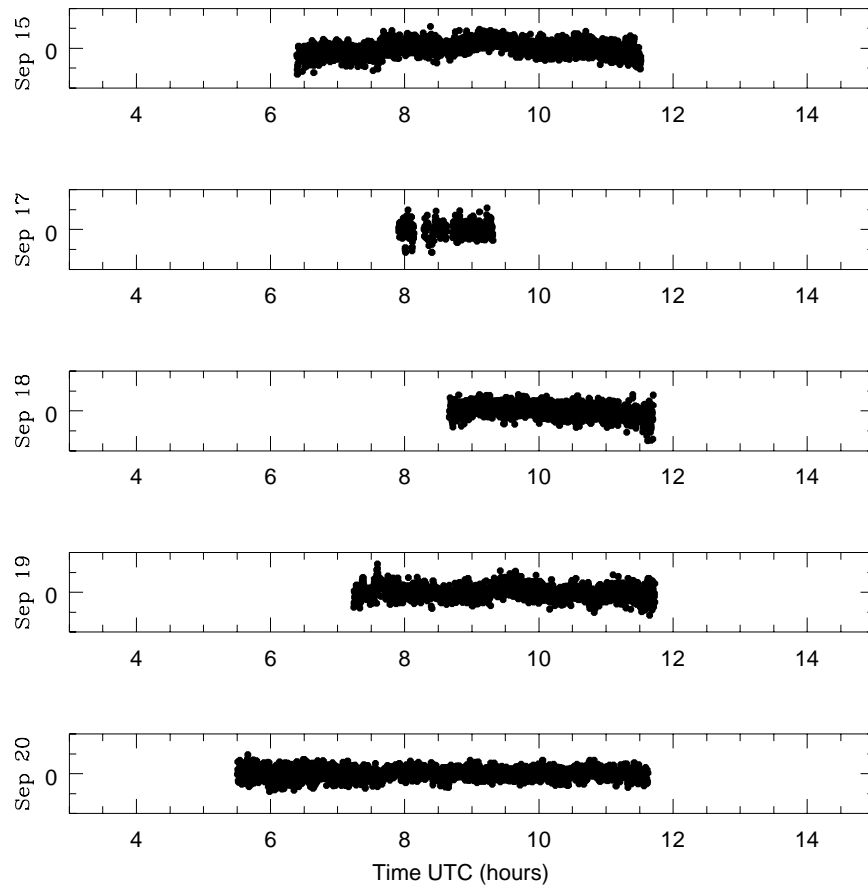
Figure 2.2.—: Light Curve of the reduced data on R548 from September 15 - 20, 1999
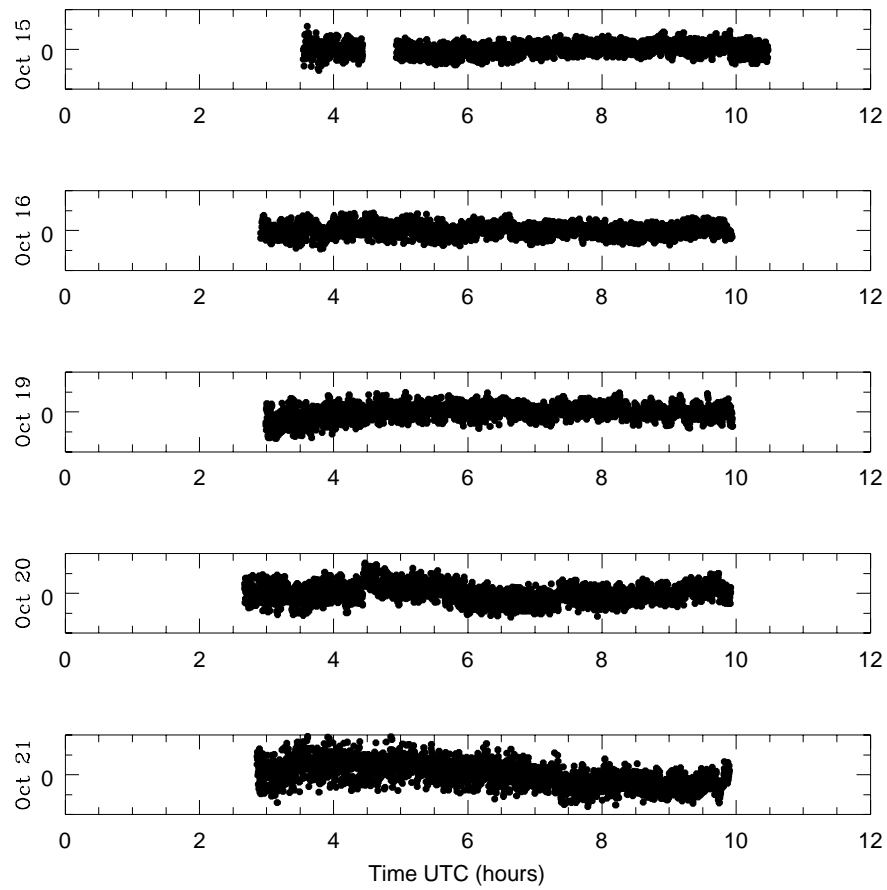
Figure 2.3.—: Light Curve of the reduced data on R548 from October 15 - 21, 1999
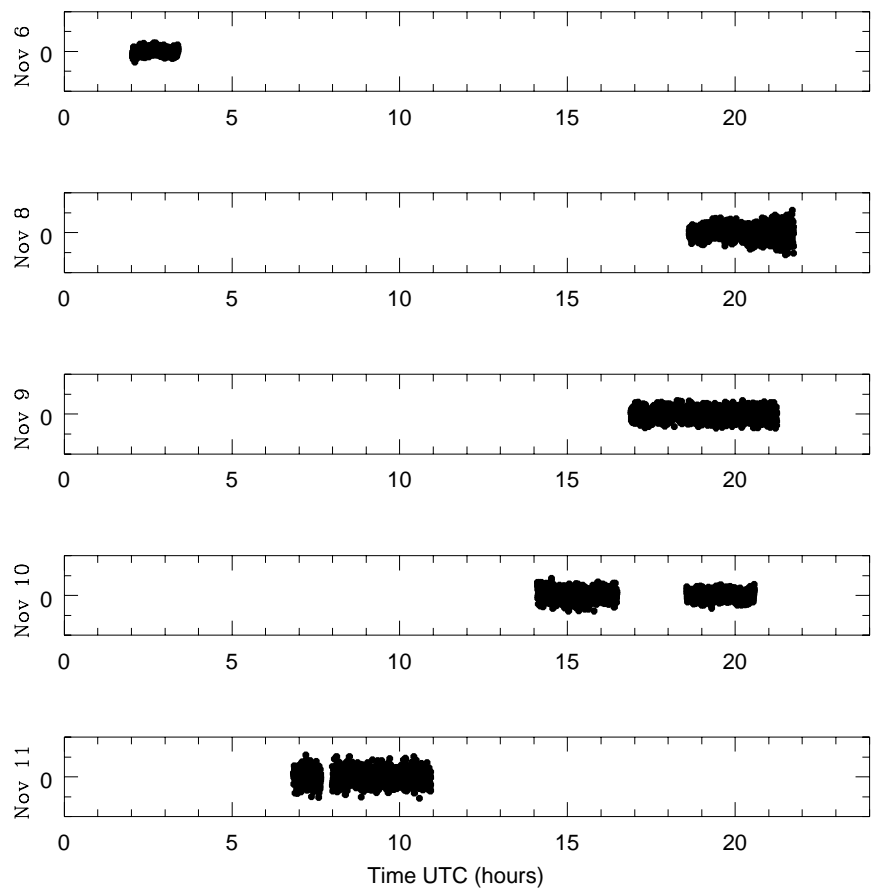
Figure 2.4.—: Light Curve of the reduced data on R548 from the WET run (November 6 - 11, 1999)
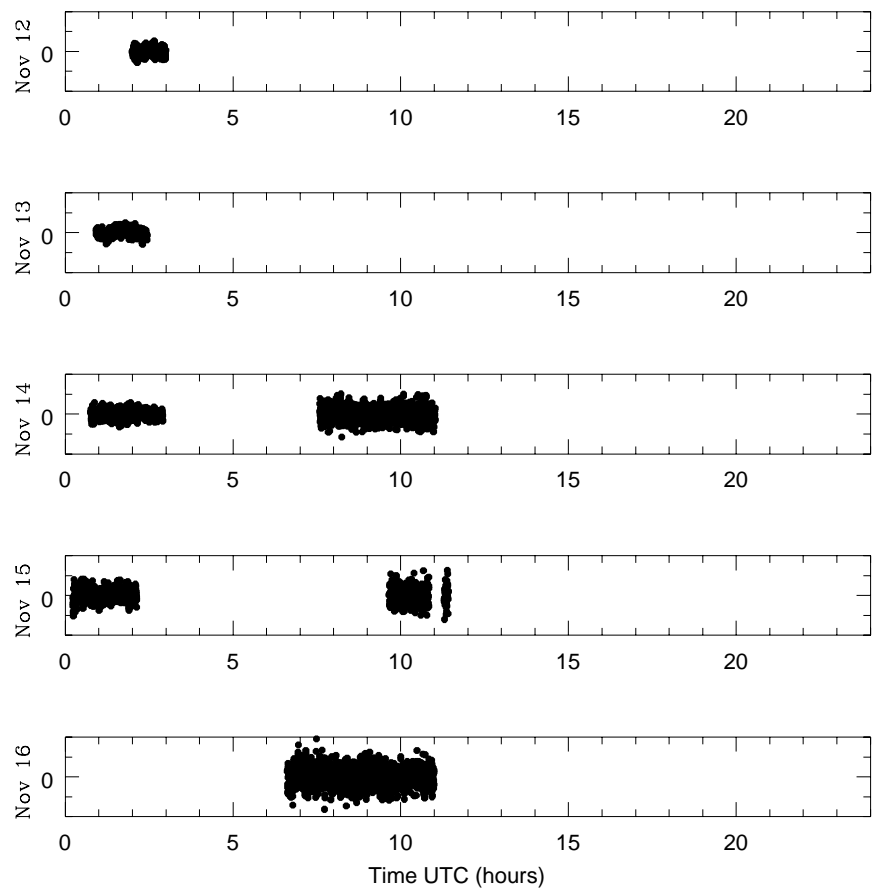
Figure 2.5.—: Light Curve of the reduced data on R548 from the WET run (November 12 - 16, 1999)

21
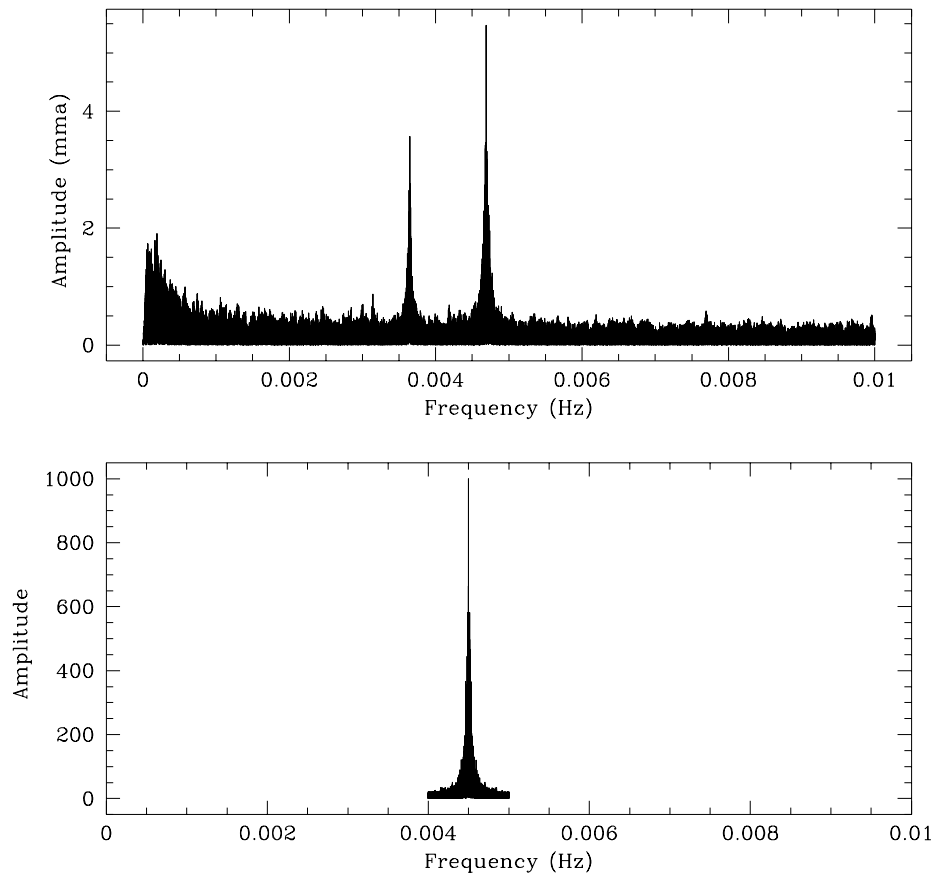
Figure 2.6.—: Fourier Transform of 1999 data on R548 with the Window Pattern

larger amplitude period in each doublet. The least squares program "LLSPHB", originally written by S. O. Kepler and modified by Scot Kleinman, gives phase and amplitude information for the two periods. Note that this program fits one period at a time. We use these values as input for a non-linear least squares program "NLSQHB", taken from Press et al, Section 14.4 and modified by Scot Kleinman. This program optimizes the period, amplitude and phase to fit the data better. Then we go back to LLSPHB and use these two better known values for the periods along with approximately known values for the two remaining periods. So, we get amplitude and phase information for all four periods, and feed it again to NLSQHB. Finally we obtain period, amplitude and phase information after fitting all four frequencies simultaneously for each data set.

2.4   Noise and Uncertainties

The uncertainties obtained from NLSQHB may be underestimated due to pattern noise. When the program tries to fit one frequency, the other frequency in the closely spaced doublet, represents a strong source of non-Gaussian noise. We call this pattern noise. Another source of non-Gaussian noise is low frequency noise. Photons arriving from R548 pass through the atmosphere and then the detection system. Systematic effects like atmospheric extinction, variations in the night transparency, cirrus, etc. introduce low frequency noise in the data. During data reduction, most of this is eliminated. However, some remnant low frequency noise can still affect the least squares fit. This indicates the importance of the polynomial correction. Due to these sources of non-random noise (chiefly pattern noise), the calculated uncertainties are under-estimated, since our calculation assumes a Gaussian distribution.

It is also interesting to see how pure noise affects the uncertainties in period, phase and amplitude respectively. An FT of white noise will show peaks at all frequencies. For the purposes of calculating some representative numbers, let us

assume that the noise amplitude is about 1 part in a thousand, i.e., 1 mma. (This is a reasonable assumption as the FT of the 1999 data sets in fig. 2.6 indicates an average noise level of 0.5 mma). Such a FT would also show higher amplitudes at lower frequencies from systematic effects introduced by the atmosphere and the detection system. This also depends on the expertise of the person who reduces the data.

Period determination is affected by the local noise band alone. The span of this local band can be determined by looking at the extent of the window, about 200 μHz for our typical FTs. Phase is also affected in the same way as period. So, we conclude that period and phase are affected by a very small portion (about 200 μHz) of pure noise spectrum (0 - 10000 μHz). To give a more quantitative picture, we quote (from non-linear least squares fits on the data sets) percentage uncertainties in period to be typically 0.001 - 0.0001%. We find typical uncertainties in phase to be 2-3 s for the 213 s doublet and 3-6 s for the 274 s doublet. The uncertainties in phase seem to be inversely related to their amplitudes. The percentage uncertainties for phase seem to be 1-2%.

To see how noise affects amplitude, we consider a light curve of the data. The noise directly adds or subtracts from the counts, and we could say that the noise amplitude is effectively adding and subtracting from the pulsation amplitude. This would incorrectly imply that the error should be as large as ± 1 mma. But we must remember that the fit is over the entire data set and this makes the measurement more reliable, thus reducing the uncertainties. Typical percentage uncertainties in amplitude seem to be about 3-5 %. Low amplitude pulsations of 2-3 mma result in larger typical uncertainties like 7-10 %. So, the amplitude determination is more strongly affected by noise than period or phase. Please bear in mind that all the numbers quoted above assume that the data set is long enough to resolve the pulsation spectrum and keep the noise level down to 1 mma. Noise in the FT will have

a higher amplitude for short data sets.

We have seen how to acquire and reduce the data. In the subsequent chapter, we will analyze the data to extract a $\dot{P}$ measurement.

Chapter 3

Data Analysis and a Summary

of the Results

There are certain necessary conditions that must be satisfied before a $\dot{P}$ measurement can be meaningful. We assume that the 4 main pulsation frequencies are resolved in the star and their amplitudes are stable. There is another critical assumption that we make. In Ed Nather's words, "We assume that the star does the same thing when we are not looking as when we are looking."

We now have various reduced data sets from 1970 to 2000. The first step is to check whether all the four frequencies are resolved in these data sets. This is important for R548, since it has two doublets with a spacing of about 0.5 s (or 7 and 8 μHz respectively, as is evident from table 2.2). If the doublets are not resolved, then the phase information will be misleading. We pre-whiten the data with 213.132 s and 274.25 s and check if the phases for 213.768 s and 274.77 s remain the same before and after pre-whitening. If they do, then those data sets can be used in the determination of $\dot{P}$ since we will have meaningful phases. After we carried out this step, data sets from the following years survived, 1970, 1975, 1980, 1986, 1991, 1993, 1999 and 2000. For each of these, we have a value of period, phase and amplitude

for all the 4 pulsations. Now, we can consider using the O-C technique to improve the period estimates and to find the value of $\dot{P}$ for all four pulsations.

3.0.1   O-C Technique

The O-C technique (e.g. Kepler et al. 1991) can be used to improve the period estimate for any periodic phenomena. The O stands for observed value of the time of maximum (or time of zero) that occurs in a data set. The C stands for its calculated value. If O-C is not zero, then we need to improve our estimate of the period or the period is not constant.

Consider a periodic phenomena with period P. The time of occurrence of the maximum, is a function of the cycle count E.

$$t_{max} = t_{max}(E) \tag{3.1}$$

Expanding in a Taylor series about $E = E_0$, we have

$$t_{max} = t_{max}|_{E_0} + \frac{dt_{max}}{dE}|_{E_0}(E - E_0) + \frac{1}{2}\frac{d^2 t_{max}}{dE^2}|_{E_0}(E - E_0)^2 + \cdots \tag{3.2}$$

This is a reasonable approach as this is normally a rapidly convergent series. For a time-span of a few years, the second order term can be neglected for a DAV like R548, as the cooling time-scale is a few billion years, assuming the pulsation is dominated by the cooling time-scale and not by a local effect in the star. It gains significance only in greater time-spans like a decade. Assuming the pulsation is strictly periodic with period P, we can identify

$$\frac{dt_{max}}{dE} = P \tag{3.3}$$

$$\frac{d^2 t_{max}}{dE^2} = \frac{dP}{dE} \tag{3.4}$$

$$\frac{d^2 t_{max}}{dE^2} = \frac{dt}{dE}\frac{dP}{dt} \tag{3.5}$$

27

$$\frac{d^2 t_{max}}{dE^2} = P\dot{P} \tag{3.6}$$

Neglecting the higher order terms (implying that $\dot{P}$ is constant),

$$t_{max} = t_{max}|_{E_0} + P|_{E_0}(E - E_0) + \frac{1}{2}P|_{E_0}\dot{P}(E - E_0)^2 \tag{3.7}$$

Now, we define O as t_{max}^{obs} and obtain its value by fitting the relevant number of frequencies to a data set with our guess periods.

$$C \equiv t_{max}^{cal} = t_{max}^{bv}|_{E_0} + P^{bv}|_{E_0}(E - E_0) \tag{3.8}$$

where the superscript "bv" stands for the best value.

$$O - C = \Delta E_0 + \Delta P E + \frac{1}{2}P\dot{P}E^2 \tag{3.9}$$

where

$$\Delta E_0 = t_{max}|_{E_0} - t_{max}^{bv}|_{E_0} \tag{3.10}$$

$$\Delta P = P|_{E_0} - P^{bv}|_{E_0} \tag{3.11}$$

ΔP is the correction in period. Using this basic theoretical recipe, we should be able to determine a point on the O-C *vs.* E diagram corresponding to each data set. We could then use a linear least squares fit and obtain the parameters ΔP and $\dot{P}$.

3.0.2 Bootstrapping with the O-C technique

The above O-C technique assumes the knowledge of a period to such a high accuracy that you are able to calculate the phase for the next data set with an error less than 10% of the pulsation cycle, i.e., a cycle count with certainty. Bootstrapping (Winget et al. 1985) is the technique to achieve this amazing feat. Our data sets have an average gap of 5-6 years. We use the period from one data set and calculate the phase for the subsequent data set. We force the calculated and observed values of phase to match by tweaking the period. So, we neglect the $\dot{P}$ term, since we are

dealing with a time-span of a few years. We also bootstrap from the second data set to the first one. An average of the two rectified periods is now our best value and their difference divided by a factor of 2 is the error in that value. It is more accurate and the error is comparable to a data set spanning the entire duration right from the first season of observations to the second one, a time-span of 5-6 years. Ordinarily, one would bootstrap a night of observations to the next and thus build up a complete data set for a season. Then continue the process as we described above to bootstrap between data sets. However, the doublets in R548 are closely spaced and it takes about 35 hours of data in principle to resolve them. In practice,it takes almost a week of observations to resolve the doublets as the data has gaps and noise. Therefore, we could only bootstrap from one season to another. Using this new period, we can bootstrap to the next data set. In order to determine phases for the next data set, we used a linear least squares fit on all four frequencies simultaneously. This program, called "LLSP4S", was originally written by S.O. Kepler and modified by Scot Kleinman. Bootstrapping to the data sets further on, gives you a refinement in the period estimates and reduces the uncertainties involved with each consecutive data set.

3.0.3 Cycle Count Errors

Bootstrapping assumes that we know the period well enough to predict the phase for the next data set without an ambiguity of a cycle count. This may not always be the case. When faced with this difficulty, we compute corrections to period for cycle count E as well as $E \pm 1$. Since we had reason to believe that the uncertainties in phase quoted by the least squares program maybe underestimated, we checked for cycle errors up to $E \pm 2$. Then, we plot an O-C diagram with each of these periods and the one that yields the lowest phase dispersion is the most probable solution. An equivalent mathematical statement would be to say that of these five possibilities,

the one that yields the smallest correction in period is the most probable solution. We checked all the possibilities using both these tests for each gap between the data sets. They always indicated the same answer and were consistent with each other. This is also the appropriate juncture to point out that we assume the lowest phase dispersion or the smallest correction in period is the best solution because we already have an idea in our minds of what the $\dot{P}$ should look like. (As mentioned earlier, cooling of the DAV is one of the slowest changes). To do a more objective and assumption-free search in a larger parameter space of P and $\dot{P}$ in order to verify the uniqueness of this solution, is a computationally intensive task, and we hope to do it eventually. All the bootstrapping values and the O-C diagrams for both periods of the 213 s doublet have been shown in the Appendix.

Here, we present our results for the best Period and $\dot{P}$ values obtained for the 213 s doublet in tables 3.1 - 3.2. We also indicate our final O-C values, which have been plotted in figure 3.1. The zero Epoch corresponds to a reference Tzero of 2446679.833986 TCB. We obtain $\dot{P} = (2.3 \pm 4.2) \times 10^{-15}$ s/s for the period $P = 213.13260565 \pm 5.3 \times 10^{-7}$ s. We also found $\dot{P} = (-4.5 \pm 7.9) \times 10^{-15}$ s/s for the period $P = 212.76842930 \pm 1.0 \times 10^{-6}$ s.

O-C (s)	Error in O-C (s)	Epoch	Season
3.9	3.7	-2346428	1970
2.2	1.7	-1617531	1975
1.9	2.5	-862740	1980
0.0	2.8	0	1986
7.4	1.1	743874	1991
3.1	2.0	1049404	1993
6.4	1.5	1924342	Sep-Oct 1999
3.7	1.7	1949381	Nov 1999
2.5	2.3	2067847	2000

Table 3.1: O-C table for Period 213.13260565 s and $\dot{P} = (2.3 \pm 4.2) \times 10^{-15}$ s/s

The uncertainties would be more reliable if there were a larger number of
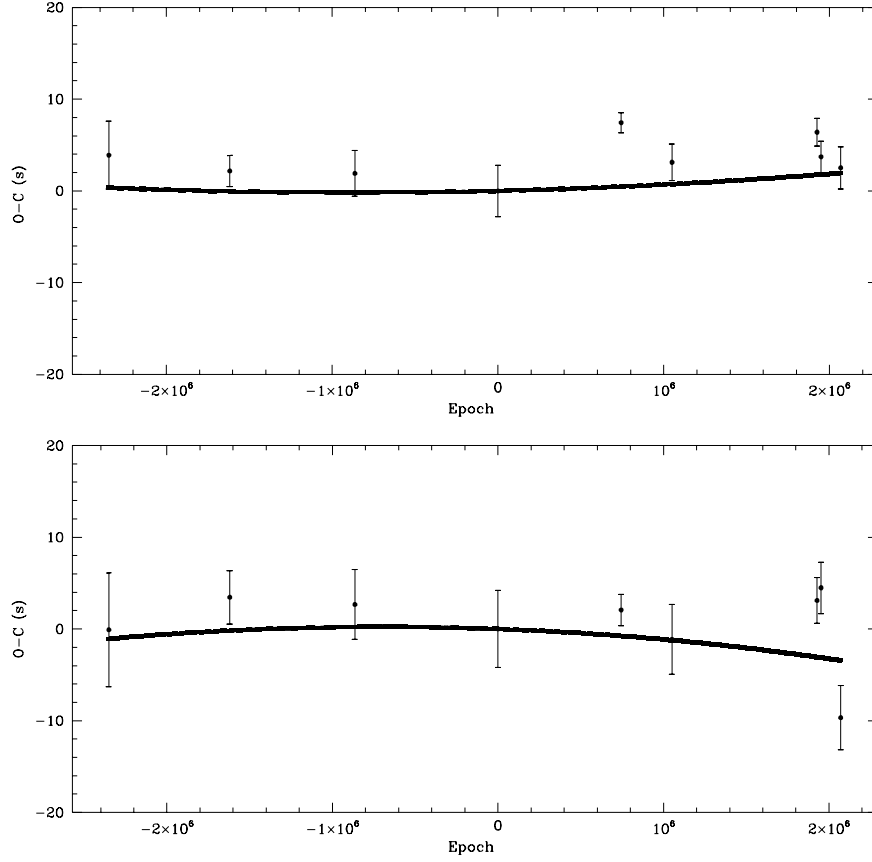
Figure 3.1.—: The 1991 data set spans over 5 days, while the other data sets are a month long on average. Hence, it is not alarming to see that the 1991 data point does not lie on the best fit within errors. Also, note that the errors are under-estimated as has clearly been demonstrated in the Monte-Carlo section.

points on the O-C diagram. Let us compare the results that we have obtained with previous values of $\dot{P}$ for the 4 pulsations. Tomaney (1987) published his best value, which was $\dot{P} < 9.6 \times 10^{-15}$ s/s at the 68% confidence level. He concluded that $\mid \dot{P} \mid \leq 300 \times 10^{-15}$ s/s for all the four modes at the 1σ level. Kepler et al. (1995) constrained it further and showed that $\mid \dot{P} \mid \leq 200 \times 10^{-15}$ s/s at the 1σ level for both the doublets. So, our results for the 213 s doublet are a further refinement due to the larger time-base, and they are consistent with previous results.

The 274 s doublet seems to be changing on a time-scale, that is 100 times faster than the 213 s doublet. Thus, the same gaps between data sets become too large to nail down the cycle counts. Also, there maybe short-term variations of the order of a few months to a few years, swamping out the parabolic effect of the cooling. We find that the O-C diagrams for both modes in the 274 s doublet do not fit a parabola and are not indicative of cooling. The O-C diagrams for the 274 s doublet have not been plotted, but the appendix does give our best O-C tables C.1 and C.2 for both periods in the doublet. The tables may have cycle count errors.

3.1 Second Verification using a Non-Linear Least Squares Fit

This technique consists of a non-linear least squares fit on all the data from 1970 to 2000 for a single period. We used the NLSPDOT program (Costa, Kepler & Winget 1999), written by S. O. Kepler. The inputs to the program are period, phase and amplitude and a guess value for $\dot{P}$. Of these, it optimizes only the period, phase and $\dot{P}$ to minimize the residuals. The amplitude is fixed. This method differs from the O-C technique in the following way. The O-C technique uses the entire data set to get the best value for the first time of maximum. While, the non-linear least squares technique utilizes all the data and therefore all the times of maxima, occurring in

32

a data set. This increases the reliability of the $\dot{P}$ value. Another advantage is that we can now include all the data, irrespective of whether the doublets are resolved or not in individual sets.

Note that this technique also suffers from cycle count errors in gaps between data sets, just like the O-C method. We input a guess value for $\dot{P}$ and by doing that, we are effectively feeding in cycle counts for the various epochs. The same bootstrapping process is implicitly applied here. So, the program will converge to the closest peak, whether it is real or not. Again, to search more objectively in a larger P, $\dot{P}$ grid would be computationally intensive.

The results for the O-C technique are consistent with the non-linear least squares fit within the uncertainties and are presented in table 3.3. The uncertainties quoted below may be underestimated due to pattern noise.

3.2   Other Techniques to determine $\dot{P}$

Determining a number of the order of 10^{-15} s/s from 3 decades of data, worrying about timing errors in each of those data sets, always dealing with numbers that possess 7 to 8 significant digits, etc. has certainly not been an easy task. If we can measure this number in other ways, then that is an opportunity to be sought by all means. Different techniques have different advantages and different sources of uncertainties. So, we hereby discuss some other techniques to determine $\dot{P}$.

1. **Direct Method :**   Ideally, we should be able to estimate the periods from each data set and plot Period *vs.* Time to find the slope $\dot{P}$. This brute force direct approach has a difficulty. Periods determined from individual data sets have large uncertainties and this manifests itself as a large uncertainty in the optimal best fit slope. However, we can still find the largest slope possible and use it to constrain $\dot{P}$. It turns out that this is a much weaker constraint than

the O-C method. This is easy to understand since $\dot{P}$ enters as a second order effect in the O-C diagram, while it is a first order term as far as the direct method is concerned. Therefore it is possible to place a tighter constraint on $\dot{P}$ using the O-C technique. One of the advantages of the direct method over the O-C technique is that it does not suffer from cycle count errors in gaps between data sets.

In figures 3.2 and 3.3, we have plotted the best determined periods *vs.* an average time for each data set for the 213 s and the 274 s doublets respectively. The time in seconds is with respect to the same reference tzero as in the O-C diagram. The following tables 3.4 to 3.7 give the best periods from individual sets along with the uncertainties. The table 3.8 gives the results from a weighted linear least squares fit, where the weights are inversely proportional to the uncertainty in period.

Another avenue that we explored was trying to pre-whiten 3 frequencies from the data sets. The remnant frequency would then have much smaller uncertainties for period and phase (Costa, Kepler & Winget 1999). That should have solved our problem, leading to a better constraint on $\dot{P}$. However, such pre-whitening procedures for R548 can prove dangerous. Pre-whitening the other doublet is a harmless matter. But, when we pre-whiten one frequency in a doublet, we effectively modify the other one, since the pre-whitening frequency is not exactly the same as the true frequency and the doublet is closely spaced. This results in unreliable phases and the answer cannot be trusted. So, this pre-whitening technique can only be applied to pulsation periods that are far away from the period of interest.

2.   **Maximum Likelihood Estimation :**   There are possible cycle count errors in the O-C tables C.1 and C.2, indicated for the 274 s doublet. If we could reverse the clock and gather more data, as Ed Robinson had once suggested

O-C (s)	Error in O-C (s)	Epoch	Season
-0.1	6.2	-2350444	1970
3.5	2.9	-1620300	1975
2.7	3.8	-864217	1980
0.0	4.2	0	1986
2.1	1.7	745148	1991
-1.1	3.8	1051200	1993
3.1	2.5	1927636	Sep-Oct 1999
4.5	2.8	1952718	Nov 1999
-9.7	3.5	2071386	2000

Table 3.2: O-C table for Period 212.76842930 s and $\dot{P} = (-4.5 \pm 7.9) \times 10^{-15}$ s/s

Period (s)	$\dot{P}$ 10^{-15} s/s	$\sigma_{\dot{P}}$ 10^{-15} s/s
213.132607	4.6	2.1
212.768429	3.5	3.6

Table 3.3: Results for Period and $\dot{P}$ from a Non-linear Least Squares Fit

Period (s)	σ_P (10^{-4}s)	Season
213.132576	4.1	1970
213.132423	0.9	1975
213.132547	1.3	1980
213.132823	3.9	1986
213.131804	7.0	1991
213.131256	4.2	1993
213.132725	1.0	Sep-Oct 1999
213.131411	9.0	Nov 1999
213.133629	1.7	2000

Table 3.4: Best fits for Period 213.132 s from individual sets

35

Period (s)	σ_P (10^{-4}s)	Season
212.768371	6.6	1970
212.768267	1.5	1975
212.768313	2.0	1980
212.768170	5.9	1986
212.778197	11.0	1991
212.769150	8.4	1993
212.768484	1.5	Sep-Oct 1999
212.766154	13.0	Nov 1999
212.770448	2.5	2000

Table 3.5: Best fits for Period 212.768 s from individual sets

Period (s)	σ_P (10^{-4}s)	Season
274.250359	9.1	1970
274.250501	2.1	1975
274.251657	4.0	1980
274.250586	6.9	1986
274.281072	22.0	1991
274.250889	11.0	1993
274.250844	2.6	Sep-Oct 1999
274.247696	25.0	Nov 1999
274.251187	4.1	2000

Table 3.6: Best fits for Period 274.25 s from individual sets

Period (s)	σ_P (10^{-4}s)	Season
274.775408	12.0	1970
274.774109	3.2	1975
274.774513	6.0	1980
274.774011	8.5	1986
274.804359	28.0	1991
274.774715	17.0	1993
274.774015	3.7	Sep-Oct 1999
274.771008	31.0	Nov 1999
274.772920	5.4	2000

Table 3.7: Best fits for Period 274.77 s from individual sets

| Period (s)	σ_P (s)	$\dot{P}$ 10^{-17} s/s	$\sigma_{\dot{P}}$ 10^{-17} s/s
213.132807	0.00008	1.6	0.2
212.769141	0.00014	2.8	0.4
274.251316	0.0002	18	0.5
274.774379	0.00024	-2.7	0.7

Table 3.8: Results from Direct Method using a Weighted linear least squares fit
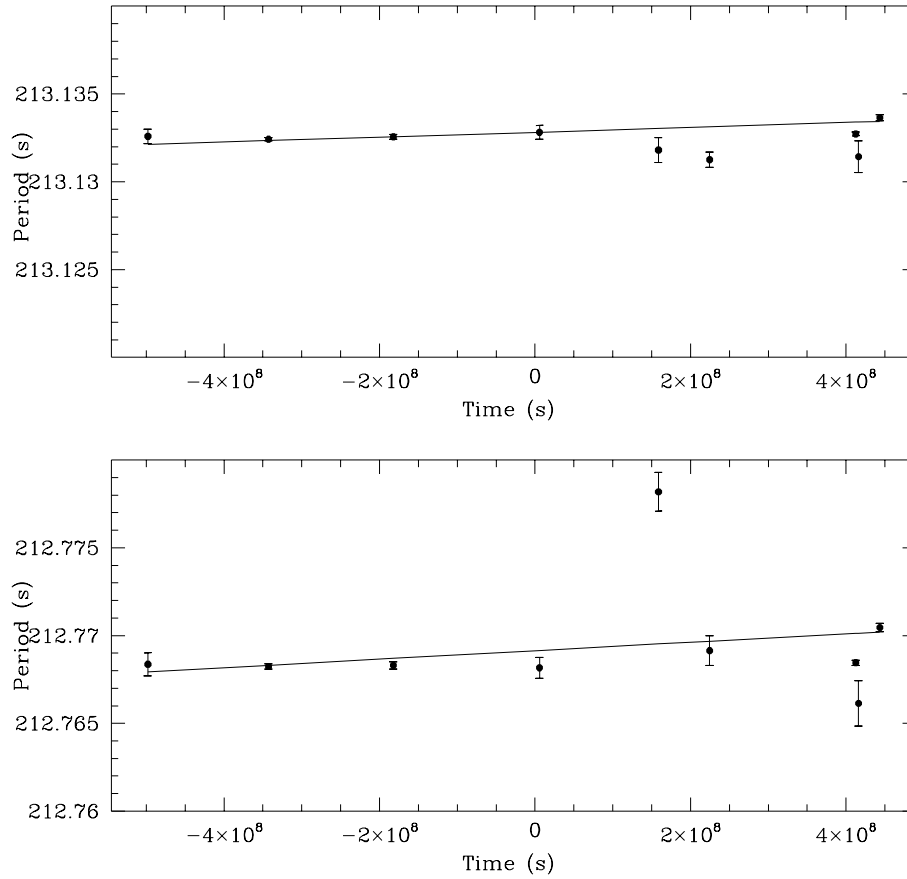
Figure 3.2.—: The 1991 data set spans over 5 days, while the other data sets are a month long on average. Hence, it is not alarming to see that the 1991 data point does not lie on the best fit within errors. Also, note that the errors are under-estimated as has clearly been demonstrated in the Monte-Carlo section.

37
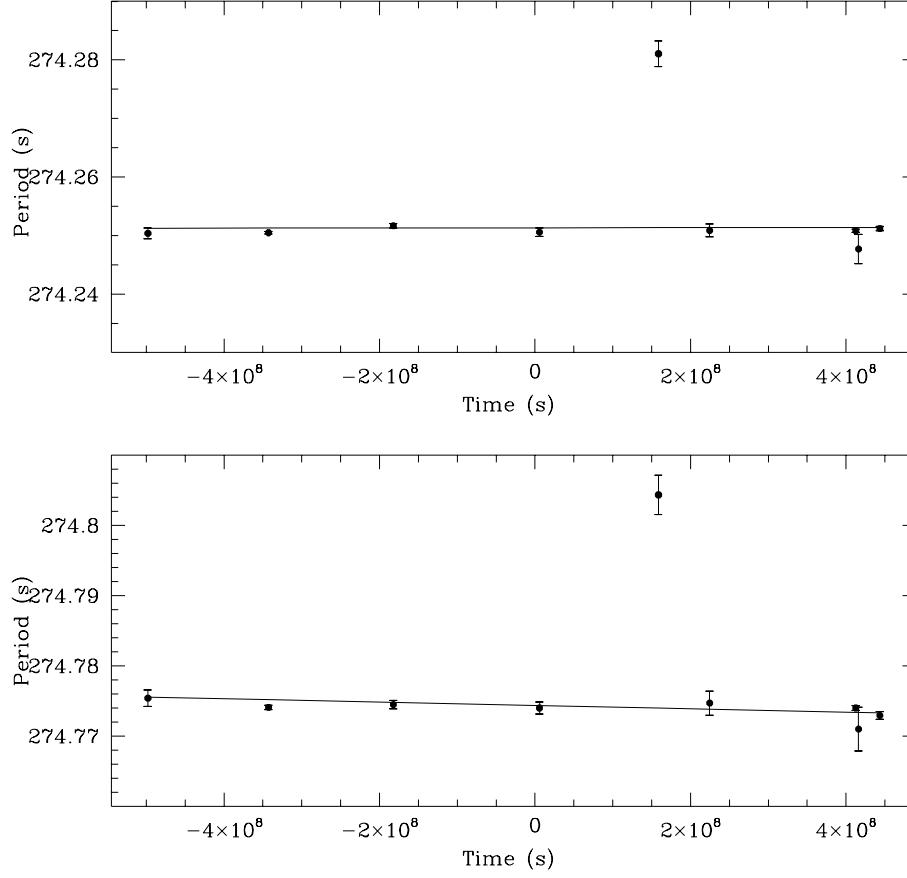
Figure 3.3.—: The 1991 data set spans over 5 days, while the other data sets are a month long on average. Hence, it is not alarming to see that the 1991 data point does not lie on the best fit within errors. Also, note that the errors are under-estimated as has clearly been demonstrated in the Monte-Carlo section.

to me, we could perhaps unambiguously declare both the sign and magnitude of the $\dot{P}$. Since this is not feasible, we could turn to statistics for the best answer, but not necessarily the correct one, since we would be dealing with low number statistics, 9 points to be exact. There do exist multiple techniques to achieve this goal, the most elegant of which is called the Maximum Likelihood Estimation (MLE).

MLE is a computationally cumbersome technique, which involves determining the χ^2 for each possible P and $\dot{P}$ solution, given the observed phases from the various data sets. Initially, we would define a range of P and $\dot{P}$ values. The resolution of these grids would be of the order of the uncertainties in P and $\dot{P}$ respectively. For each possible (P,$\dot{P}$) pair, we would initially determine the epochs, given the observed set of phases. Using the $\dot{P}$, we would then determine the correction in period. Using all these values, we could then see how well the observed phases fit and obtain a χ^2 value. The global minimum for χ^2 would be indicative of the best answer for period and $\dot{P}$. If however, the $\ddot{P}$ term is significant, as suggested in the next chapter, then this technique would have to be suitably modified to include a second order term. That would take even more computation time.

3.3 Best Value for an evolutionary $\dot{P}$

We conclude that the periods of the 213 s doublet are exceptionally stable. We found that the 274 s doublet does not indicate cooling and so we will only focus on the 213 s doublet. We measured $\dot{P}$ for both periods of the 213 s doublet using the O-C technique, non-linear least squares fit and the direct method. Of these, results from the non-linear least squares fit are most reliable as it utilizes all the data to get a best fit. While, the O-C and the direct method base their answers on 9 points and are in the domain of low number statistics. We obtained (4.6 $\pm$

2.1) $\times 10^{-15}$ s/s and $(3.5 \pm 3.6) \times 10^{-15}$ s/s for the periods 213.13260565 s and 212.76842930 s respectively. Since these $\dot{P}$ values are only upper limits and not yet true measurements, the uncertainties gain more importance than the numbers themselves as they are indicators of reliability. So, our best value for an evolutionary $\dot{P}$ for R548 is $(4.6 \pm 2.1) \times 10^{-15}$ s/s. Henceforth, we will be using this value for all our subsequent calculations.

3.4   Other Possibilities regarding the 274 s Doublet

We conducted the following tests to eliminate some other possibilities, that maybe causing the O-C diagram for the 274 s doublet to look different. Implications of what could be going on with the 274 s doublet are discussed at length in the next chapter.

1. **Variations in $\dot{P}$ at time-scales of a few days to a month :** We wanted to check whether there were any variations in $\dot{P}$ at shorter time-scales like a few days to a month, which averaged out over a longer time-span, but could be enough to swamp out the parabolic shape of the O-C diagram for the 274 s doublet. We chose to investigate the 1999 data set, since it has the greatest density of data and spreads over September, October and November. If the pulsation period of the star varies at time-scales of a few days to a month, then that would render itself as broader (broader compared to the corresponding peaks in the window) peaks in the FT. We simulated a doublet with constant periods and compared the FWHMs for the true peaks in the FT to the FWHMs from the real data set. We could not find any conclusive evidence that the FWHMs in the real data set were wider and had to abandon the idea that any such short term variations might have taken place.

2. **Interaction between the 213 s doublet and the 274 s doublet at time-scales of a few decades :** We checked whether the two doublets are truly resolved in the chosen data sets. We pre-whitened the data sets, thus eliminating the 213 s doublet as best as we could. (Some residual power will always remain since the amplitudes are never accurately determined due to gaps in the data and low signal to noise ratio. We found that the amplitudes from the single site 3.6m CFHT data taken in 1991 were higher by about 1 mma compared to single site data on the 0.9m at McDonald Observatory). Next, we obtained the phase information, using our best guesses for the 274 s period values, taken from the O-C diagram. We found that the phases did not differ significantly. This shows that if there exists an interaction between the two doublets, then it would have to be on time-scales longer than three decades.

3.5   Monte-Carlo Simulation Technique for Improved Errors

The value of $\dot{P}$ obtained for the 213 s doublet is only an upper limit and hence the uncertainties become more important than the value itself. Costa, Kepler & Winget (1999) demonstrated that the uncertainties obtained for phases from a linear least squares fit are under-estimated. Costa (1996) used a method based on Monte-Carlo simulations to derive more realistic values of σ_{P_i}. We did this computationally cumbersome calculation for R548, since the doublets are closely spaced and we could be severely under-estimating the uncertainties due to pattern noise. Such a calculation will give us a better idea of the reliability of the phases for each individual data set and thus of the $\dot{P}$ obtained.

3.5.1   The Technique :

The basic idea is to choose random values within the known uncertainties to generate a pulsation spectrum similar to that of R548. Next, process the simulated light curve in exactly the same manner as real data and then obtain a least squares fit. The difference between the initially chosen values and the values obtained in the fit will give us the true uncertainties. By repeating this process about 2000 to 2500 times, we can plot an error distribution for period, phase and amplitude. The details are given in the following paragraphs.

Initially, we select a frequency between $4689\mu Hz$ and $4695\mu Hz$. This represents the first mode. Then, we add $8\mu Hz$ to it and get the second pulsation mode. This results in a doublet at a period close to 213 s and with the same spacing as the corresponding one in R548. Next, we select amplitudes randomly within the ranges 5.4 - 6.6 mma and 3.4 - 4.6 mma for the 2 modes, such that the mode with the higher period gets the higher amplitude range. Next, we select another frequency between $3643\mu Hz$ and $3649\mu Hz$. By subtracting $7\mu Hz$ from it, we get the second mode. Thus we generate another doublet at 274 s, and select amplitudes in the ranges 3.4 - 4.6 mma and 2.4 to 3.6 mma, such that the mode with lower period gets the higher amplitude range. Phases for all 4 modes are chosen in a range of 210 s, beginning from the first point of the data set under consideration. So, we have randomly generated a pulsation spectrum similar to R548.

Next, we simulate a light curve using the periods, amplitudes and phases that we chose. However, we also need to sample the data in a realistic manner with gaps from daytime, clouds, etc. So, suppose we are considering the 1970 data set, then the program that simulates the light curve also reads in the real 1970 data. The program will then generate a point of data only when there exists a corresponding point in the real data set. This implies that the simulated data has the same duration, the same gaps and the same data density as the real set. We also

add Gaussian noise of amplitude 1 mma to it. Henceforth, we subject the simulated data to a procedure exactly identical to real data.

Initially, we take an FT and identify the frequencies. We use these approximate values as input to the LLSPHB and NLSQHB programs, thus obtaining best fits. However, it is neither practical nor feasible to actually take an FT 2500×9 times. So, what we feed in as input guesses to the least squares program are randomly chosen numbers in a range of $\pm 1 \mu Hz$ of the true frequency. Giving a guess value $\pm 1 \mu Hz$ away from the true frequency is conservative enough because the resolutions of the corresponding FTs of real data sets are as good as $0.1 \mu Hz$ to $0.01 \mu Hz$. One would naively think that if the resolution of the FT is $0.1 \mu Hz$, the true uncertainty in the frequency is only $\pm 0.1 \mu Hz$. But, the true peak need not be the highest one and hence the guess value needs to be given further away from the chosen frequency.

The difference between the best fits obtained and the numbers used to simulate the data give us the true uncertainties. Repeating this entire procedure about 2500 times or so gives us an error distribution, which will reveal how under-estimated uncertainties quoted by the NLSQHB program are. We can only emphasize the importance of deciding how far away the guess value should be from the true frequency. If we give a guess value that is too close to the right answer, we will be under-estimating the uncertainties. If the guess value is too far away from the true frequency, the least squares programs might have a severe convergence problem and we could also end up over-estimating the uncertainties. So, it is necessary to feed in a guess value that is realistic within the measured uncertainties.

We ran the entire simulation 2500 times for all the data sets. We came across a convergence problem for a few of the data sets. For these, about 700-1200 iterations would not converge. In table 3.9, we have listed the number of iterations that did not converge on the first guess, for each individual data set. We dealt with

43

this problem by trying out a second guess for the non-convergent iterations. The results from the second set of simulations are given in the third column. A fraction of 5-10% of non-convergent iterations are quite acceptable. We stopped trying different guesses when the number of non-convergent iterations dropped below 250.

Now that we have a suitable number of simulations for each data set, we can plot out histograms showing the error distribution in period, phase and amplitude for each data set. The Half Width at Half Maximum (HWHM) of these distributions is an error of 1σ. Since we have four periods, we will get 4 sets of uncertainties for period, phase and amplitude for each of the individual data sets. These are outlined in tables 3.10 to 3.13. Comparing the values in one table *vs.* another allows us to estimate the effect of the signal to noise ratio on the error distributions, since the 4 modes have different amplitudes. We have also listed the uncertainties given by the non-linear least squares program for the real data sets in those seasons.

3.5.2 Period Error Distributions

The period error distributions definitely managed to surprise us, as shown in fig. 3.4. We originally suspected our programs and felt that our choice of periods might be quantized, thus resulting in a quantized error distribution. We plotted out a distribution of the randomly chosen periods. We also plotted out a distribution of the periods from the best fits obtained. Both these histograms showed a random distribution; but a difference of the two would always result in a non-Gaussian quantized distribution. As we looked at the error distributions from different data sets, we realized that the spacings between the peaks is of the order of $\frac{1}{T}$. This implied that we were looking at aliases, from gaps of the order of a month. This high frequency structure is a manifestation only of the month-long gaps and it would not be present for good multi-site coverage or for short data sets. We do find that both our WET data sets from Sep-Oct 93 and November 1999 show a Gaussian
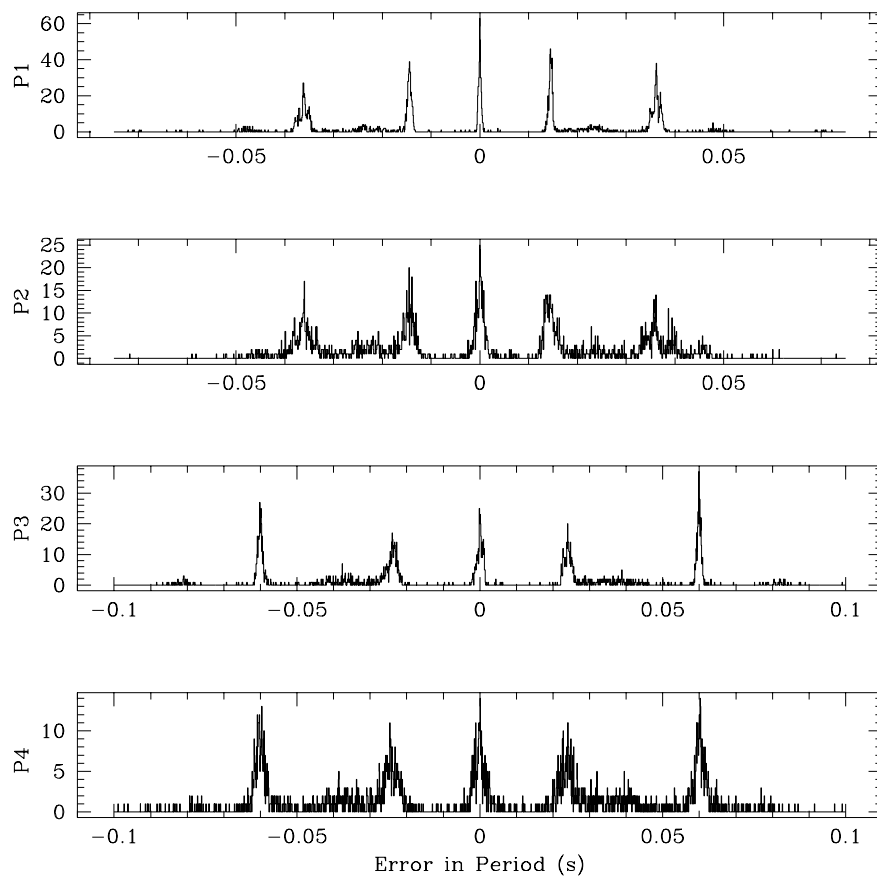
Figure 3.4.—: Error in Period is the difference between the value chosen to simulate the light curve and the best fit obtained

error distribution. The short data sets such as 1991 also show a Gaussian error distribution in period. That is evidently because they are only a week or 2 weeks long and therefore should have no aliases from month long gaps.

The quantized or non-Gaussian error distribution is the chief cause of all the convergence problems. Note that the 1991 and November 1999 data sets did not have a convergence problem and both of them show Gaussian error distributions. The 1975 data set did not have a convergence problem either, but the envelope of the quantized error distribution looks Gaussian.

The immediate problem we faced was uncertainty quantification since we did not have anything similar to a normal distribution. We then came up with the following idea. Consider a generalized distribution which need not be Gaussian or centered at zero, but it has to be somewhat symmetric. We start from a bin in the histogram, about which the distribution is symmetric. We then move outwards in both directions and stop only when we have accounted for 34% of the simulations on either side. In between the two final bins lie the errors from 68% of the simulations and we quote half of this number as a 1σ uncertainty. Since the distribution is not normal, $2 \times \sigma$ will not account for the errors from 95% of the simulations. We will have to repeat the same procedure and find an equivalent 2σ. When the distribution is not symmetric, we choose the central bin such that there is equal area on both sides. Please note that the central bin is chosen after looking at a print-out of the histogram. It is very subjective and prone to error. The 1σ uncertainties that we quote have to be taken with a grain of salt, specially for non-symmetric distributions.

Examining the tables 3.10 to 3.13, we find that the uncertainties in period are severely under-estimated by factors like 30 to 70 for quite a few data sets and in some pathological cases, a factor of 100 and more. For seasons that showed a Gaussian error distribution, the uncertainties are under-estimated by a factor of 2-4.

46

3.5.3   Amplitude Error Distributions

A striking feature of most amplitude error distributions is that they are not centered at zero. This implies that the least squares program always under-estimates the amplitudes. This is a systematic effect and it seems to be quite apparent for composite data sets like Sep-Oct 99 and Aug-Sep-Oct 2000, as shown in fig. 3.5.

As we are plotting $A_{\text{calc}} - A_{\text{input}}$, it should be centered on zero, but we notice a very definite pattern in all data sets that show an off-center distribution. We find that the offset is largest for the high amplitudes as compared to the low amplitudes. The offsets are listed in columns 8 in the tables to 3.10 to 3.13. This is counter-intuitive.

To explore this systematic effect, we eliminated the 1 mma noise that we add to the simulated light curve. Now, we are dealing with noiseless simulated light curves with realistic gaps. When we plotted out the error distribution for amplitude, we find that the systematic effect does not vanish. It is either a result of the gaps or of the least squares programs. However, since we are able to get well-centered Gaussian distributions for 1991, Sep-Oct 1993 and November 1999, we conclude that this systematic effect is a result of the gaps in the data. Furthermore, we plotted out an error distribution for the 4 periods, choosing only those simulations that resulted in significantly lower amplitudes. The resulting plot is shown in fig. 3.6. Evidently, these simulations have converged to an alias, which has a lower amplitude than the true frequency. This results in a peak in the error distribution that is centered at $(A_t - A_a)$, where A_t is the amplitude of the true frequency and A_a is the amplitude of the alias.

We conducted a few other tests. For fig. 3.5, the amplitudes for the 213.132 s, 212.768 s, 274.25 s and 274.77s are in the ranges of 6 ± 0.6, 4 ± 0.6, 4 ± 0.6 and 3 ± 0.6 respectively. We simulated light curves with larger amplitudes than before to study the amplitude correlation. We chose amplitudes for the 213.132 s, 212.768
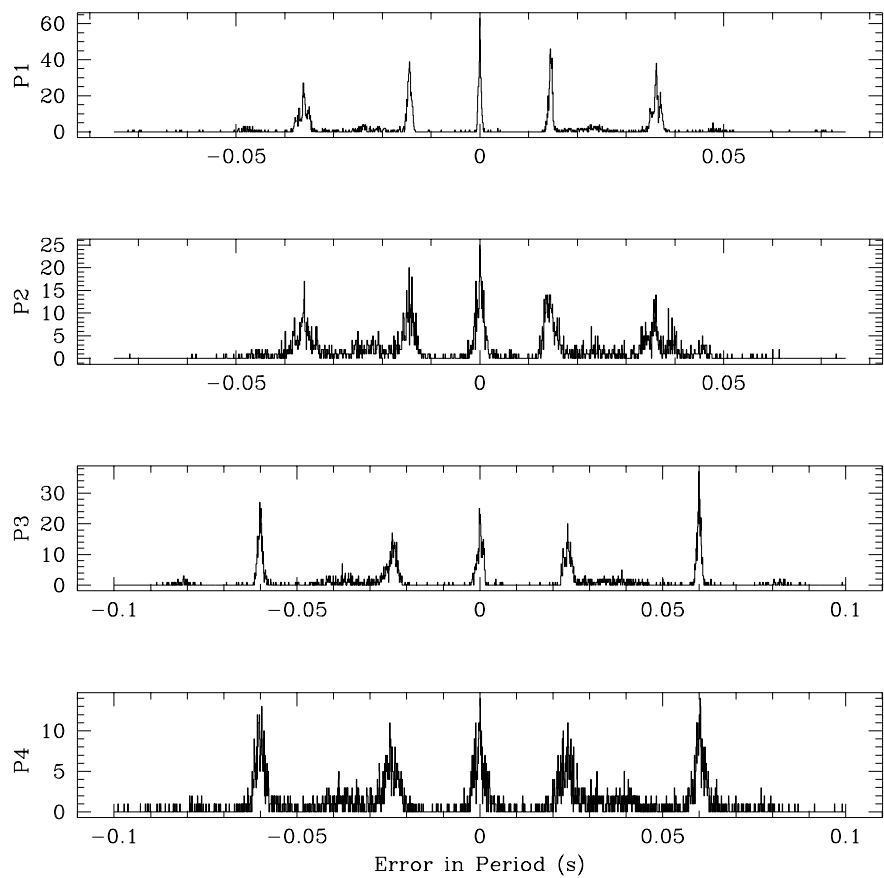
Figure 3.5.—: Error in Amplitude is the difference between the value chosen to simulate the light curve and the best fit obtained
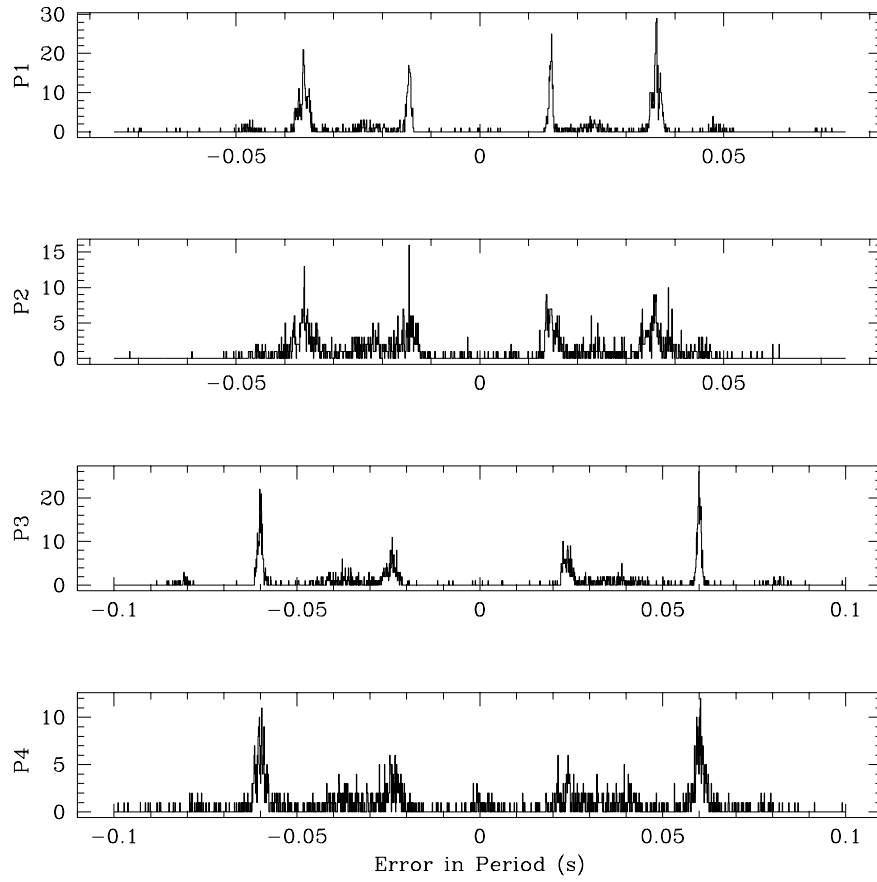
Figure 3.6.—: Period Error Distribution for Sep-Oct 99 from simulations resulting in severely under-estimated amplitudes

49

s, 274.25 s and 274.77s to be in the ranges 15 ± 0.6, 8 ± 0.6, 8 ± 0.6 and 6 ± 0.6 respectively. The resulting error distribution showed peaks that were further away from zero than before by a ratio $\frac{A_1}{A_2}$, where A_1 indicates the new amplitude and A_2 indicates the earlier choice of amplitude. This has been shown in fig. 3.7. This amplitude correlation can be easily explained. When we enhance the amplitude, we are effectively scaling the whole window function to that new value. In other words, we are altering the amplitude of the true frequency and the aliases as well. More specifically, we are scaling the difference $(A_t - A_a)$ by the ratio $\frac{A_1}{A_2}$. So, we should expect a peak in the error distribution that is further away from zero by the amount of scaling.

Next, we tried to see if this systematic effect persists when we run simulations for a single frequency near 213 s and at 274 s, instead of doublets. We found that the effect does remain as can be expected from our understanding of it. This clearly implies that gaps in the data are more destructive than the fact that we are dealing with a doublet. So, alias-noise is more harmful than pattern noise. This realization leads us to appreciating the significance of instruments like the WET, which are a must for studying periodic phenomena.

We found no traces of the systematic effect discussed above in the error distributions for the 1991, Sep-Oct 1993 and November 1999 data sets. Instead, they showed a random distribution centered at zero. This is due to white noise. Imagine noise at a frequency similar to the pulsation modes. It can have a phase that either adds to the pulsation amplitude or subtracts from it, thus resulting in a normal distribution. There is, however, a small bias of over-estimating the amplitude. This bias is proportional to the square of the random noise amplitude and hence this is a really tiny effect. We do not see it in any of our distributions.

The uncertainties in amplitude are under-estimated by a factor of 1.5 to 5 or so, and in some cases, even by a factor of 10.

Figure 3.7.—: Amplitude Error Distribution for Sep-Oct 99 from simulations with enhanced amplitudes

3.5.4 Phase Error Distributions

Most of the error distributions for phase show a near-Gaussian distribution, implying that we could proceed with the Maximum Likelihood Technique. However, for the 1975 and Sep-Oct 99 data sets (fig. 3.8), we find a quantized error distribution that shows multiple peaks instead of a single Gaussian peak. The size of the implied error shows that the least squares programs under-estimate the error in phase by a factor of 1.2 to 5 and in certain cases a factor of 30, depending on the sampling of the data.

The first question that needs to be answered is whether our O-C analysis still holds. It is not surprising to us that the phase uncertainties are under-estimated by a factor of 10 on average. When we did the O-C analysis, we were always conservative and considered the error to be 10 times larger than that shown by the least squares fit. So, this does not change or modify any of the results.

Also, these uncertainties come from a non-linear least squares fit, wherein the period, amplitude and phase for all 4 pulsation modes are simultaneously varied to obtain the best fit. But when we do the O-C analysis, we use the phases from a least squares fit. Intuition tells us that if we fix the period, we should expect the uncertainties in amplitude and phase to be smaller than their counterparts from the non-linear least squares fit, provided we have a good value for the period. The uncertainties from linear least squares fit may also be under-estimated, but probably not as severely. We use a period from bootstrapping the various data sets, and it is far more accurate than periods from individual seasons. Another key-point is that a significant fraction of the simulations converged to an alias and this resulted in larger uncertainties in phase as well as amplitude. However, since we are certain that we always had the right periods in all the data sets for the 213 s doublet, we should re-evaluate the phase uncertainties, taking into account only those simulations that converged to the right frequency. Please note that we can be so certain about
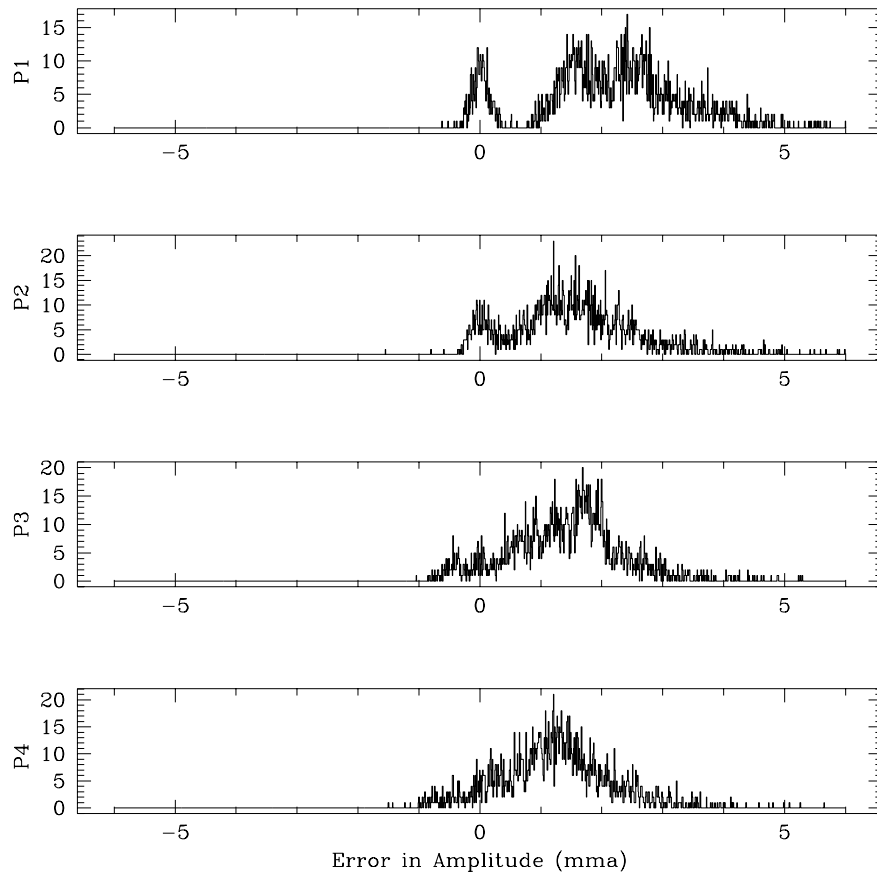
Figure 3.8.—: Error in Phase is the difference between the value chosen to simulate the light curve and the best fit obtained

knowing the right frequency since we have 3 decades of data on the star. A similar statement may not be valid for the 274 s doublet since the periods are changing at a rate that is at least a 100 times faster and hence it is possible that we are picking out aliases in some of the data sets. That would affect the results of an O-C diagram drastically.

3.6   New Pulsation Modes

We also found three additional pulsations around 187.27 s, 318.08 s and 333.65 s, as indicated in figure 3.9. We believe they are real because we saw them clearly in the FTs of quite a few independent data sets. Also, earlier multi-site observations of R548 revealed power around 333 s, 320 s and 187 s, indicating the presence of small amplitude pulsations (Kepler et al. 1995). These modes had been suspected to exist for a long time now. Table 3.14 gives our best estimates for the periods and amplitudes for the various years of observation.

The amplitudes of these modes is small enough that nailing down the precise frequencies is difficult. With the discovery of three additional modes in R548, we now have 7 known modes. This would help in mode identification and lead to constraints in the stellar structure, through asteroseismology.

3.7   Correction due to Proper Motion

Pulsating WDs also have a non-evolutionary secular period change due to proper motion. The size of this effect on $\dot{P}$ was evaluated to be of the order of 10^{-15} s/s (Pajdosz 1995). This effect is insignificant for the DOV and PNNV stars because their evolutionary $\dot{P}$ is several orders of magnitude larger. However, it is of the same order as the $\dot{P}$ measured for hot DAVs like R548 and G117-B15A. R548, at a distance of 55 parsec, does have a measured proper motion. Any motion (with a uniform velocity) of a DAV along the line of sight will manifest itself as a correction in the period estimate for the pulsations and will not affect $\dot{P}$. However, motion perpendicular to the line of sight is equivalent to a centripetal acceleration,

54

Season	Number of iterations that did not converge			
	First Guess	Second Guess	Third Guess	Fourth Guess
1970	1221	672	382	226
1975	151			
1980	1170	602	313	160
1986	1173	557	275	139
1991	153			
1993	874	299	109	
Sep-Oct 1999	719	207		
Nov 1999	247			
2000	298	32		

Table 3.9: Number of non-convergent iterations for the various data sets

Season	σ_P (10^{-3}s)		σ_{ph} (s)		σ_A (mma)		Offset (mma)
	MCS	Real Data	MCS	Real Data	MCS	Real Data	MCS
1970	29	0.4	19	6	1.9	0.7	2.8
1975	30	0.09	40	1.4	1.1	0.2	1.5
1980	27	0.1	11.3	1.4	0.9	0.24	0.4
1986	27	0.4	46	12	0.75	0.5	0.3
1991	1.5	0.7	1.8	0.7	0.15	0.1	0
1993	23	8.4	28	26	0.6	2.34	
Sep-Oct 1999	35.6	0.1	43.4	1.34	1.4	0.14	1.8
Nov 1999	0.55	0.9	1.5	2.5	0.1	0.18	0
2000	29	0.2	13.5	2.9	1.3	0.17	1.0

Table 3.10: 1σ Uncertainties in period, phase and amplitude for the 213.1326 s period

Season	σ_P (s)		σ_{ph} (s)		σ_A (mma)		Offset (mma)
	MCS	Real Data	MCS	Real Data	MCS	Real Data	MCS
1970	31	0.7	30	9.0	1.7	0.7	1.8
1975	31	0.2	41	2.4	0.9	0.2	1.2
1980	30	0.2	14	2.3	1.1	0.24	0.2
1986	36	0.6	69	18	1.1	0.5	0.3
1991	2.5	1.1	2.7	1.14	0.15	0.1	0
1993	17.5	20	46	63	1.5	2.34	
Sep-Oct 1999	34	0.15	47	1.9	1.1	0.14	1.3
Nov 1999	1.0	1.3	2.8	3.65	0.12	0.18	0
2000	29	0.3	31	4.2	1.25	0.17	0.7

Table 3.11: 1σ Uncertainties in period, phase and amplitude for the 212.7684 s period

Season	σ_P (s)		σ_{ph} (s)		σ_A (mma)		Offset (mma)
	MCS	Real Data	MCS	Real Data	MCS	Real Data	MCS
1970	45	0.9	28	10	1.2	0.6	1.8
1975	51	0.2	51	2.6	0.7	0.2	1.1
1980	47	0.4	16.3	3.0	0.85	0.2	0.3
1986	50	0.7	61	16	0.54	0.5	0.3
1991	4.1	2.2	3.5	1.65	0.16	0.094	0
1993	8.3	10.9	28.5	26	1.5	2.3	
Sep-Oct 1999	59.4	0.3	55	2.7	0.85	0.14	1.4
Nov 1999	1.4	2.5	2.9	5.2	0.1	0.19	0
2000	49	0.5	11.6	5.2	0.96	0.16	0.8

Table 3.12: 1σ Uncertainties in period, phase and amplitude for the 274.2508 s period

Season	σ_P (s)		σ_{ph} (s)		σ_A (mma)		Offset (mma)
	MCS	Real Data	MCS	Real Data	MCS	Real Data	MCS
1970	50	1.2	40	13	1.1	0.6	1.4
1975	52	0.3	54	4.0	0.6	0.2	0.75
1980	50	0.6	21	4.5	0.9	0.2	0.3
1986	58	0.9	90	19	0.7	0.5	0.3
1991	6.6	2.8	5.2	2.1	0.17	0.094	0
1993	30.5	16.4	63	40	1.2	2.3	
Sep-Oct 1999	58.5	0.4	57	4	0.9	0.14	1.2
Nov 1999	3.7	3.1	7.3	6.4	0.13	0.19	0.01
2000	49	0.7	27.5	7.1	0.9	0.16	0.7

Table 3.13: 1σ Uncertainties in period, phase and amplitude for the 274.7745 s period

	1991	1993	Sep-Oct 1999	Nov 1999	2000
Period (s)	187.272	187.267			
Amplitude (mma)	0.93	0.85			
Period (s)	318.049		318.075	318.082	318.080
Amplitude (mma)	0.85		0.93	0.82	0.67
Period (s)	333.636		333.642	333.634	333.668
Amplitude (mma)	0.64		0.51	1.31	0.67

Table 3.14: New pulsation modes
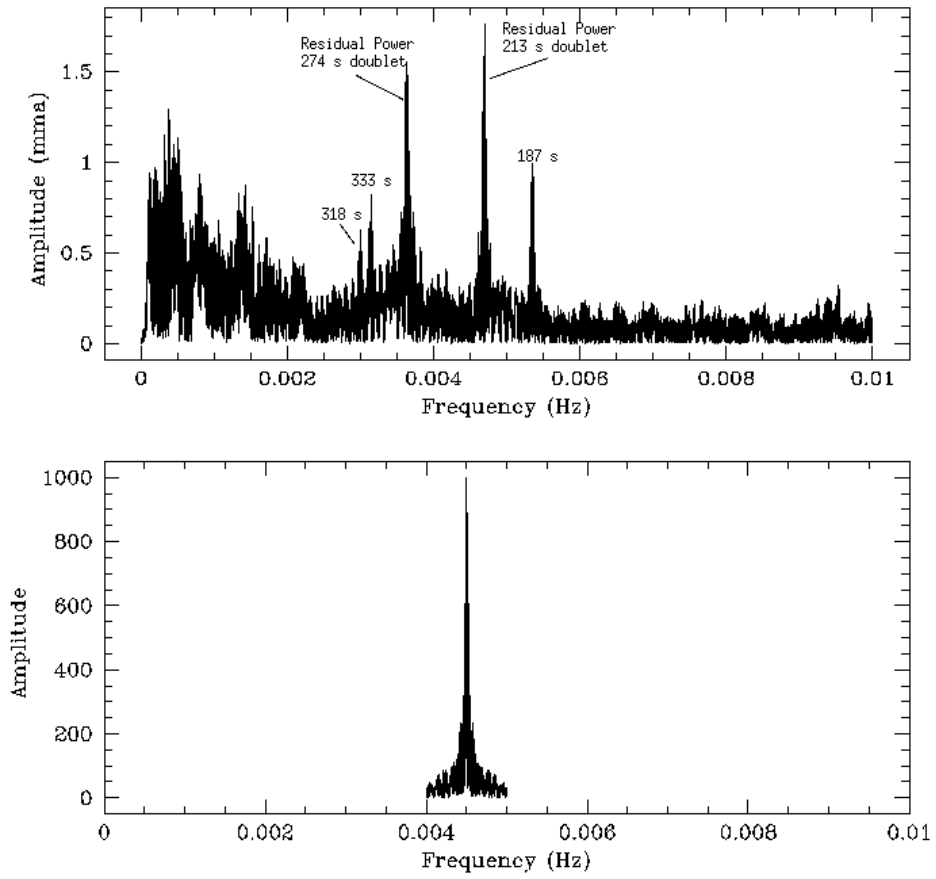
Figure 3.9.—: Pre-whitened Fourier Transform of the 1991 data set, clearly showing the new modes

with Earth as the reference. This causes a $\dot{P}_{pm}$. Pajdosz (1995) has evaluated this to be:

$$\dot{P}_{pm} = \frac{P\dot{v}_r}{c} \qquad (3.12)$$

Pajdosz (1995) evaluates the tangential acceleration to be

$$\dot{v}_r = \frac{v_t^2}{r} \qquad (3.13)$$

He concludes that it is always positive and hence the proper motion correction must always be subtracted from the measured $\dot{P}$. We disagree because this is based on a model of the WD revolving around the Sun. With this model, you would always get a centripetal acceleration directed towards the Sun. We contend that the tangential acceleration can be positive or negative depending on the motion of the WD, thus flipping the sign of the correction term accordingly. This issue needs to be investigated thoroughly and we will do so pretty soon.

Pajdosz (1995) evaluates the correction for proper motion to be

$$\dot{P}_{pm} = 2.43 \times 10^{-18} P[s](\mu["/yr])^2 (\pi["])^{-1} \qquad (3.14)$$

where μ is the proper motion and π is the parallax. Using $\mu = 0.236"/year$ and $\pi = 0.013"$ (Pajdosz 1995), we have evaluated the $\dot{P}_{pm}$ for the 4 periods as indicated in table 3.15.

Period (s)	$\dot{P}_{pm}$ 10^{-15} s/s	$\sigma_{\dot{P}_{pm}}$ 10^{-15} s/s
213.13260565	2.22	0.36
212.76842930	2.22	0.36
274.25080355	2.86	0.46
274.77450046	2.86	0.46

Table 3.15: Correction to $\dot{P}$ due to Proper Motion

At least in the case of the 213 s doublet, the proper motion correction is comparable to $\dot{P}_{obs}$. So, the true $\dot{P}_{cooling}$ for the 213 s doublet could be $(2.4 \pm 2.1)10^{-15}$ s/s or $(6.8 \pm 2.1)10^{-15}$ s/s. This is still a constraint on the evolutionary models. Bradley (1996) gives a theoretical 3σ upper limit of $\dot{P} \leq 6.5 \times 10^{-15}$ s/s, for R548, corresponding to a time-scale ≥ 1.2 Gyr.

Chapter 4

Discussion of the Results in an Astrophysical Context

In this chapter, we will discuss the results of measuring an evolutionary $\dot{P} = (4.6 \pm 2.1) \times 10^{-15}$ s/s for R548. We found the O-C diagram for the 274 s doublet to be different from the 213 s modes. We also discovered some new pulsation modes. We will now be taking a look at some of the implications and applications of this work in an astrophysical context.

4.1 $\dot{P}$ obtained for the 213s doublet

We conclude that the $\dot{P} \leq (4.6\pm2.1)10^{-15}$ s/s is consistent with cooling. Detailed theoretical calculations using evolutionary models (Bradley, Winget & Wood 1992) as well as the $\dot{P}$ measurement for G117-B15A indicate similar values. We have therefore achieved our goal of constraining stellar evolution. The stability of these modes, both the 215 s mode in G117-B15A and the 213 s doublet in R548, is simply amazing and there is a plausible explanation for that.

4.1.1   Stability of the 213 s Doublet

The HDAV (Hot DAV) stars, which include R548, exhibit extreme amplitude and frequency stability, making them reliable clocks. This stability maybe associated with two different

effects: low k modes and mode trapping.

1. **Low k Modes :** Low k modes sample the deep interior and thus have a rate of period change that reflects cooling alone. High k modes have regions of period formation further out in the star and so can be easily affected by magnetic fields, rotation, convection and non-linear interactions among other effects. Using $\dot{P} = 4.6 \times 10^{-15}$ s/s, we calculate the evolutionary time-scale $P/\dot{P}$ to be 1.5 Gyr. Bradley (1996) gives a 3σ upper limit of $\dot{P} \leq 6.5 \times 10^{-15}$ s/s, corresponding to a time-scale ≥ 1.2 Gyr.

2. **Mode Trapping :** In WDs, compositional stratification occurs due to gravitational settling and prior nuclear shell burning. Hydrogen, if present, floats on the surface long before the WD reaches the DAV instability strip. In such WDs, there is a mechanical resonance effect between the local g-mode oscillation wavelength and the thickness of one of the compositional layers (Wood & Winget 1988). This mechanical resonance serves as a stabilizing mechanism in model calculations. The resonantly trapped modes are more stable than un-trapped modes. For a mode to be trapped in the outer H layer, it needs to have a resonance with the He/H transition region, such that its vertical and horizontal displacements both have a node near this interface (Montgomery 1998; Brassard, Fontaine, Wesemael & Hansen 1992). Note that the H/He interface can also result in confinement or trapping of modes in the core. Mode trapping has the greatest effect when a mode is trapped in the outer envelope (Bradley 1993). Trapped modes are energetically favored, as the amplitudes of their eigenfunctions below the H/He interface are smaller than un-trapped modes. Modes trapped in the envelope can have kinetic oscillation energies lower by six orders of magnitude, as compared to the adjacent non-trapped modes (Winget, Van Horn & Hansen 1981). This filter mechanism may very well explain why all the modes expected from theoretical models are not actually observed in the ZZ Ceti stars (Winget, Van Horn & Hansen 1981; Brassard, Fontaine, Wesemael & Hansen 1992). The period spacing between trapped modes depends directly on the location of the H/He discontinuity in models and therefore on the thickness of the outer hydrogen layer (Brassard, Fontaine, Wesemael & Hansen 1992). Theoretical calculations indicate that trapped modes should have a $\dot{P}$ smaller than that produced in the un-trapped

modes due to cooling by a factor ≤ 2 (Bradley, Winget & Wood 1992; Bradley 1993).

If the 213 s doublet in R548 consists of trapped modes, then indeed we could be measuring the stability of the trapping mechanism and not the cooling. Bradley (1998) identified the 213 s doublet as $\ell=1$, k=2. This suggests that the modes are stable because they are low k modes and we are measuring a $\dot{P}$ due to cooling. However, low k modes can also be trapped. Since we have an upper limit for $\dot{P}$ and not yet a true measurement, we cannot tell whether or not these modes are trapped.

The uncertainties in measuring $\dot{P}$ go down as the square of the time-base. This implies that to decrease the uncertainties by a factor of 10, we would need about 90 years of data! One way to do this in a lifetime is to get more accurate values for the phases, which can be achieved using a bigger telescope or a longer data set, (remembering that we must have 35-40 hours to resolve the 2 doublets and that the 1991 data set already includes 3.6m CFHT data), every few years or even every decade.

4.2 $\dot{P}$ indicated for the 274 s Doublet

The implied $\dot{P}$ from the O-C diagram for the 274 s doublet is a 100 times larger than the $\dot{P}$ for the 213 s doublet. It is thus different from the 213 s doublet and therefore unexpected. We should remind ourselves that the two doublets sample different regions of the star. Theoretical evolutionary models imply that $\dot{P}$ should be positive and of the order of 10^{-15} s/s. We do not know yet what the O-C diagram implies, but we know that it is not consistent with cooling. By looking at the periods obtained in the various FTs, we can plot P *vs.* time. The maximum slope $\frac{\Delta P}{\Delta t}$ possible after accounting for the uncertainties gives us an upper limit on the $\dot{P}$ value, provided the uncertainties are not severely underestimated. This limit turns out to be 10^{-11} s/s. The minimum dispersion in the O-C diagram, which does not fit a parabola, allows us to set a lower limit $\frac{\Delta P}{\Delta t} \approx 10^{-13}$ s/s. The uncertainties maybe underestimated by a factor of 10. Taking that into account, our upper limit changes to 5×10^{-11} s/s. To be extremely conservative, we could limit the time-scale to be between 5×10^{-11} s/s and 10^{-14} s/s.

Some possibilities of what could be happening are :

1. **An Avoided Crossing :** Modes of differing k sample slightly different regions in the star with correspondingly different evolutionary time-scales. Hence, we expect each mode to have a different rate of period change (Wood & Winget 1988). Consider two such modes, one changing faster than the other. If the two modes have frequencies very close to each other, then it is possible to interchange their natures. Such an interaction is termed as an avoided crossing (Aizenman, Smeyers & Weigert 1977; Christensen-Dalsgaard 1981). Stable modes can thus become unstable after such an avoided crossing (Montgomery & Winget 1999; Wood & Winget 1988). In other words, if you were monitoring the $\dot{P}$ for any of these modes, you would observe a rapid change during the crossing, i.e., the $\ddot{P}$ term would be important. Montgomery and Winget (1999) have done the most detailed calculation to date, showing how the g-mode periods evolve as the crystallized mass fraction is slowly increased. Their results, plotted in fig. 9. of their paper, clearly show many "kinks" or avoided crossings. Wood & Winget (1988) also saw similar behavior in their evolutionary calculations, when they included H and He layers in their models. The 274 s doublet in R548 could be undergoing an avoided crossing, but this issue needs to be investigated more thoroughly.

2. **Short term Phase Variations :** It is possible that the 274 s doublet is unstable because it samples regions of the star that could be undergoing changes at time-scales shorter compared to 3 decades. We may have variations in $\dot{P}$ at short time-scales of the order of a few months to a few years, super-imposed on the secular cooling. (Note that we investigated for variations in phase at time-scales from a few days to a month or so and found none). Possibly, such short-term behavior averages out in the long run, since from figure 3.3, we can see stability at some level. We cannot place any limits on the short-term behavior, as we have large gaps between data sets. Such short-term phase variations could render a parabolic fit to the O-C diagram difficult, thus swamping out $\dot{P}$ due to cooling.

We hope to eventually attempt to unravel this mystery, by getting both multi-site and extensive single-site data in a season. Since both the 213 s doublet in R548 and the 215 s mode in G117-B15A show the same $\dot{P}$, it would be worthwhile to find out if the 270

s mode in G117-B15A misbehaves like the 274 s doublet in R548. If so, then it would be a vital clue. We would like to request the readers of this document to contact us, if they have any archival data on R548. We would really appreciate it.

4.3 Implications and Applications

The various implications and applications brought about as a result of this work are as follows .

1. **Aiding White Dwarf Cosmochronometry :** The $\dot{P}$ value is an upper limit on the rate of cooling. This helps in constraining theoretical evolutionary models. Along with the $\dot{P}$ measurements for PG-1159 (Costa, Kepler & Winget 1999) and G117-B15A (Kepler et al. 2000), we can calibrate the cooling curve. This will result in more accurate ages for a WD. This will reduce one of the theoretical uncertainties in WD cosmochronology, as explained in the introduction.

2. **Reliable Clock :** WDs such as R548 and G117-B15A are the most reliable clocks known . They are more stable than atomic clocks, pulsars, etc. We assume that the atomic clock is perfect and determine a $\dot{P}$ on that basis. Since we are able to measure a stability of order 10^{-15} s/s for pulsating WDs, we can safely conclude that the uncertainty in atomic clocks is smaller than 10^{-14} s/s (as claimed by NIST) by at least a factor of 2. There is one millisecond pulsar PSR 1937+21 that does match these amazing WDs in stability (Rawley, Taylor, Davis & Allan 1987). Its frequency stability is at least as good as 6×10^{-14} for averaging times longer than 4 months. It has a period of 1.56 ms and a measured $\dot{P} = 0.11 \times 10^{-18}$ s/s (Kaspi, Taylor & Ryba 1994c). The relevant time-scale is then $P/\dot{P} \approx 4.5$ Gyrs. The evolutionary time-scale that we computed for R548 is 1.5 Gyrs. R548 can be used to measure the relative drift of atomic clocks, pulsars and even G117-B15A. R548 can also be used to calibrate GPS software.

3. **Core Composition :** The rate of cooling of a WD depends on core composition and stellar mass. There is a family of cooling curves for different core compositions. The heavier the core, faster it cools. By estimating the rate of cooling for R548,

and by comparing it to theoretical evolutionary models, we are effectively measuring the mean atomic weight of the core, A. Bradley, Winget & Wood (1992) obtained theoretical $\dot{P}$ values around 5 -7 $\times 10^{-15}$ s/s from detailed calculations for un-trapped modes in O core 0.5 $M_\odot$ models with periods close to 215 s. This implies that our current limit of 4.6×10^{-15} s/s indicates a C/O core and eliminates substantially heavy cores like Fe or Mg, for example.

4. **Crystallization and Phase Separation :** For a 0.6 $M_\odot$ Wood (1992) model, the onset of crystallization is at $T_{eff} = 6000$ K for a C core ($t_{cool} \simeq 2$ Gyr, $L \simeq 10^{-3.8} L_\odot$), and at $T_{eff} = 7200$ K for an O core. These temperatures are much cooler than the DAV instability strip from 11 000-12 000 K. So, ordinarily, one would not be able to study effects such as crystallization and phase separation using $\dot{P}$ values for the DAVs. However, massive stars like BPM 37093 ($M \simeq 1\ M_\odot$) should be crystallized pulsators (Winget et al. 1997; Montgomery & Winget 1999; Nitta et al. 1999) and provide us with a unique opportunity to study these effects. (Spectroscopic $\log g$ values suggest that R548 has a mass of 0.52 $M_\odot$ (Bergeron et al. 1995) and therefore it is clearly not a crystallized pulsator). Crystallization affects $\dot{P}$ in the following ways; it releases latent heat and delays the cooling and, secondly, the outward moving crystallization front causes the periods to increase.

When faced with uncertainties like crystallization and phase separation, we can scale our measurements to compute the evolutionary $\dot{P}$ expected of a massive WD. The observed $\dot{P}$ of a crystallized pulsator should be a sum of $\dot{P}_{crys}$ and $\dot{P}_{cooling}$ and is expected to be measurable with a 10 year baseline. Montgomery (1998) calculated $\dot{P}_{crys}$ to be $\sim 7 \times 10^{-15}$ s/s for periods less than 1000 s and $\sim 5 \times 10^{-15}$ s/s for periods between 500 - 700 s. By comparing the observed $\dot{P}$ of a crystallized pulsator with the evolutionary $\dot{P}$ expected of a massive WD, we could estimate the size of effects like crystallization and phase separation. Note that there is yet no proof to demonstrate that BPM 37093 is crystallized. The existent data is not sufficient for a $\dot{P}$ measurement. There are no other known candidates for crystallized pulsators, though the massive WDs discovered in the various surveys are a good starting point to look for one.

65

5. **Orbital companion :** If R548 had an unseen orbital companion, another star or a planet, then its motion about the center of mass of the system would manifest itself as a sinusoidal variation of the arrival time of maximum pulsation. This sinusoidal variation could, in principle, be distinguishable from the parabolic signature due to cooling of the WD. This could serve as a means of detection of planetary systems or other binary companions. The period of the sinusoid would be the orbital period and the amplitude of the sinusoid would help in deducing the mass and/or distance of the orbital companion. The deviation from a sine curve would tell us something about the ellipticity of the orbit and the angle of inclination of the orbit in the sky. A Doppler effect that would result from the orbital motion of the clock would cause a $\dot{P}_{orb}$ (Kepler et al. 1991), given by

$$\dot{P}_{orb} = \frac{P}{c}\frac{Gm}{a^2} \tag{4.1}$$

where P is the pulsation period, m is the mass of the orbital companion and a is the separation between the components. The $\dot{P}_{orb}$ is not caused by the motion towards or away from us, but by the acceleration in the motion. Any uniform motion along the line of sight would just be interpreted as a correction in pulsation period, ΔP.

The O-C diagrams for R548, G117-B15A and L19-2 do not show any discernible sinusoidal variations. G117-B15A is in a binary system, but the orbital companion with a mass of 0.39 $M_\odot$ and a separation of 925 A.U. is not detectable using the O-C technique (Kepler et al. 1991). We can set the following limits on the physical parameters for an orbital companion. Suppose that the O-C diagram consists of points that span 3 decades and have an average spacing of a year. We observe the DAV at about the same time of the year, so we are de-sensitized to observing an orbital period of a year, as we would find it to be in the same phase every orbit. Suppose the orbital period is shorter than a year, then every O-C point would sample it in a different phase and we would be able to uncover such a pattern eventually. The orbital period could only be longer than 6 decades, if no sinusoidal variations or the like are seen. Using this limit on the period and Kepler's third law, we then set a limit on the orbital radius r for the companion. The amplitude A of the sinusoid (orbital light travel time) is less than the average uncertainties of the points in the

66

O-C diagram and hence we do not detect it. This sets a limit on the orbital radius $r_\star$ for the DAV, which also has to go around the common center of mass of the system with the same orbital period P.

$$(2A)c = 2r_\star \sin(i) \tag{4.2}$$

where i is the angle of inclination. Note the role played by the angle of inclination. If the plane of the orbit is perpendicular to the line of sight, then we will not see a sinusoid in the O-C diagram. In that context, the limits that we are setting on the mass and radius of the orbital companion have a factor from the angle of inclination, entangled with them. Remembering that the orbital radii should be in inverse ratio of their masses, we have

$$\frac{m}{M_\star} = \frac{r}{r_\star} \tag{4.3}$$

We can now set a limit on the mass m of the orbital companion. Note that the orbital separation a is the sum of r and $r_\star$. Let us find out the sensitivity of detecting an orbital companion using this technique. We could ask if we can detect planets like Earth at 1 A.U. For a period of 213.132 s, equation (3) gives

$$\dot{P}_{orb}^{\text{Earth}} = \frac{213.132 \text{ s}}{3 \times 10^8 \text{ m/s}} \frac{6.6 \times 10^{-11} \text{ N m}^2/\text{kg}^2 \cdot 6 \times 10^{24}\text{kg}}{\left(1.5 \times 10^{11} \text{ m}\right)^2} \tag{4.4}$$

$$\dot{P}_{\text{orb}}^{\text{Earth}} = 12.5 \times 10^{-15} \text{ s/s} \tag{4.5}$$

This technique is ultimately sensitive enough to find planets like Earth at 1 A.U. as the $\dot{P}_{orb}$ is about 5 times larger than $\dot{P}_{cooling}$. For a planet like Jupiter ($M = 318 \, M_\oplus$) at 5.2 A.U., we have

$$\dot{P}_{\text{orb}}^{\text{Jupiter}} = 12.5 \times 10^{-15} \frac{318}{\left(5.2\right)^2} \tag{4.6}$$

$$\dot{P}_{\text{orb}}^{\text{Jupiter}} = 1.5 \times 10^{-13} \text{ s/s} \tag{4.7}$$

Thus, planets the size of Jupiter at 5 A.U. are easier to detect than Earth-like planets at 1 A.U. If R548 were to be in a binary system with a brown dwarf ($M_\star = 0.08 M_\odot$), then what could be their maximum separation for the brown dwarf to be detectable, assuming that the plane of the orbit is not perpendicular to the line of sight. The

angle of inclination plays a role in the size of $\dot{P}_{\mathrm{orb}}$, apart from the mass and size of the orbital companion.

$$9.2 \times 10^{-15} = 12.5 \times 10^{-15} \, \frac{26\,635}{a^2 \sin i^2} \qquad (4.8)$$

where we have assumed the total upper limit of the observed $\dot{P} \simeq 9.2 \times 10^{-15}$ to be due to binary nature, and a mass for the companion of $26\,635 \, M_\oplus \, (0.08 M_\odot)$.

$$a_{\mathrm{max}} \sin i = 190 A.U. \qquad (4.9)$$

We will be able to detect a brown dwarf companion of $0.08 M_\odot$ even at a distance of 190 A.U. at the very least. For other values of the angle of inclination, we might be able to detect a brown dwarf at greater distances than 190 A.U.

6. **Asteroseismology :** With the discovery of three new modes in R548, we now have 7 known modes. This would help in mode identification and lead to constraining the stellar structure, through asteroseismology. It would also assist Kleinman, Kawaler & Bischoff (2000) in their work on ensemble asteroseismology of DAVs.

Metcalfe, Nather & Winget (2000; in press) have applied an optimization method utilizing a genetic algorithm for fitting white dwarf pulsation models to asteroseismological data. They are using this global approach to investigate the completeness and adequacy of our understanding of the principles governing white dwarf interiors by parameterizing the constitutive physics of our models and using a genetic algorithm to search for all of the solutions that produce observationally indistinguishable behavior. To make these calculations practical, they have configured a specialized computational instrument, a meta-computer. The idea is to use period spacings, derived from observed periods in WDs, as a criterion for estimating the χ^2 of how the models fit the observed data. By changing the input physics and parameters that go into a model and by observing how the fit improves or degrades, they are actually doing the inverse problem. For the success of this technique, they require at least 7 to 8 observed modes. With the additional modes discovered in R548, they can now tackle it. R548 demonstrates sinusoidal variations and is a linear pulsator. This makes it an attractive candidate for such work.

4.4 Future Work

1. **Improving the $\dot{P}$ value for the 213 s Doublet :** The error in $\dot{P}$ goes down as the square of time. So, we will continue to derive a better value by extending our time-base of observations. This is effectively a life-time side project.

2. **Unraveling the 274 s Doublet :** There is also something very exciting going on with the 274 s doublet. We need to investigate this doublet, both theoretically and observationally as well.

3. **Ensemble Asteroseismology :** Since both the 213 s doublet in R548 and the 215 s mode in G117-B15A show the same $\dot{P}$, it would be worthwhile to find out if the 270 s mode in G117-B15A misbehaves like the 274 s doublet in R548.

4. **Maximum Likelihood Estimation :** As was clearly pointed out in earlier sections, we already assume something about the size of $\dot{P}$ before we measure it. To do a more objective and assumption-free search for the true solution in a P, $\dot{P}$ grid defined over a reasonably large parameter space, is one of our future goals. This may prove important for the 274 s doublet.

4.5 Conclusion

Our best upper limit for $\dot{P}$ for R548 is $(4.6 \pm 2.1) \times 10^{-15}$ s/s, which constrains secular cooling. Using $\dot{P} = 4.6 \times 10^{-15}$ s/s, we calculate the evolutionary time-scale $P/\dot{P}$ to be 1.5 Gyr. Bradley (1996) gives a theoretical 3σ upper limit of $\dot{P} \leq 6.5 \times 10^{-15}$ s/s, corresponding to an evolutionary time-scale ≥ 1.2 Gyr.

The 274 s doublet behaves differently than the 213 s doublet. For both modes of the 274 s doublet, we could never achieve a clear minimization of phase dispersion. The uncertainties in phase are larger for the 274 s doublet as it has a lower amplitude compared to the 213 s doublet. However, both 212.768 s and 274.25 s periods have similar amplitudes. Rather, the O-C diagrams are suggestive of behavior, apart from cooling. We obtain an O-C diagram with ambiguous cycle counts and all the points do not lie on a parabola within error bars. This can lead to a plausible thought that $\dot{P}$ for the 274 s doublet is not constant

and the $\dddot{P}$ term is significant. If so, then we could be seeing something very exciting, that needs further investigation.

<div align="center">

That's all folks!

</div>

Appendix A

A.1 Bootstrapping for the Period 213.13260656 s

We present bootstrapping values for the 213.132 s period. We decided to start from 1970 since there were quite a few data sets in that decade and it would be easier to initiate the bootstrapping process. Note that we have not explicitly stated the corrections in period at each stage. When we looked at individual data sets, we found that we could bootstrap between most gaps expecting cycle errors up to ± 2. When we do the actual bootstrapping with a period that improves with each step and is far more accurate than individual seasons, we know for certain that if we check for cycle counts up to ± 2, we will be fine. This is true for both periods of the 213 s doublet.

A.1.1 Bootstrapping from 1970 to 1975

The respective periods from individual data sets in 1970 and 1975 were $213.132576 \pm 4.1 \times 10^{-4}$ s and $213.132423 \pm 8.9 \times 10^{-5}$ s. A gap of 5 years will have about 739821 cycles. Multiplying the error in period by the number of cycles will yield the error in the calculated value of phase. It turns out to be 66 s or 0.3 cycles, if we bootstrap from 1975 to 1970. If we go the other way from 1970 to 1975, the error in calculated phase becomes 303 s or 1.4 cycles. If the uncertainties in phases are truly underestimated by the least squares fit, then the true error could be larger than 1 or 2 cycles, rendering it difficult to nail down the number of cycles in the gap. We faced a problem in bootstrapping from 1975 to 1970. With hindsight, we can see that the period from 1970 is closer to the true period than 1975, though it has a larger error. True period only implies the best value that we could obtain

from 30 years of data on R548. However, luckily for us, when we plotted five O-C diagrams and checked for cycle errors up to ±2, we could easily spot the correct number of epochs between 1970 and 1975. The unambiguous number of epochs from 1970 to 1975 for period 213.132604 s turned out to be 728897, as seen from figures A.2 to A.6.
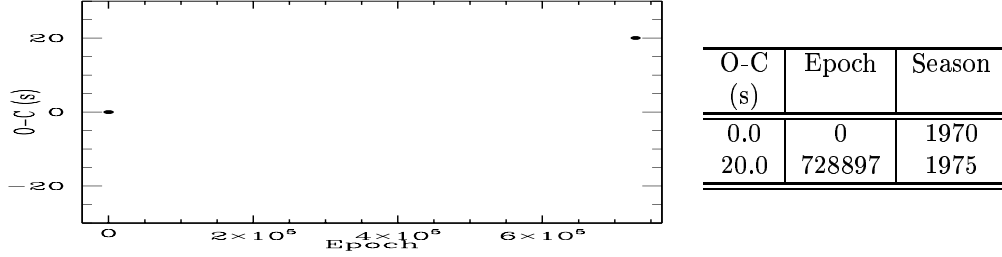
Figure A.1.—: O-C Diagram for Period = 213.132576 s for data sets 1970 & 1975

O-C (s)	Epoch	Season
0.0	0	1970
20.0	728897	1975

From the O-C diagram in fig. A.1, we obtain the following corrections to P for the five possibilities E, E$\pm$1 and E$\pm$2. We have neglected the $\dot{P}$ term in computing these corrections.

Epoch	Correction in Period $(10^{-5}$ s$)$	New Period (s)
E-2=728895	61.231	213.133188
E-1=728896	031.9905	213.132896
E=728897	2.75002	213.132604
E+1=728898	-26.4904	213.132311
E+2=728899	-55.7307	213.132019

Table A.1: Corrections in Period for varying cycle counts between 1970 & 1975

The smallest correction in period has been obtained for E = 728897 and is already suggestive of the right answer. We will see if this mathematical expectation tallies with the O-C minimization. To help us pick out the right answer, we have also plotted a point corresponding to the 1980 data set, though it has not been utilized in the calculations. Please note that whenever you come across a point marked with a cross on the O-C diagram, it indicates additional information being displayed and the data set has not been utilized in the calculations for that subsection. But that data set will be utilized in the next subsection and its epoch will be varied to yield minimum phase dispersion.

O-C (s)	Epoch	Season
0.0	0	1970
0.5	728895	1975
-11.4	1483684	1980
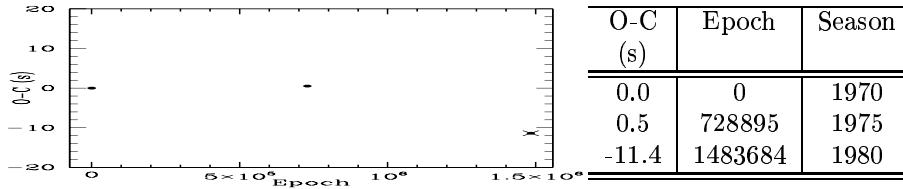
Figure A.2.—: O-C Diagram for Period = 213.133188 s for E-2

73

O-C (s)	Epoch	Season
0.0	0	1970
0.1	728896	1975
-5.3	1483686	1980
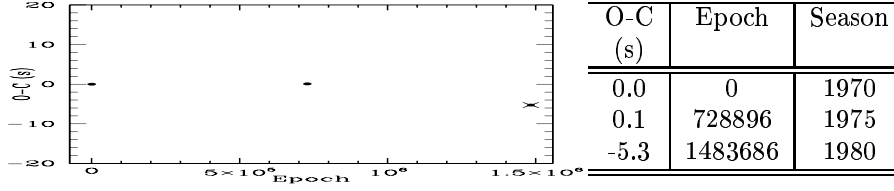
Figure A.3.—: O-C Diagram for Period = 213.132896 s for E-1

O-C (s)	Epoch	Season
0.0	0	1970
-0.4	728897	1975
1.0	1483688	1980
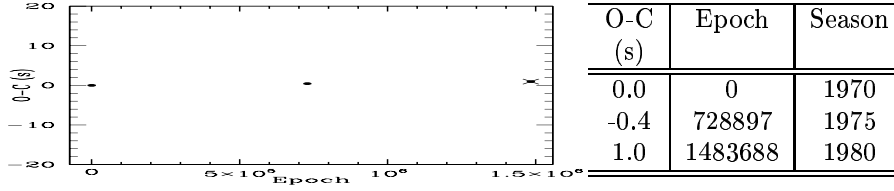
Figure A.4.—: O-C Diagram for Period = 213.132604 s for E

O-C (s)	Epoch	Season
0.0	0	1970
-0.3	728898	1975
8.6	1483690	1980
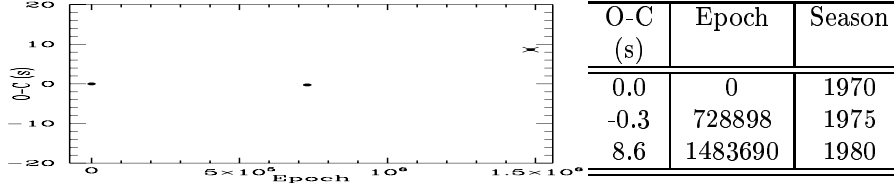
Figure A.5.—: O-C Diagram for Period = 213.132311 s for E+1

O-C (s)	Epoch	Season
0.0	0	1970
-0.1	728899	1975
14.9	1483692	1980
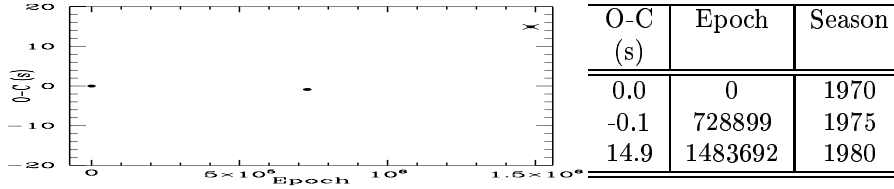
Figure A.6.—: O-C Diagram for Period = 213.132019 s for E+2

A.1.2   Bootstrapping from 1975 to 1980

Having established that the cycle count between 1970 and 1975 is positively 728897, we obtain the new corrections to Period by varying the cycle count between 1975 and 1980. Again, though we plot a point for 1986, it is just additional information being displayed and that point does not play a role in any of the calculations. The new period estimates are tabulated below.

Using these period estimates we plot O-C diagrams, shown in fig. A.7 to A.11. We can clearly see that E=1483688 is the correct number of epochs for the 1980 data set.

Epoch	Correction in Period (10^{-5} s)	New Period (s)
E-2=1483686	23.1843	213.132836
E-1=1483687	011.6122	213.132720
E=1483688	0.04008	213.132604
E+1=1483689	-11.532	213.132489
E+2=1483690	-23.1042	213.132373

Table A.2: Corrections in Period for varying cycle counts between 1975 & 1980

O-C (s)	Epoch	Season
0.0	0	1970
43.6	728896	1975
83.1	1483686	1980
91.0	2346425	1986
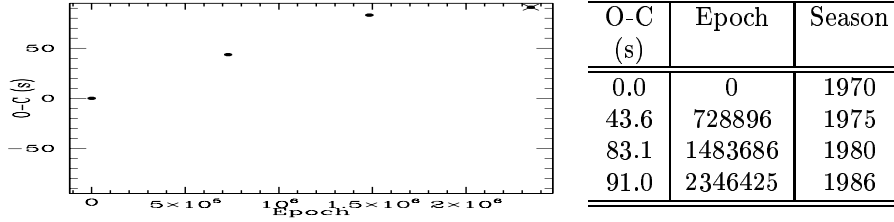
Figure A.7.—: O-C Diagram for Period = 213.132836 s for E-2

O-C (s)	Epoch	Season
0.0	0	1970
-85.0	728897	1975
41.8	1483687	1980
-61.1	2346427	1986
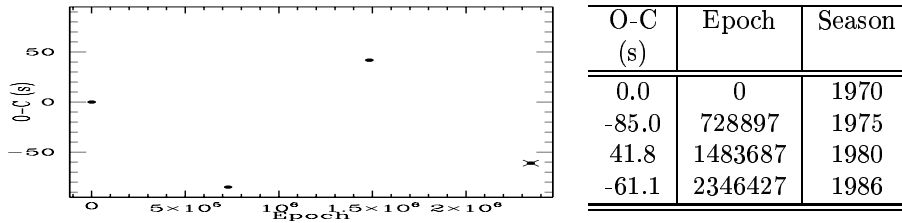
Figure A.8.—: O-C Diagram for Period = 213.132720 s for E-1

O-C (s)	Epoch	Season
0.0	0	1970
-0.5	728897	1975
0.4	1483688	1980
0.0	2346428	1986
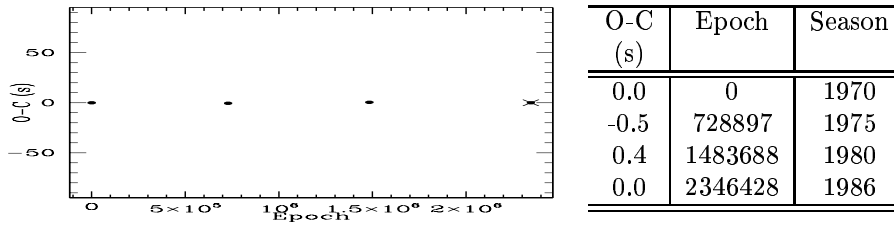
Figure A.9.—: O-C Diagram for Period = 213.132604 s for E

O-C (s)	Epoch	Season
0.0	0	1970
83.1	728897	1975
-42.3	1483689	1980
58.7	2346429	1986
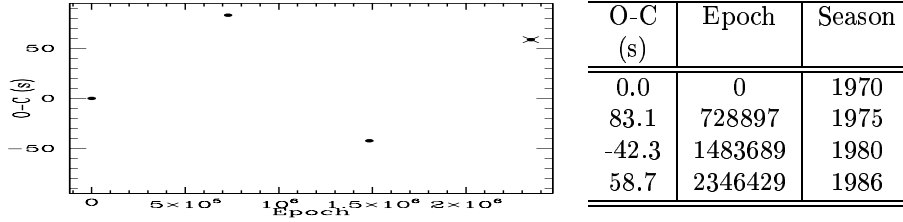
Figure A.10.—: O-C Diagram for Period = 213.132489 s for E+1

O-C (s)	Epoch	Season
0.0	0	1970
-45.5	728898	1975
-83.6	1483690	1980
-93.3	2346431	1986
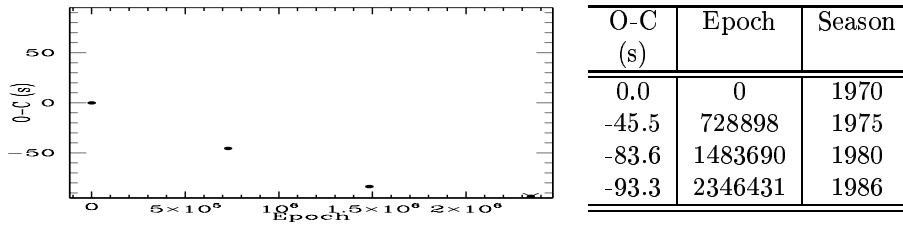
Figure A.11.—: O-C Diagram for Period = 213.132373 s for E+2

A.1.3 Bootstrapping from 1980 to 1986

Using the O-C diagram in fig. A.9, we obtain the following corrections to P for the five possibilities E, E±1 and E±2.

Epoch	Correction in Period (10⁻⁵ s)	New Period (s)
E-2=2346426	12.144	213.132725
E-1=2346427	6.0736	213.132665
E=2346428	0.00319	213.132604
E+1=2346429	-6.0672	213.132543
E+2=2346430	-12.1376	213.132483

Table A.3: Corrections in Period for varying cycle counts between 1980 & 1986

O-C (s)	Epoch	Season
0.0	0	1970
-88.6	728897	1975
34.4	1483687	1980
-72.9	2346427	1986
62.0	3090300	1991
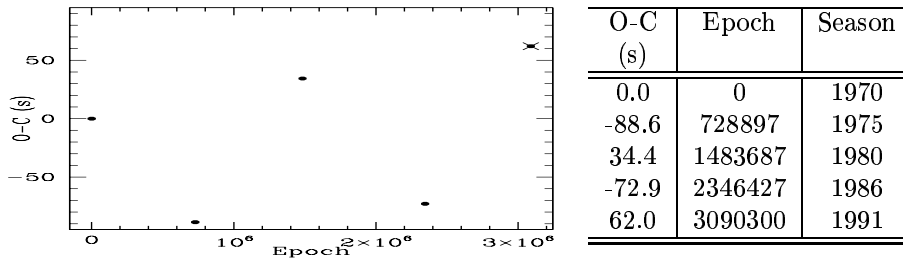
Figure A.12.—: O-C Diagram for Period = 213.132725 s for E-2

O-C (s)	Epoch	Season
0.0	0	1970
-44.9	728897	1975
-89.8	1483688	1980
68.95	2346427	1986
33.8	3090301	1991
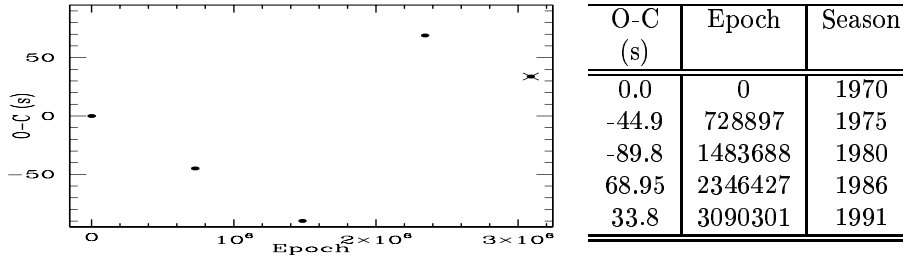
Figure A.13.—: O-C Diagram for Period = 213.132665 s for E-1

O-C (s)	Epoch	Season
0.0	0	1970
-0.5	728897	1975
0.4	1483688	1980
0.0	2346428	1986
8.6	3090302	1991
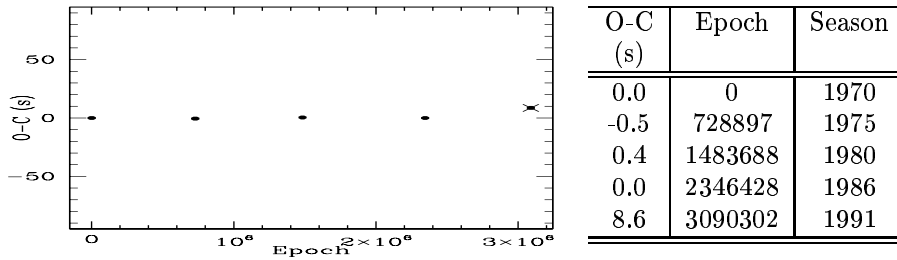
Figure A.14.—: O-C Diagram for Period = 213.132604 s for E

77

O-C (s)	Epoch	Season
0.0	0	1970
43.9	728897	1975
90.8	1483688	1980
-68.9	2346429	1986
-16.5	3090303	1991
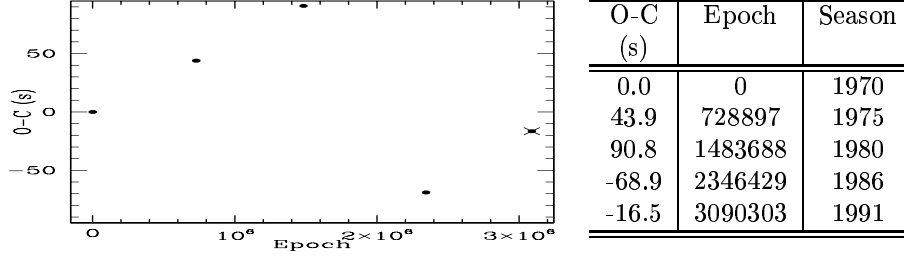
Figure A.15.—: O-C Diagram for Period = 213.132543 s for E+1

O-C (s)	Epoch	Season
0.0	0	1970
87.5	728897	1975
-33.4	1483689	1980
72.8	2346429	1986
-44.8	3090304	1991
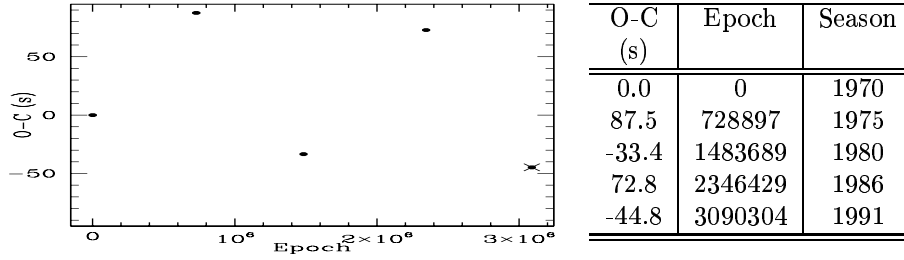
Figure A.16.—: O-C Diagram for Period = 213.132483 s for E+2

From figures A.12 to A.16, we conclude that E=2346428 is the correct number of cycles for the 1986 data set.

A.1.4 Bootstrapping from 1986 to 1991

From the O-C diagram of fig. A.14, we obtain the following corrections to P for the five possibilities E, E$\pm$1 and E$\pm$2.

Epoch	Correction in Period $(10^{-5}$ s)	New Period (s)
E-2=3090300	7.5569	213.13267957
E-1=3090301	03.85426	213.13264254
E=3090302	0.15158	213.13260552
E+1=3090303	-3.5511	213.13256849
E+2=3090304	-7.2538	213.13253146

Table A.4: Corrections in Period for varying cycle counts between 1986 & 1991

O-C (s)	Epoch	Season
0.0	0	1970
-55.6	728897	1975
101.7	1483687	1980
34.5	2346427	1986
-11.1	3090301	1991
-38.2	3395831	1993
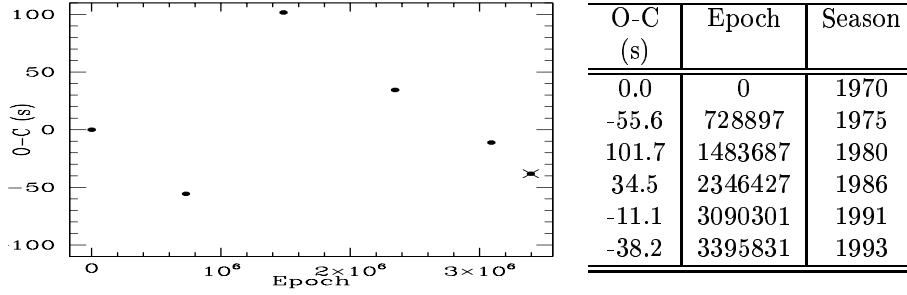
Figure A.17.—: O-C Diagram for Period = 213.13267957 s for E-2

O-C (s)	Epoch	Season
0.0	0	1970
-28.6	728897	1975
-56.7	1483688	1980
-91.1	2346428	1986
103.1	3090301	1991
87.4	3395831	1993
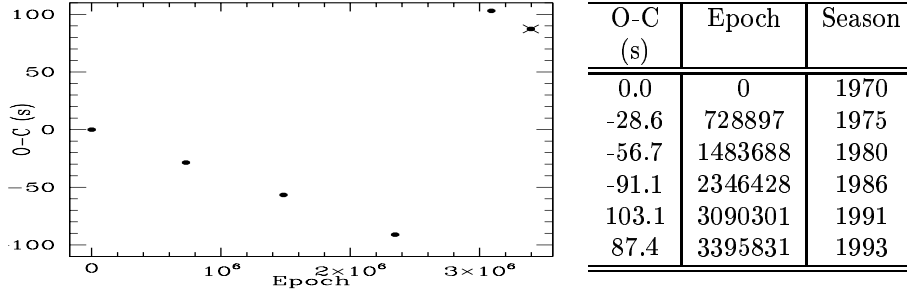
Figure A.18.—: O-C Diagram for Period = 213.13264254 s for E-1

O-C (s)	Epoch	Season
0.0	0	1970
-1.64	728897	1975
-1.8	1483688	1980
-3.6	2346428	1986
3.97	3090302	1991
-0.35	3395832	1993
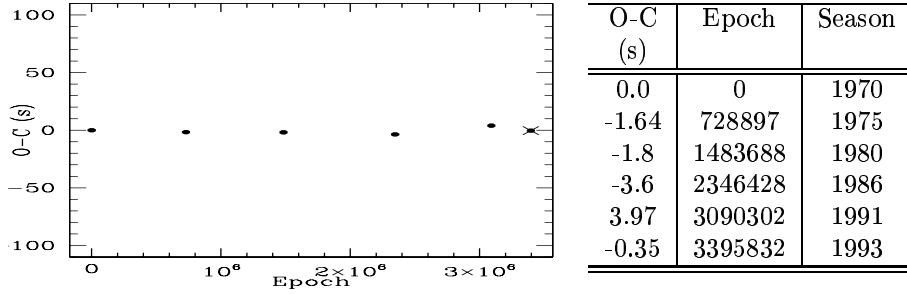
Figure A.19.—: O-C Diagram for Period = 213.13260552 s for E

Epoch	Correction in Period $(10^{-5}$ s)	New Period (s)
E-2=3395830	4.9326	213.13265485
E-1=3395831	02.4641	213.13263016
E=3395832	-0.0044	213.13260548
E+1=3395833	-2.4729	213.13258079
E+2=3395834	-4.9414	213.13255611

Table A.5: Corrections in Period for varying cycle counts between 1991 & 1993

79

O-C (s)	Epoch	Season
0.0	0	1970
25.3	728897	1975
53.04	1483688	1980
84.0	2346428	1986
-95.0	3090303	1991
-88.0	3395833	1993
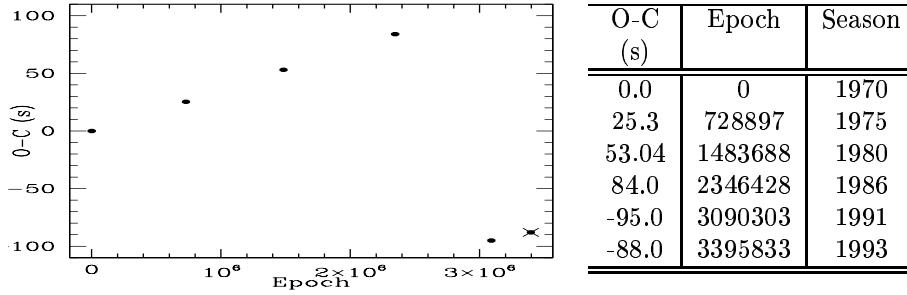
Figure A.20.—: O-C Diagram for Period = 213.13256849 s for E+1

O-C (s)	Epoch	Season
0.0	0	1970
52.3	728897	1975
-105.2	1483689	1980
-41.7	2346429	1986
19.1	3090303	1991
37.5	3395833	1993
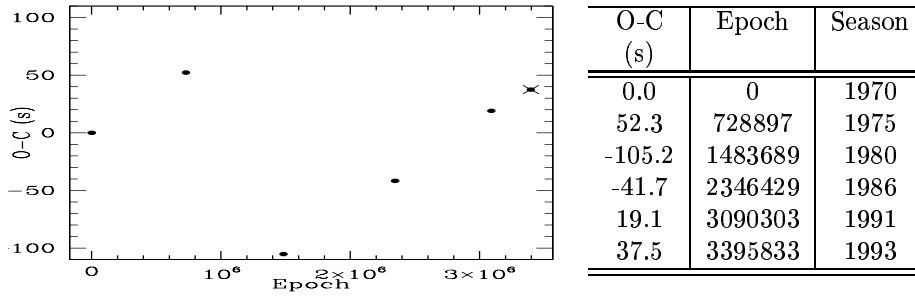
Figure A.21.—: O-C Diagram for Period = 213.13253146 s for E+2

From figures A.17 to A.21, E=3090302 is evidently the right number of epochs for 1991

A.1.5   Bootstrapping from 1991 to 1993

From the O-C diagram shown in fig. A.19, we obtain the following corrections to Period for the five possibilities E, E±1 and E±2.

O-C (s)	Epoch	Season
0.0	0	1970
-37.6	728897	1975
-74.8	1483688	1980
92.9	2346427	1986
65.04	3090301	1991
45.6	3395831	1993
5.7	4270769	Sep-Oct99
1.9	4295808	Nov 99
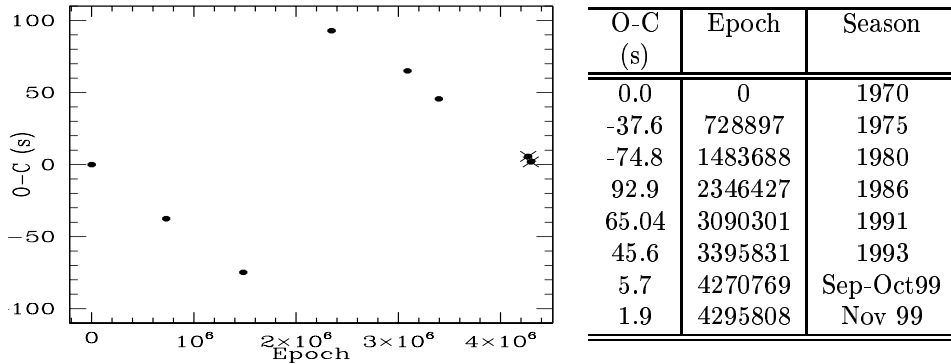
Figure A.22.—: O-C Diagram for Period = 213.13265485 s for E-2

80
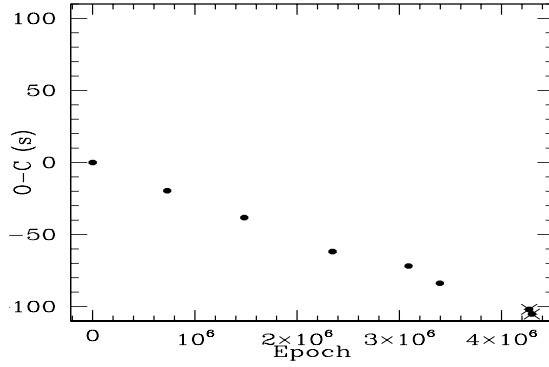
O-C (s)	Epoch	Season
0.0	0	1970
-19.6	728897	1975
-38.25	1483688	1980
-61.8	2346428	1986
-71.9	3090302	1991
-83.8	3395832	1993
-101.9	4270770	Sep-Oct99
-105.2	4295809	Nov 99

Figure A.23.—: O-C Diagram for Period = 213.13263016 s for E-1
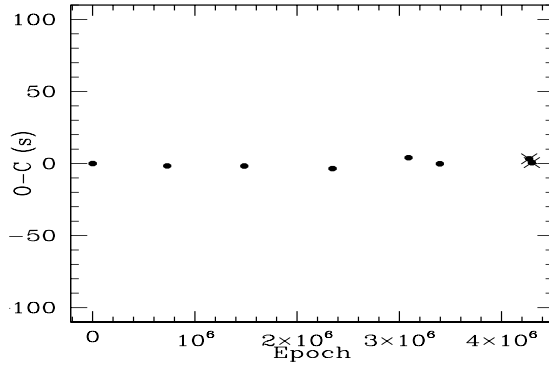
O-C (s)	Epoch	Season
0.0	0	1970
-1.64	728897	1975
-1.7	1483688	1980
-3.5	2346428	1986
4.1	3090302	1991
-0.2	3395832	1993
3.3	4270770	Sep-Oct99
0.6	4295809	Nov 99

Figure A.24.—: O-C Diagram for Period = 213.13260548 s for E
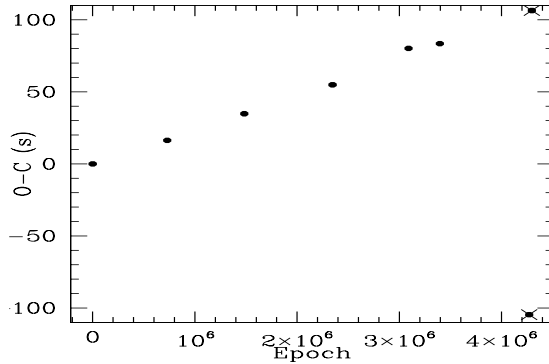
O-C (s)	Epoch	Season
0.0	0	1970
16.3	728897	1975
34.8	1483688	1980
54.9	2346428	1986
80.2	3090302	1991
83.5	3395832	1993
-104.6	4270771	Sep-Oct99
106.4	4295809	Nov 99

Figure A.25.—: O-C Diagram for Period = 213.13258079 s for E+1

81

O-C (s)	Epoch	Season
0.0	0	1970
34.4	728897	1975
71.5	1483688	1980
-99.9	2346429	1986
-56.8	3090303	1991
-46.0	3395833	1993
0.6	4270771	Sep-Oct99
-0.8	4295810	Nov 99
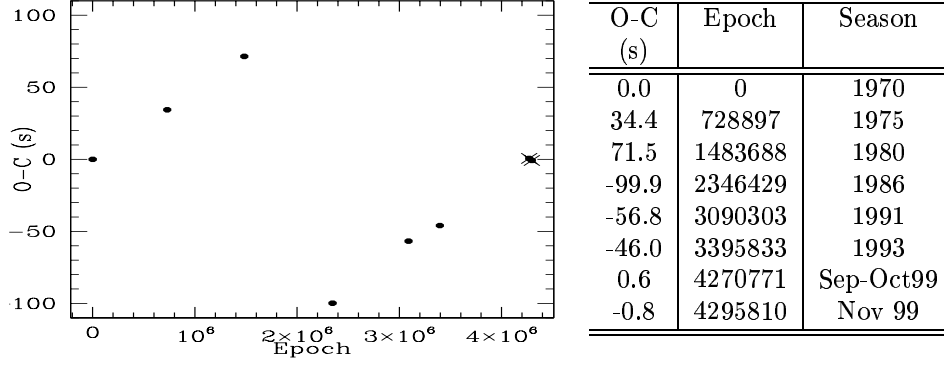
Figure A.26.—: O-C Diagram for Period = 213.13255611 s for E+2

From figures A.22 to A.26, we can see that E=3395832 is the correct number of cycles for 1993

A.1.6 Bootstrapping from 1993 to 1999

From the O-C diagram in fig. A.24, we compute the following corrections to period for varying the epochs of both the 1999 data sets simultaneously for the 5 possibilities E, E±1 and E±2.

Epoch	Correction in Period (10^{-6} s)	New Period (s)
E-2=4270768	27.9636	213.13263347
E-1=4270769	14.1414	213.13261960
E=4270770	0.31924	213.13260573
E+1=4270771	-13.503	213.13259186
E+2=4270772	-27.3252	213.13257799

Table A.6: Corrections in Period for varying cycle counts between 1993 & 1999

Epoch	Correction in Period (10^{-6} s)	New Period (s)
E-2=4414273	21.9323	213.13262766
E-1=4414274	10.9284	213.13261666
E=4414275	-0.07547	213.13260565
E+1=4414276	-11.0794	213.13259465
E+2=4414277	-22.0833	213.13258365

Table A.7: Corrections in Period for varying cycle counts between 1999 & 2000

82
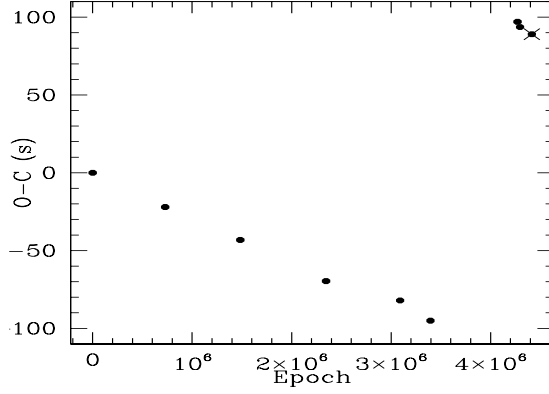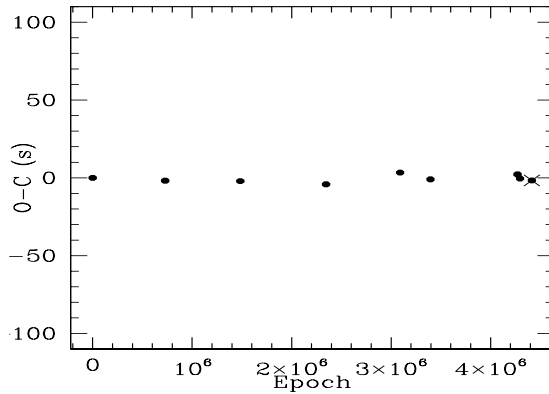
O-C (s)	Epoch	Season
0.0	0	1970
-22.0	728897	1975
-43.2	1483688	1980
-69.6	2346428	1986
-82.1	3090302	1991
-95.0	3395832	1993
97.0	4270769	Sep-Oct99
93.7	4295808	Nov 99
89.1	4414274	2000

Figure A.27.—: O-C Diagram for Period = 213.13263347 s for E-2
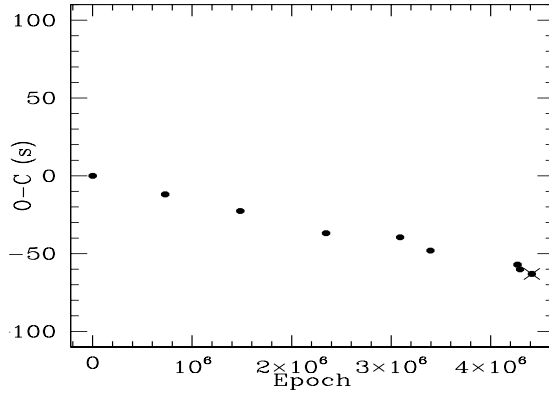
O-C (s)	Epoch	Season
0.0	0	1970
-11.9	728897	1975
-22.6	1483688	1980
-36.9	2346428	1986
-39.5	3090302	1991
-48.0	3395832	1993
-57.1	4270770	Sep-Oct99
-60.1	4295809	Nov 99
-63.1	4414275	2000

Figure A.28.—: O-C Diagram for Period = 213.13261960 s for E-1

O-C (s)	Epoch	Season
0.0	0	1970
-1.8	728897	1975
-2.1	1483688	1980
-4.1	2346428	1986
3.4	3090302	1991
-0.95	3395832	1993
2.2	4270770	Sep-Oct99
-0,4	4295809	Nov 99
-1.6	4414275	2000

Figure A.29.—: O-C Diagram for Period = 213.13260573 s for E

83

O-C (s)	Epoch	Season
0.0	0	1970
8.3	728897	1975
18.4	1483688	1980
28.8	2346428	1986
46.0	3090302	1991
46.0	3395832	1993
61.3	4270770	Sep-Oct99
59.0	4295809	Nov 99
59.5	4414275	2000
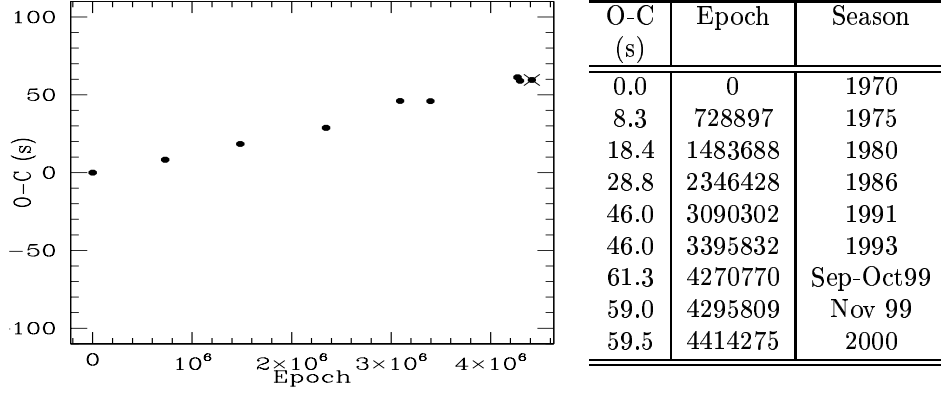
Figure A.30.—: O-C Diagram for Period = 213.13259186 s for E+1

O-C (s)	Epoch	Season
0.0	0	1970
18.3	728897	1975
39.1	1483688	1980
61.4	2346428	1986
88.7	3090302	1991
92.9	3395832	1993
-92.8	4270771	Sep-Oct99
-94.9	4295810	Nov 99
-92.5	4414276	2000
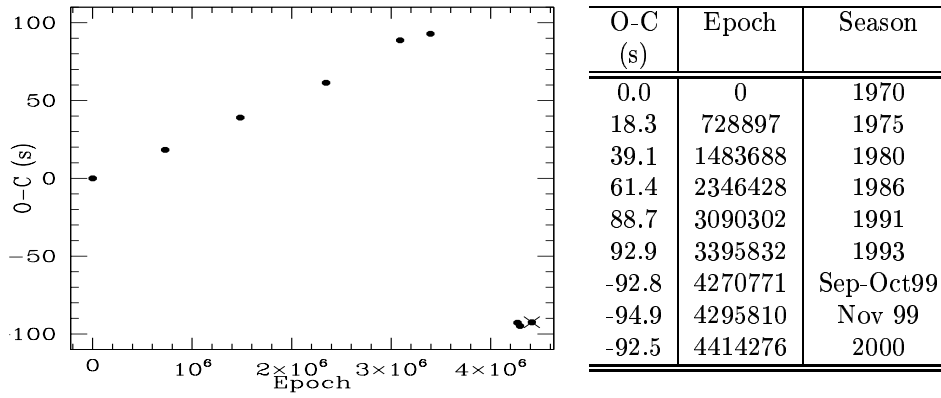
Figure A.31.—: O-C Diagram for Period = 213.13257799 s for E+2

From figures A.27 to A.31, we conclude that E=4270770 and E=4295809 are the right number of epochs for Sep-Oct 1999 and November 1999 respectively.

A.1.7 Bootstrapping from 1999 to 2000

From fig. A.29, we vary the epoch for the 2000 data set and calculate the following corrections to the period.

O-C (s)	Epoch	Season
0.0	0	1970
-17.8	728897	1975
-34.5	1483688	1980
-56.0	2346428	1986
-64.2	3090302	1991
-75.3	3395832	1993
-91.3	4270770	Sep-Oct99
-94.5	4295809	Nov 99
-98.4	4414275	2000
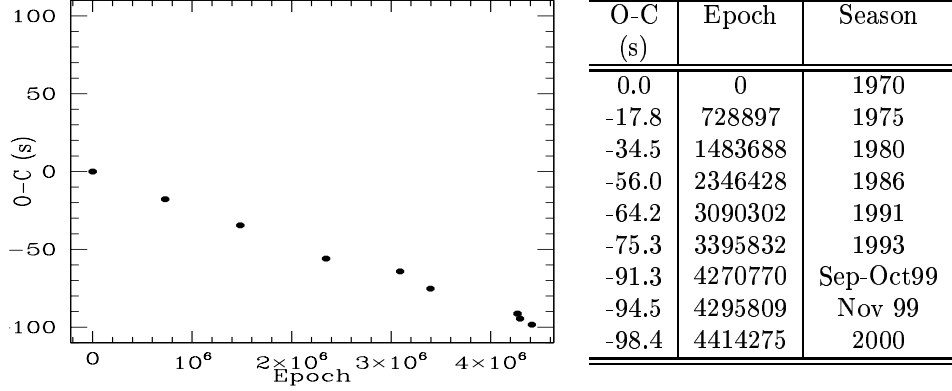
Figure A.32.—: O-C Diagram for Period = 213.13262766 s for E-2

O-C (s)	Epoch	Season
0.0	0	1970
-9.8	728897	1975
-18.3	1483688	1980
-29.9	2346428	1986
-30.3	3090302	1991
-38.0	3395832	1993
-44.4	4270770	Sep-Oct99
-47.4	4295809	Nov 99
-49.9	4414275	2000
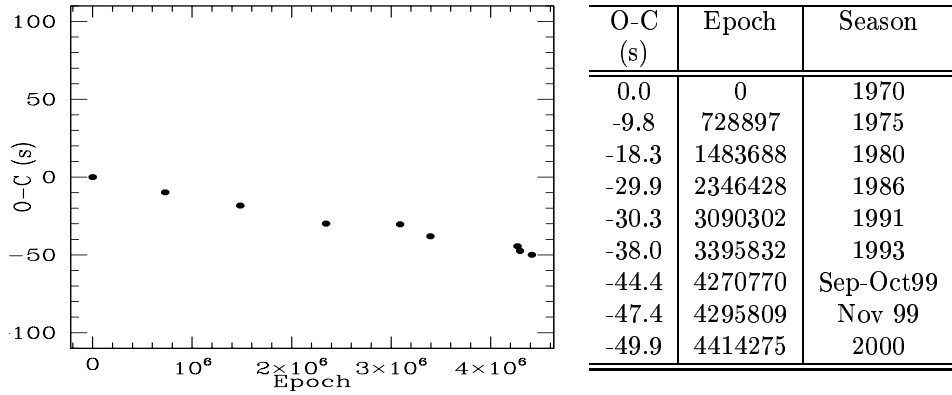
Figure A.33.—: O-C Diagram for Period = 213.13261666 s for E-1

85

O-C (s)	Epoch	Season
0.0	0	1970
-1.7	728897	1975
-2.0	1483688	1980
-4.0	2346428	1986
-3.5	3090302	1991
-1.0	3395832	1993
2.4	4270770	Sep-Oct99
-0.3	4295809	Nov 99
-1.5	4414275	2000
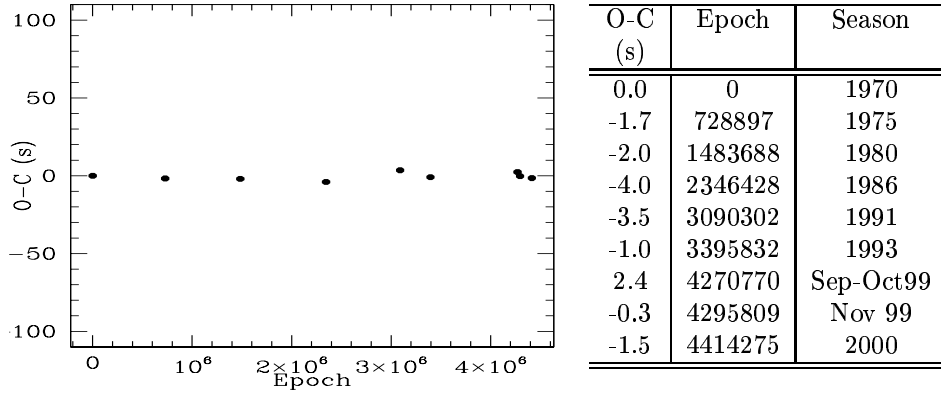
Figure A.34.—: O-C Diagram for Period = 213.13260565 s for E

O-C (s)	Epoch	Season
0.0	0	1970
6.3	728897	1975
14.3	1483688	1980
22.1	2346428	1986
37.4	3090302	1991
36.5	3395832	1993
49.2	4270770	Sep-Oct99
46.8	4295809	Nov 99
47.0	4414275	2000
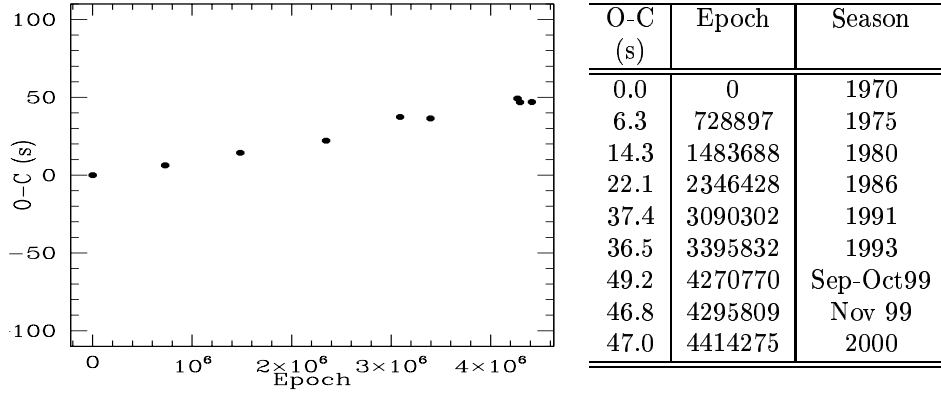
Figure A.35.—: O-C Diagram for Period = 213.13259465 s for E+1

O-C (s)	Epoch	Season
0.0	0	1970
14.2	728897	1975
30.6	1483688	1980
48.0	2346428	1986
71.4	3090302	1991
73.7	3395832	1993
96.3	4270770	Sep-Oct99
94.2	4295809	Nov 99
95.8	4414275	2000
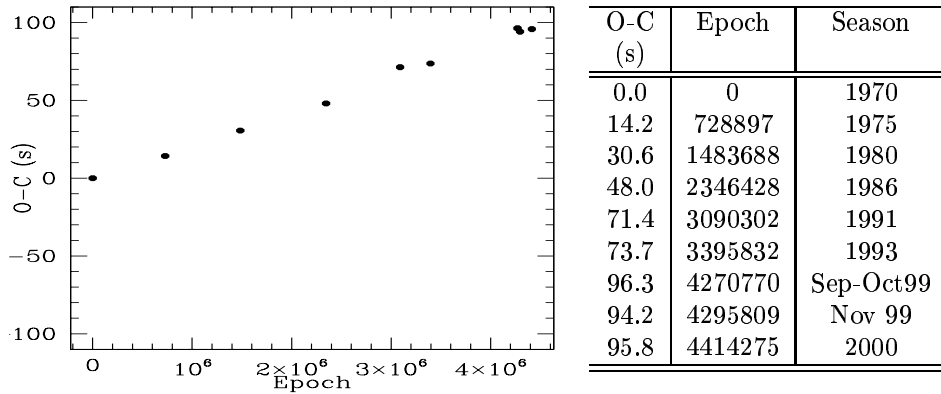
Figure A.36.—: O-C Diagram for Period = 213.13258365 s for E+2

From figures A.32 to A.36, we can evidently see that E=4414275 for the 2000 data set.

86

A.1.8 Changing the Tzero from 1968 to 1986

The error in the calculated value of phase C for a point on the O-C diagram is a product of the error in period and number of epochs from Tzero. To reduce this error in C, we should choose a suitable Tzero that lies in between the observations from 1970 to 2000. This suggests that the 1986 data set will prove to be a suitable reference point. Below, in fig. A.37, we present our final and best O-C diagram for the period 213.13260565 s.

O-C (s)	Epoch	Season
3.9	-2346428	1970
2.2	-1617531	1975
1.9	-862740	1980
0.0	0	1986
7.4	743874	1991
3.1	1049404	1993
6.4	1924342	Sep-Oct99
3.7	1949381	Nov 99
2.5	2067847	2000

Figure A.37.—: O-C Diagram for Period = 213.13260565 s for Tzero 1986

87

Appendix B

B.1 Bootstrapping values for the Period 212.76842949 s

In this section, we will indicate the O-C diagrams that led to establishing the period and $\dot{P}$ for the 212.768 s mode.

B.1.1 Bootstrapping from 1970 to 1975

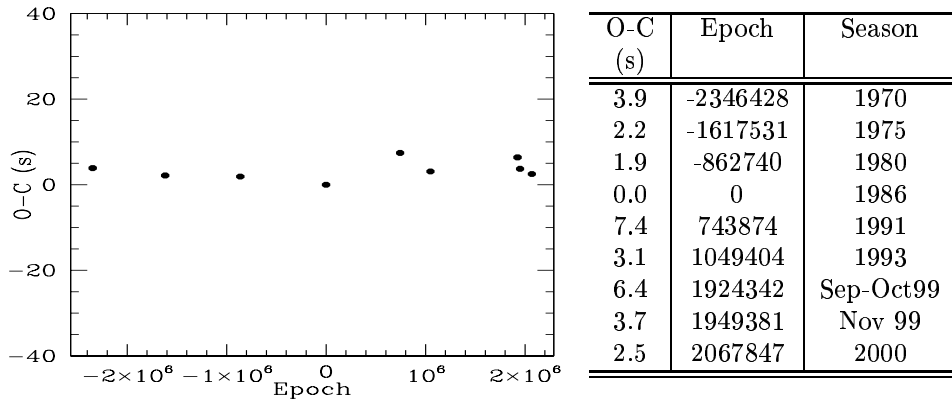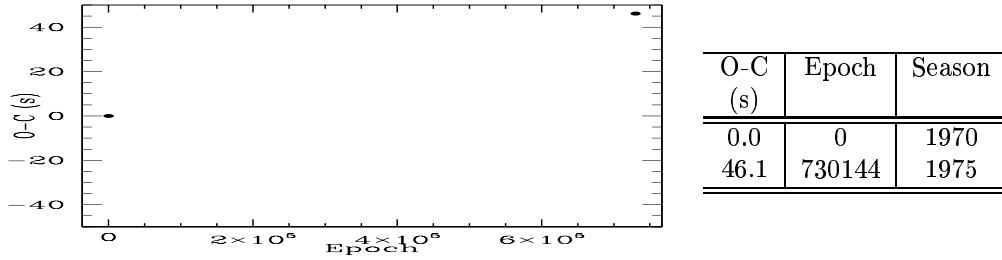Figure B.1.—: O-C Diagram for Period = 212.768371 s for data sets 1970 & 1975

O-C (s)	Epoch	Season
0.0	0	1970
46.1	730144	1975

From the O-C diagram in fig. B.1, we obtain the following corrections to Period for the five possibilities E, E±1 and E±2.

Epoch	Correction in Period (10^{-5} s)	New Period (s)
E-2=730142	64.6004	212.769017
E-1=730143	035.4596	212.768726
E=730144	6.319	212.768434
E+1=730145	-22.8216	212.768143
E+2=730146	-51.9621	212.767851

Table B.1: Corrections in Period for varying cycle counts between 1970 & 1975

The smallest correction in period has been obtained for E = 730144 and is already suggestive of the right answer. To help us pick out the right answer, we have also plotted a point corresponding to the 1980 data set, though it has not been utilized in the calculations.

O-C (s)	Epoch	Season
0.0	0	1970
-1.6	730142	1975
-20.6	1486223	1980
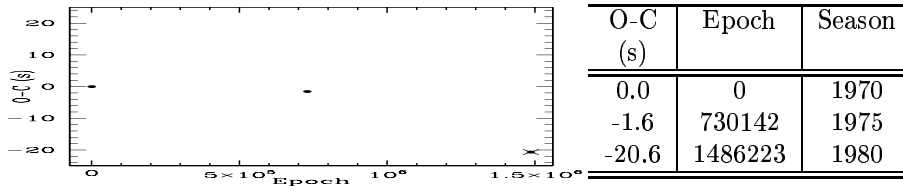
Figure B.2.—: O-C Diagram for Period = 212.769017 s for E-2

O-C (s)	Epoch	Season
0.0	0	1970
-1.2	730143	1975
-12.7	1486225	1980
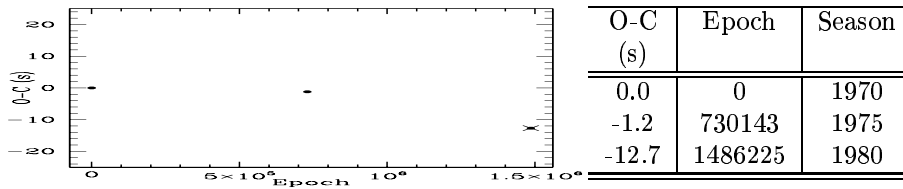
Figure B.3.—: O-C Diagram for Period = 212.768726 s for E-1

O-C (s)	Epoch	Season
0.0	0	1970
0.1	730144	1975
-3.3	1486227	1980
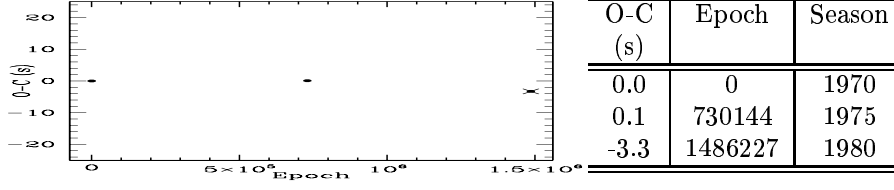
Figure B.4.—: O-C Diagram for Period = 212.768434 s for E

O-C (s)	Epoch	Season
0.0	0	1970
1.1	730145	1975
4.8	1486229	1980
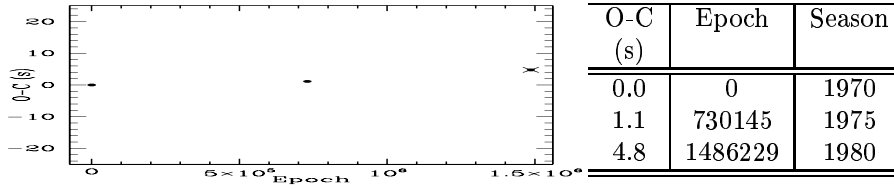
Figure B.5.—: O-C Diagram for Period = 212.768143 s for E+1

O-C (s)	Epoch	Season
0.0	0	1970
3.0	730146	1975
14.2	1486231	1980
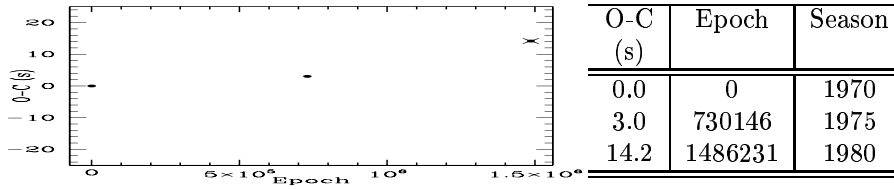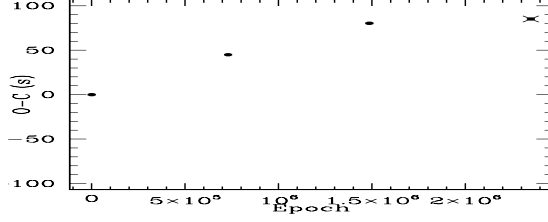
Figure B.6.—: O-C Diagram for Period = 212.767851 s for E+2

B.1.2 Bootstrapping from 1975 to 1980

Having concluded that E=730144 is the right number of cycles between 1970 and 1975, we now proceed to nailing down the number of epochs for the 1980 data set.
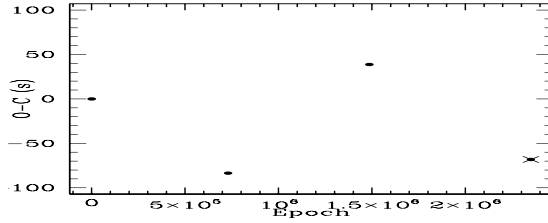
Epoch	Correction in Period (10^{-5} s)	New Period (s)
E-2=1486225	22.8896	212.768663
E-1=1486226	011.357	212.768548
E=1486227	-0.1757	212.768432
E+1=1486228	-11.7083	212.768317
E+2=1486229	-23.2409	212.768202

Table B.2: Corrections in Period for varying cycle counts between 1975 & 1980
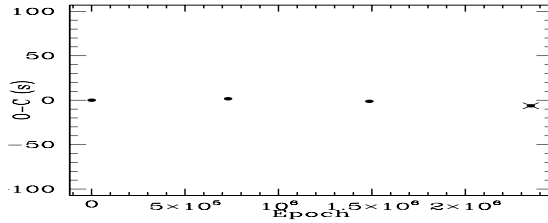
O-C (s)	Epoch	Season
0.0	0	1970
44.9	730143	1975
80.3	1486225	1980
85.1	2350441	1986

Figure B.7.—: O-C Diagram for Period = 212.768663 s for E-2
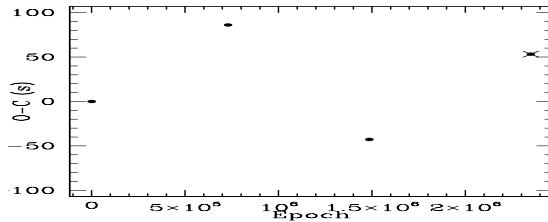
O-C (s)	Epoch	Season
0.0	0	1970
-83.5	730144	1975
38.7	1486226	1980
-68.1	2350443	1986

Figure B.8.—: O-C Diagram for Period = 212.768548 s for E-1

O-C (s)	Epoch	Season
0.0	0	1970
1.6	730144	1975
-1.3	1486227	1980
-6.3	2350444	1986

Figure B.9.—: O-C Diagram for Period = 212.768432 s for E

O-C (s)	Epoch	Season
0.0	0	1970
86.1	730144	1975
-42.8	1486228	1980
53.2	2350445	1986

Figure B.10.—: O-C Diagram for Period = 212.768489 s for E+1

91

O-C (s)	Epoch	Season
0.0	0	1970
-42.2	730145	1975
-84.2	1486229	1980
-100.0	2350447	1986
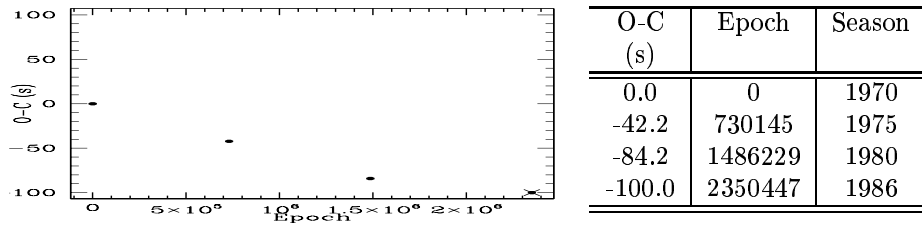
Figure B.11.—: O-C Diagram for Period = 212.768202 s for E+2

We conclude that E=1486227 is the right number of cycles for the 1980 data set.

B.1.3   Bootstrapping from 1980 to 1986

From the O-C values plotted in fig. B.9, we compute the following corrections to the period.

Epoch	Correction in Period (10^{-5} s)	New Period (s)
E-2=2350442	119112	212.768551
E-1=2350443	5.86154	212.768491
E=2350444	-0.18814	212.768430
E+1=2350445	-6.2378	212.768370
E+2=2350446	-12.2875	212.768309

Table B.3: Corrections in Period for varying cycle counts between 1980 & 1986

O-C (s)	Epoch	Season
0.0	0	1970
-85.7	730144	1975
34.3	1486226	1980
-75.2	2350443	1986
51.6	3095590	1991
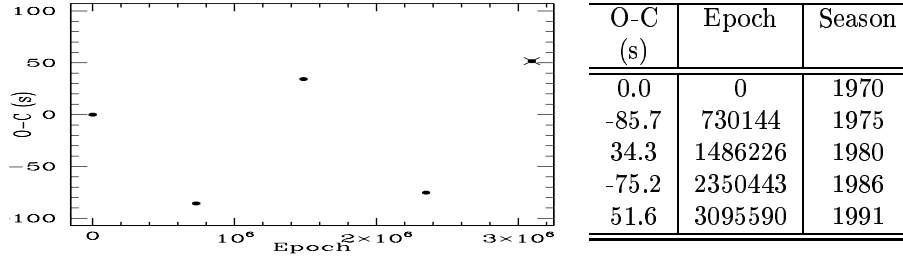
Figure B.12.—: O-C Diagram for Period = 212.768551 s for E-2

O-C (s)	Epoch	Season
0.0	0	1970
-41.6	730144	1975
-89.1	1486227	1980
66.7	2350443	1986
24.2	3095591	1991
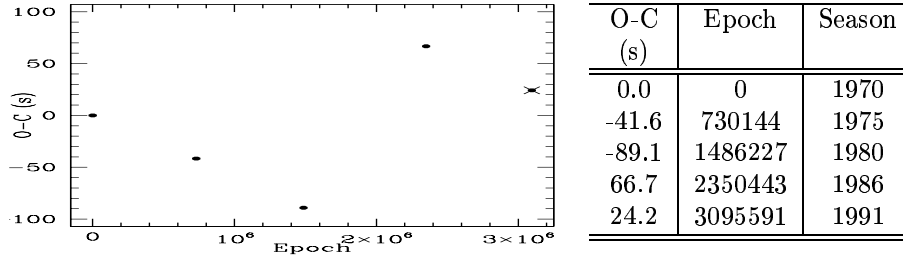
Figure B.13.—: O-C Diagram for Period = 212.768491 s for E-1

O-C (s)	Epoch	Season
0.0	0	1970
3.1	730144	1975
1.8	1486227	1980
-1.6	2350444	1986
0.0	3095592	1991
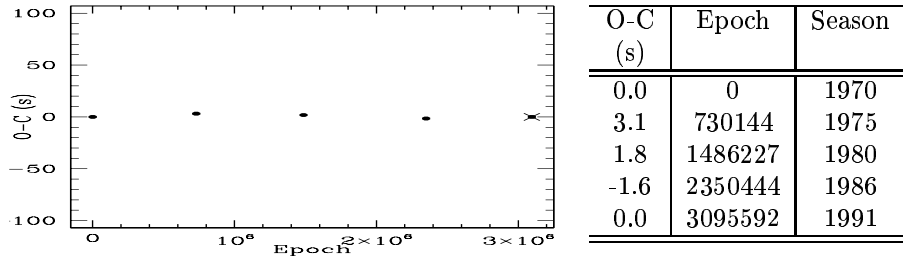
Figure B.14.—: O-C Diagram for Period = 212.768430 s for E

93

O-C (s)	Epoch	Season
0.0	0	1970
47.1	730144	1975
91.1	1486227	1980
-72.2	2350445	1986
-27.3	3095593	1991
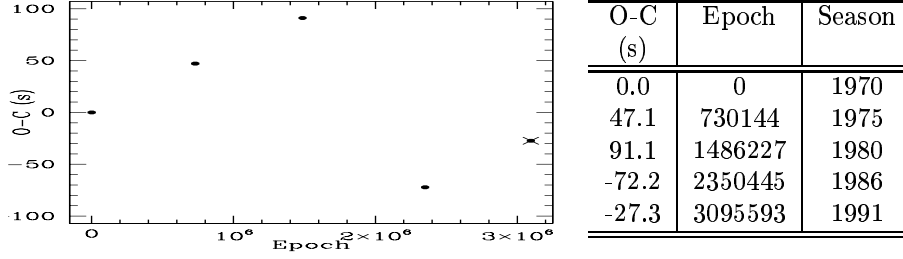
Figure B.15.—: O-C Diagram for Period = 212.768370 s for E+1

O-C (s)	Epoch	Season
0.0	0	1970
92.0	730144	1975
-30.8	1486228	1980
72.1	2350445	1986
-51.6	3095594	1991
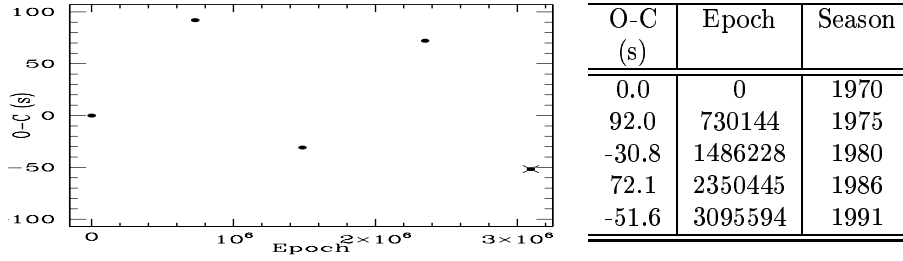
Figure B.16.—: O-C Diagram for Period = 212.768309 s for E+2

We can evidently see that the correct number of epochs for the 1986 data set is E=2350444.

B.1.4   Bootstrapping from 1986 to 1991

Using the O-C values indicated in fig. B.14, we have calculated the following corrections in period for the 5 possibilities E, E±1 and E±2.

Epoch	Correction in Period (10^{-6} s)	New Period (s)
E-2=3095590	73.8743	212.76850387
E-1=3095591	036.9739	212.76846697
E=3095592	0.07352	212.76843007
E+1=3095593	-36.8269	212.76839317
E+2=3095594	-73.7272	212.76835627

Table B.4: Corrections in Period for varying cycle counts between 1986 & 1991

Epoch	Correction in Period (10^{-6} s)	New Period (s)
E-2=3401642	48.7644	212.76847883
E-1=3401643	024.1638	212.76845423
E=3401644	-0.4369	212.76842963
E+1=3401645	-25.0376	212.76840503
E+2=3401646	-49.6382	212.76838043

Table B.5: Corrections in Period for varying cycle counts between 1991 & 1993
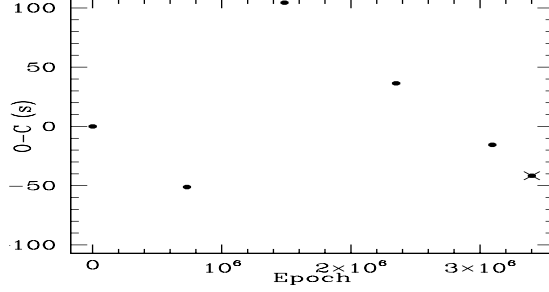
O-C (s)	Epoch	Season
0.0	0	1970
-51.1	730144	1975
104.5	1486226	1980
36.4	2350443	1986
-15.6	3095591	1991
-41.6	3401643	1993

Figure B.17.—: O-C Diagram for Period = 212.76850387 s for E-2
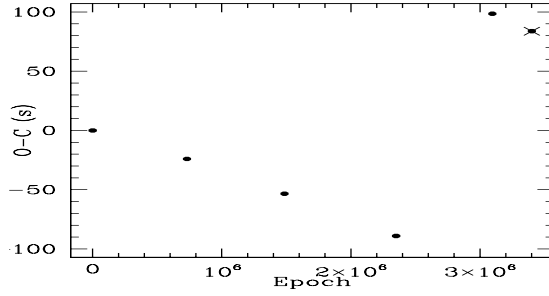
O-C (s)	Epoch	Season
0.0	0	1970
-24.0	730144	1975
-53.4	1486227	1980
-89.0	2350444	1986
98.5	3095591	1991
83.8	3401643	1993

Figure B.18.—: O-C Diagram for Period = 212.76846697 s for E-1
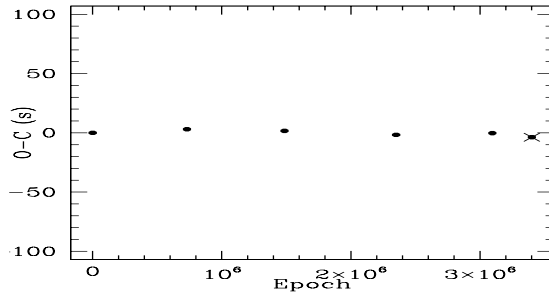
O-C (s)	Epoch	Season
0.0	0	1970
3.0	730144	1975
1.6	1486227	1980
-1.7	2350444	1986
-0.3	3095592	1991
-3.7	3401644	1993

Figure B.19.—: O-C Diagram for Period = 212.76843007 s for E

95

O-C (s)	Epoch	Season
0.0	0	1970
30.2	730144	1975
56.6	1486227	1980
85.6	2350444	1986
-99.0	3095593	1991
-91.0	3401645	1993
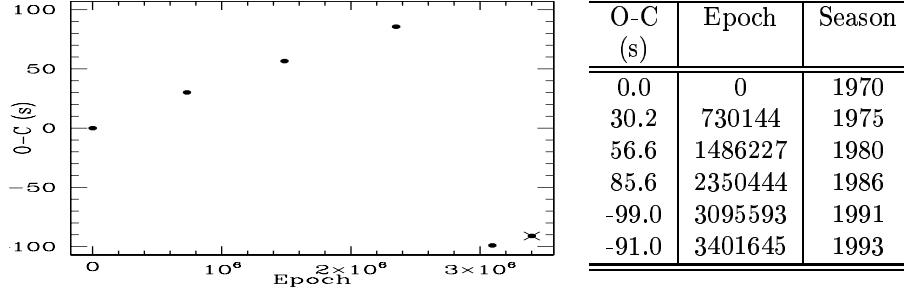
Figure B.20.—: O-C Diagram for Period = 212.76839317 s for E+1

O-C (s)	Epoch	Season
0.0	0	1970
57.2	730144	1975
-101.2	1486228	1980
-39.8	2350445	1986
15.0	3095593	1991
34.3	3401645	1993
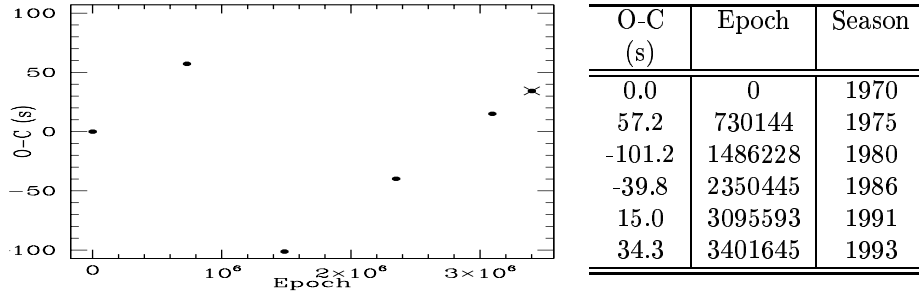
Figure B.21.—: O-C Diagram for Period = 212.76835627 s for E+2

E=3095592 seems to be the right answer from all the 5 possibilities investigated.

B.1.5 Bootstrapping from 1991 to 1993

Utilizing the O-C table in fig. B.19, we evaluated the following corrections to the period.

O-C (s)	Epoch	Season
0.0	0	1970
-32.8	730144	1975
-71.0	1486227	1980
95.6	2350443	1986
61.9	3095591	1991
43.5	3401643	1993
4.1	4278079	Sep-Oct99
4.4	4303161	Nov99
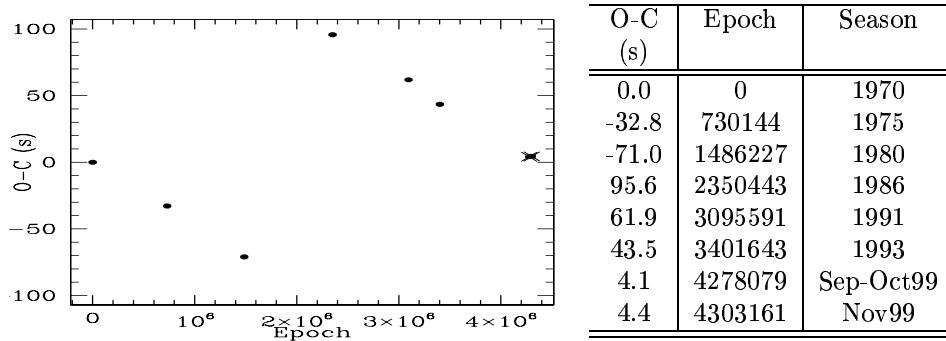
Figure B.22.—: O-C Diagram for Period = 212.76847883 s for E-2

96

O-C (s)	Epoch	Season
0.0	0	1970
-14.7	730144	1975
-34.4	1486227	1980
-58.9	2350444	1986
-74.9	3095592	1991
-85.7	3401644	1993
-103.3	278080	Sep-Oct99
-102.5	303162	Nov99
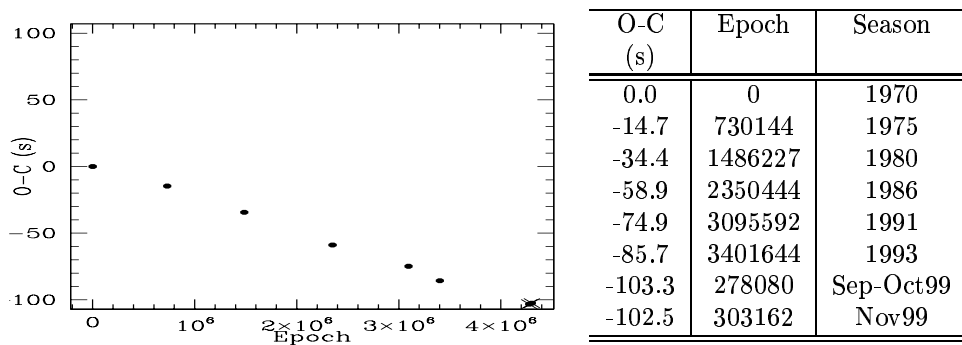
Figure B.23.—: O-C Diagram for Period = 212.76845423 s for E-1
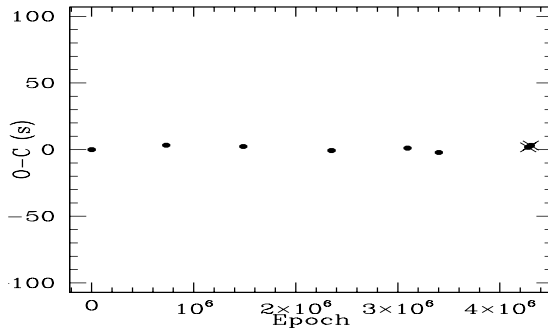
O-C (s)	Epoch	Season
0.0	0	1970
3.3	730144	1975
2.3	1486227	1980
-0.7	2350444	1986
1.1	3095592	1991
-2.1	3401644	1993
1.7	278080	Sep-Oct99
3.1	303162	Nov99

Figure B.24.—: O-C Diagram for Period = 212.76842963 s for E
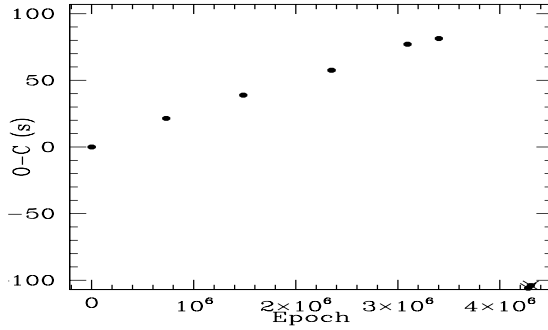
O-C (s)	Epoch	Season
0.0	0	1970
21.4	730144	1975
38.9	1486227	1980
57.5	2350444	1986
77.1	3095592	1991
81.4	3401644	1993
-105.9	4278081	Sep-Oct99
-103.9	4303163	Nov99

Figure B.25.—: O-C Diagram for Period = 212.76840503 s for E+1
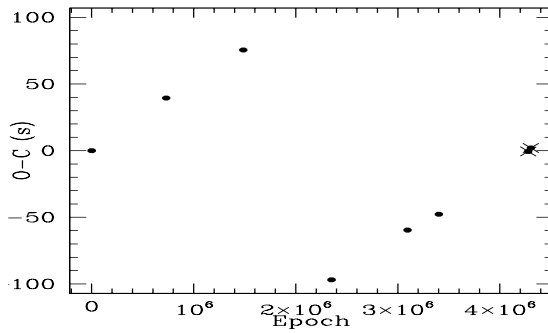
O-C (s)	Epoch	Season
0.0	0	1970
39.5	730144	1975
75.5	1486227	1980
-96.9	2350445	1986
-59.6	3095593	1991
-47.7	3401645	1993
-0.6	4278081	Sep-Oct99
2.0	4303163	Nov99

Figure B.26.—: O-C Diagram for Period = 212.76838043 s for E+2

We can conclude that E=3401644 is the correct number of cycles for the 1993 data set.

B.1.6   Bootstrapping from 1993 to 1999

From the O-C values indicated in fig. B.24, we calculate the following corrections to the period.

98

Epoch	Correction in Period (10^{-6} s)	New Period (s)
E-2=4278078	27.9636	212.76845759
E-1=4278079	14.1414	212.76844377
E=4278080	0.31924	212.76842995
E+1=4278081	-13.503	212.76841613
E+2=4278082	-27.7325	212.76840230

Table B.6: Corrections in Period for varying cycle counts between 1993 & 1999
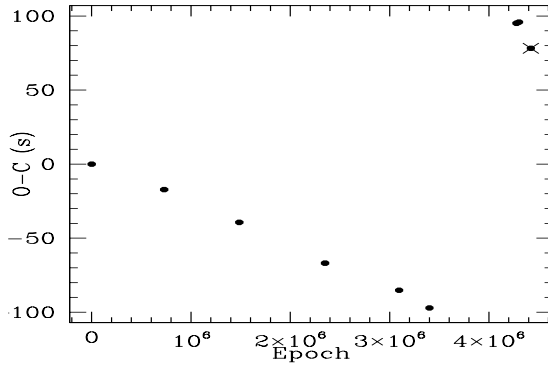
O-C (s)	Epoch	Season
0.0	0	1970
-17.2	730144	1975
-39.3	1486227	1980
-66.8	2350444	1986
-85.2	3095592	1991
-97.1	3401644	1993
95.1	4278079	Sep-Oct99
95.9	4303161	Nov99
78.2	4421829	2000

Figure B.27.—: O-C Diagram for Period = 212.76845759 s for E-2
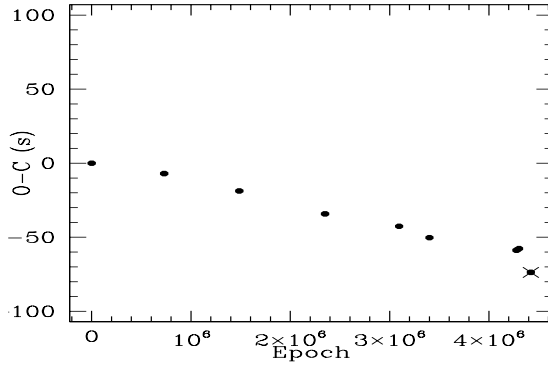
O-C (s)	Epoch	Season
0.0	0	1970
-7.0	730144	1975
-18.7	1486227	1980
-34.2	2350444	1986
-42.6	3095592	1991
-50.3	3401644	1993
-58.8	4278080	Sep-Oct99
-57.7	4303162	Nov99
-73.7	4421830	2000

Figure B.28.—: O-C Diagram for Period = 212.76844377 s for E-1

99
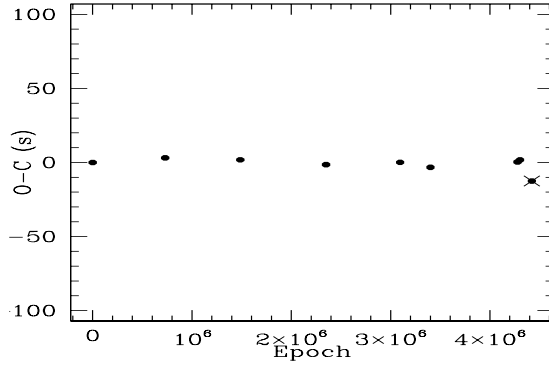
O-C (s)	Epoch	Season
0.0	0	1970
3.1	730144	1975
1.8	1486227	1980
-1.5	2350444	1986
0.1	3095592	1991
-3.3	3401644	1993
0.3	4278080	Sep-Oct99
1.7	4303162	Nov99
-12.5	4421830	2000

Figure B.29.—: O-C Diagram for Period = 212.76842995 s for E
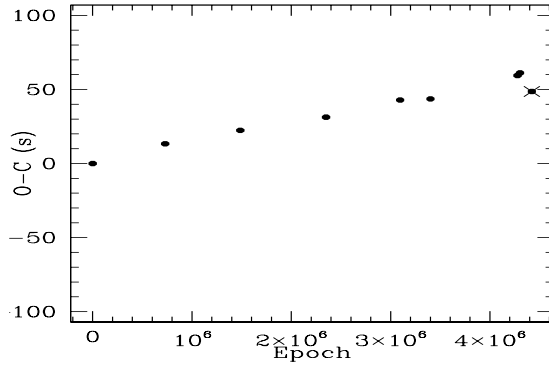
O-C (s)	Epoch	Season
0.0	0	1970
13.3	730144	1975
22.4	1486227	1980
31.3	2350444	1986
42.9	3095592	1991
43.6	3401644	1993
59.4	4278080	Sep-Oct99
61.2	4303162	Nov99
48.6	4421830	2000

Figure B.30.—: O-C Diagram for Period = 212.76841613 s for E+1
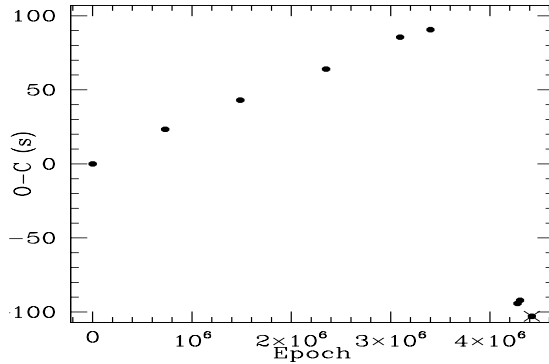
O-C (s)	Epoch	Season
0.0	0	1970
23.3	730144	1975
43.0	1486227	1980
64.0	2350444	1986
85.5	3095592	1991
90.6	3401644	1993
-94.2	4278081	Sep-Oct99
-92.2	4303163	Nov99
-102.9	4421831	2000

Figure B.31.—: O-C Diagram for Period = 212.76840230 s for E+2

100

E=4278080 and E=4303162 are evidently the right number of epochs for the Sep-Oct 1999 and November 1999 data sets respectively.

B.1.7 Bootstrapping from 1999 to 2000

Utilizing the O-C values indicated in fig. B.29, we evaluate the following corrections to period for the 5 possibilities E, E±1 and E±2.

Epoch	Correction in Period (10^{-6} s)	New Period (s)
E-2=4421828	21.2815	212.76845123
E-1=4421829	10.3151	212.76844027
E=4421830	-0.6512	212.76842930
E+1=4421831	-11.6175	212.76841833
E+2=4421832	-22.5839	212.76840737

Table B.7: Corrections in Period for varying cycle counts between 1999 & 2000

O-C (s)	Epoch	Season
0.0	0	1970
-12.4	730144	1975
-29.0	1486227	1980
-51.9	2350444	1986
-65.5	3095592	1991
-75.5	3401644	1993
-90.5	4278080	Sep-Oct99
-89.6	4303162	Nov99
106.2	4421829	2000

Figure B.32.—: O-C Diagram for Period = 212.76845123 s for E-2

O-C (s)	Epoch	Season
0.0	0	1970
-4.5	730144	1975
-13.6	1486227	1980
-25.9	2350444	1986
-31.7	3095592	1991
-38.2	3401644	1993
-43.6	4278080	Sep-Oct99
-42.5	4303162	Nov99
-58.0	4421830	2000

Figure B.33.—: O-C Diagram for Period = 212.76844027 s for E-1

O-C (s)	Epoch	Season
0.0	0	1970
3.5	730144	1975
2.8	1486227	1980
0.1	2350444	1986
2.2	3095592	1991
-1.0	3401644	1993
3.3	4278080	Sep-Oct99
4.7	4303162	Nov99
-9.5	4421830	2000

Figure B.34.—: O-C Diagram for Period = 212.76842930 s for E

O-C (s)	Epoch	Season
0.0	0	1970
11.7	730144	1975
19.1	1486227	1980
26.0	2350444	1986
36.1	3095592	1991
36.3	3401644	1993
50.2	4278080	Sep-Oct99
51.8	4303162	Nov99
39.1	4421830	2000

Figure B.35.—: O-C Diagram for Period = 212.76841833 s for E+1

102

O-C (s)	Epoch	Season
0.0	0	1970
19.7	730144	1975
35.4	1486227	1980
52.0	2350444	1986
70.0	3095592	1991
73.5	3401644	1993
97.0	4278080	Sep-Oct99
98.9	4303162	Nov99
87.6	4421830	2000

Figure B.36.—: O-C Diagram for Period = 212.76840737 s for E+2

We conclude that E=4421830 is evidently the correct number of cycles for the 2000 data set.

B.1.8   Changing the Tzero from 1968 to 1986

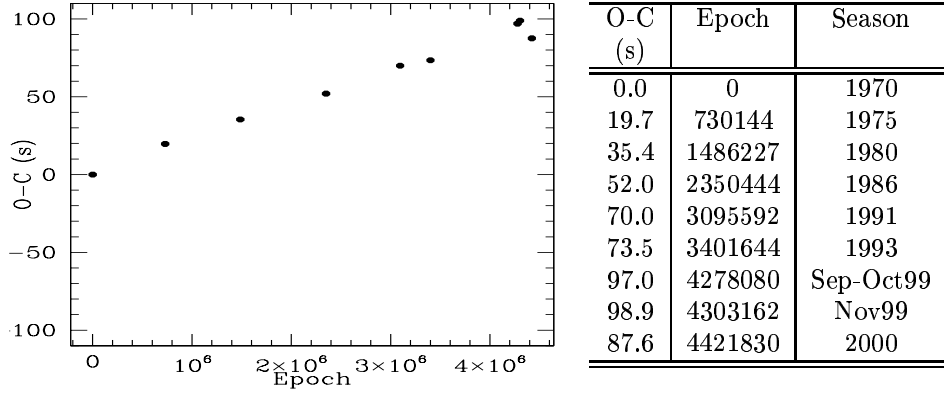As explained earlier in section A.1.8, changing the Tzero from 1968 to 1986 will reduce the uncertainties in the calculated value of phase for the various points on the O-C diagram.

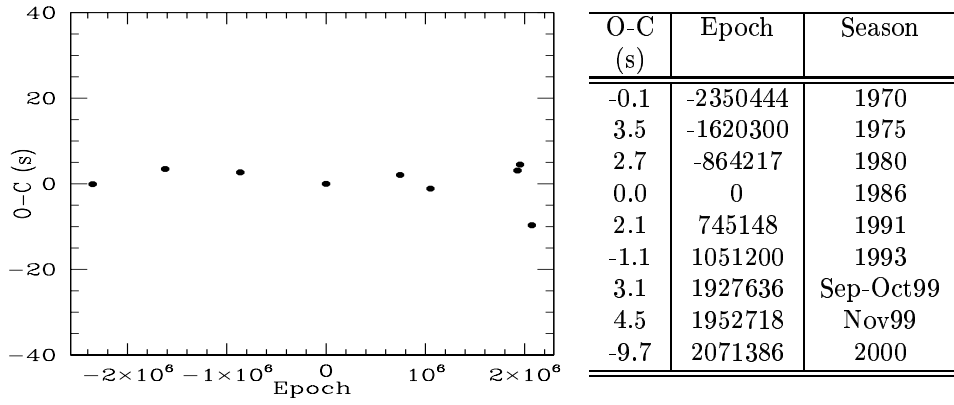| O-C (s)	Epoch	Season
-0.1	-2350444	1970
3.5	-1620300	1975
2.7	-864217	1980
0.0	0	1986
2.1	745148	1991
-1.1	1051200	1993
3.1	1927636	Sep-Oct99
4.5	1952718	Nov99
-9.7	2071386	2000

Figure B.37.—: O-C Diagram for Period = 212.76842930 s for Tzero 1986

Appendix C

C.1   Best O-C table for the 274 s Doublet

The 274 s doublet behaves differently than the 213 s doublet. For both modes of the 274 s doublet, we could never achieve a clear minimization of phase dispersion. The uncertainties in phase are larger for the 274 s doublet as it has a lower amplitude compared to the 213 s doublet. However, both 212.768 s and 274.25 s periods have similar amplitudes. We cannot blame the doublet's amplitude for not being able to find correct cycle counts. Rather, the O-C diagrams are suggestive of behavior, apart from cooling. Suppose the effect governing the 274 s doublet resulted in a constant $\dot{P}$ (at time-scales of 3 decades), then we would still have been able to minimize the phase dispersion and all the O-C points would lie on the best fit within uncertainties. In other words, uncertainty of this constant $\dot{P}$ would have been comparable to the $\dot{P}$ uncertainty shown by the 213 s doublet. However, what we actually obtain is an O-C diagram with ambiguous cycle counts and all the points do not lie on a parabola within error bars. This can lead to a plausible thought that $\dot{P}$ for the 274 s doublet is not constant and the $\ddot{P}$ term is significant. If so, then we could be seeing something very exciting, that needs further investigation.

O-C (s)	Error in O-C (s)	Epoch	Season
-55	18	-1823513	1970
-56	12	-1257055	1975
-5.4	7.3	-670474	1980
0.0	5.8	0	1986
-55.7	5.5	578099	1991
-72.0	8.6	815540	1993
-58	13	1495493	Sep-Oct 1999
-65	14	1514952	Nov 1999

Table C.1: O-C table for Period 274.25080355 s

O-C (s)	Error in O-C (s)	Epoch	Season
-35	41	-1820038	1970
17.5	28	-1254660	1975
22	16	-669196	1980
0.0	7.7	0	1986
-153	13	576996	1991
-126	20	813986	1993
-18	33	1492643	Sep-Oct 1999
-60	33	1512065	Nov 1999

Table C.2: O-C table for Period 274.77450046 s

Bibliography

[Aizenman, Smeyers & Weigert (1977)] Aizenman, M., Smeyers, P. and Weigert, A. 1977, A&A, 58, 41

[Bergeron et al.(1995)] Bergeron, P., Wesemael, F., Lamontagne, R., Fontaine, G., Saffer, R. A. & Allard, N. F. 1995, ApJ, 449, 258

[Bradley (1998)] Bradley, P. A. 1998, ApJS, 116, 307

[Bradley (1996)] Bradley, P. A. 1996, ApJ, 468, 350

[Bradley (1993)] Bradley, P. A. 1993, Ph.D. Thesis, 4

[Bradley, Winget & Wood (1992)] Bradley, P. A., Winget, D. E. and Wood, M. A. 1992, ApJ, 391, L33

[Brassard, Fontaine, Wesemael & Hansen (1992)] Brassard, P., Fontaine, G., Wesemael, F. and Hansen, C. J. 1992, ApJS, 80, 369

[Christensen-Dalsgaard (1981)] Christensen-Dalsgaard, J. 1981, MNRAS, 194, 229

[Clemens (1993)] Clemens, J. C. 1993, Baltic Astronomy, 2, 511

[Costa, Kepler & Winget (1999)] Costa, J. E. S., Kepler, S. O. & Winget, D. E. 1999, ApJ, 522, 973

[Costa (1996)] Costa, J. E. S. 1996, M. S. thesis, Inst. Fis. Univ. Federal do Rio Grande do Sul, Brazil

[Giovannini et al. (1998)] Giovannini, O., Kepler, S. O., Kanaan, A., Wood, A., Claver, C. F. and Koester, D. 1998, Baltic Astronomy, 7, 131

[Kaspi, Taylor & Ryba(1994)] Kaspi, V. M., Taylor, J. H. & Ryba, M. F. 1994, ApJ, 428, 713

[Kawaler, Winget & Hansen(1985)] Kawaler, S. D., Winget, D. E. & Hansen, C. J. 1985, ApJ, 298, 752

[Kepler, et al. (2000)] Kepler, S. O., Mukadam, A., Winget, D. E., Nather, R. E., Metcalfe, T. S., Reed, M. D., Kawaler, S. D. and Bradley, P. A. 2000, ApJ, 534, L185

[Kepler, et al. (1995)] Kepler, S. O., et al. 1995, Baltic Astronomy, 4, 238

[Kepler & Bradley (1995)] Kepler, S. O. & Bradley, P. A. 1995, Baltic Astronomy, 4, 166

[Kepler (1993)] Kepler, S. O. 1993, Baltic Astronomy, 2, 515

[Kepler, et al. (1991)] Kepler, S. O., and 28 colleagues 1991, ApJ, 378, L45

[Kleinman, Kawaler & Bischoff (2000)] Kleinman, S. J., Kawaler, S. D. and Bischoff, A. 2000, ASP Conf. Ser. 203: The Impact of Large-Scale Surveys on Pulsating Star Research, 515

[Kleinman, Nather & Phillips (1996)] Kleinman, S. J., Nather, R. E. & Phillips, T. 1996, PASP, 108, 356

[Lacombe & Fontaine (1980)] Lacombe, P. & Fontaine, G. 1980, JRASC, 74, 147

[Leggett, Ruiz & Bergeron (1998)] Leggett, S. K., Ruiz, M. T. and Bergeron, P. 1998, ApJ, 497, 294

[Liebert, Dahn & Monet (1988)] Liebert, J., Dahn, C. C. and Monet, D. G. 1988, ApJ, 332, 891

[McGraw & Robinson (1976)] McGraw, J. T. & Robinson, E. L. 1976, ApJ, 205, L155

[Mestel (1952)] Mestel, L. 1952, MNRAS, 112, 583

[Montgomery & Winget(1999)] Montgomery, M. H. & Winget, D. E. 1999, ApJ, 526, 976

[Montgomery(1998)] Montgomery, M. H. 1998, Ph.D. Thesis, 21

[Nather (1995)] Nather, R. E. 1995, Baltic Astronomy, 4, 321

[Nather, et al. (1990)] Nather, R. E., Winget, D. E., Clemens, J. C., Hansen, C. J. & Hine, B. P. 1990, ApJ, 361, 309

[Nitta et al. (1999)] Nitta, A., Kanaan, A., Kepler, S. O., Koester, D., Montgomery, M. H. and Winget, D. E. 1999, Baltic Astronomy, 9, 97

[Oswalt, Smith, Wood & Hintzen (1996)] Oswalt, T. D., Smith, J. A., Wood, M. A. and Hintzen, P. 1996, Nature, 382, 692

[Pajdosz (1995)] Pajdosz, G. 1995, A&A, 295, L17

[Rawley, Taylor, Davis & Allan(1987)] Rawley, L. A., Taylor, J. H., Davis, M. M. & Allan, D. W. 1987, Science, 238, 761

[Robinson, Kepler & Nather (1982)] Robinson, E. L., Kepler, S. O. & Nather, R. E. 1982, ApJ, 259, 219

[Standish (1998)] Standish, E. M. 1998, A&A, 336, 381

[Tomaney (1987)] Tomaney, A. B. 1987, IAU Colloq. 95: Second Conference on Faint Blue Stars, 673

[van Horn (1971)] van Horn, H. M. 1971, IAU Symp. 42: White Dwarfs, 42, 97

[Weidemann (1990)] Weidemann, V. 1990, ARA&A, 28, 103

[Winget (1998)] Winget, D. E. 1998, Journal of Physic s: Condensed Matter, 10, 11247

[Winget et al. (1997)] Winget, D. E., Kepler, S. O., Kanaan, A., Montgomery, M. H. and Giovannini, O. 1997, ApJ, 487, L191

[Winget et al. (1987)] Winget, D. E., Hansen, C. J., Liebert, J., van Horn, H. M., Fontaine, G., Nather, R. E., Kepler, S. O. and Lamb, D. Q. 1987, ApJ, 315, L77

[Winget, et al. (1985)] Winget, D. E., Robinson, E. L., Nather, R. E., Kepler, S. O. and Odonoghue, D. 1985, ApJ, 292, 606

[Winget, Hansen & van Horn (1983)] Winget, D. E., Hansen, C. J. and van Horn, H. M. 1983, Nature, 303, 781

[Winget, van Horn & Hansen (1981)] Winget, D. E., van Horn, H. M. & Hansen, C. J. 1981, ApJ, 245, L33

[Wood(1992)] Wood, M. A. 1992, ApJ, 386, 539

[Wood & Winget (1988)] ood, M. A. & Winget D. E. 1988, Multimode Stellar Pulsations, eds. G. Kovacs, L. Szabados, and B. Szeidl (Konkoly Observatory. Kultura: Budapest), p. 199

Vita

Anjum Mukadam was born on December 29, 1974 in Bombay, India. When she was 10 years old, she decided to become an astronomer, to her family's surprise and amusement. She just loved looking at the stars and was very fascinated by them. She completed her school years in St. Thomas High School and cleared the Senior Secondary Certificate Board Examination (Grade X) in April, 1990. She then joined Bhavan's Junior College to study science and passed the Higher Secondary Certificate Board Examination (Grade XII) in April, 1992. She then joined D. G. Ruparel College and got her Bachelor of Science in Physics in May, 1995. Anjum pursued physics in the Indian Institute of Technology (IIT), Bombay and was awarded Master of Science in April, 1997. She then joined Tata Institute of Fundamental Research (TIFR), Bombay as a research scholar for a year. She came to the United States in July 1998 and joined the University of Texas at Austin as a graduate student.

Permanent Address: 2502 Leon Street, Apt # M

Austin, TX - 78705

This thesis was typeset with $\text{\LaTeX}\,2_\varepsilon$[1] by the author.

---

[1] $\text{\LaTeX}\,2_\varepsilon$ is an extension of LaTeX. LaTeX is a collection of macros for TeX. TeX is a trademark of the American Mathematical Society. The macros used in formatting this thesis were written by Dinesh Das, Department of Computer Sciences, The University of Texas at Austin.